TABLE OF CONTENTS

LIST OF FIGURES

Abbreviations and Synonyms

SIS: Strange Invariant Set, an invariant set that has a fractal dimension.
UPO: Unstable Periodic Orbit.
cycle: a periodic orbit.
PDE: Partial Differential Equation.
ODE: Ordinary Differential Equation.
KSe: Kuramoto-Sivashinsky equation.
CGLe: Complex Ginzburg-Landau equation.
NSe: Navier-Stokes equation

SUMMARY

We propose a dynamical systems approach to study of turbulence (spatiotemporal chaos) based on the periodic orbit theory. The role of recurrent patterns and coherent structures is emphasized in the description. After a brief review of the periodic orbit theory in low dimensions, we discuss its possible application to the dynamics of spatially extended systems. The discussion is three-fold. First, we introduce a novel variational scheme for finding periodic orbits in general flows. Second, we check the periodic structures near the first instability of the complex Ginzburg-Landau equation and talk about its role in pattern formation. Third, we discuss the extensive numerical explorations that we have done to the Kuramoto-Sivashinsky system in the chaotic regime, including searching for periodic orbits, constructing symbolic dynamics and describing the chaotic invariant set in terms of intrinsic coordinates. In these investigations, we hope to identify and rank the nonlinear instabilities according to their relative importance.

CHAPTER I

INTRODUCTION

If I have seen less far than other men it is because I have stood behind giants.
E. A. Spiegel

In this chapter we give a sketch of dynamical system theory and turbulence study from both the historical development and methodology points of view. Since both subjects involve a huge body of literature, they are touched in a way that will provide background for and motivate our investigation later on. The bottomline is the effort that brings dynamical system theory, especially the periodic orbit theory, to the study of 1-d spatiotemporal chaos, a first step towards the real world 3-d turbulence.

1.1 From dynamical systems to periodic orbit theory

Dynamical system theory is a modern subject, but the basic elements emerged a century ago. Today, both its concepts and methodology are under intensive development. Periodic orbit theory is among the most powerful and promising of these developments. It combines many techniques for dealing with dynamical systems.

1.1.1 Historical perspective

Since the invention of calculus by Newton and Leibniz, differential equations become a focus of study, not only because of their dominant role in describing nature but also because of their intrinsic complexity and beauty and paramount importance in the development of new theories. Although more efforts are still being made to seek fundamental laws of nature in extremely high energy regime, physicists may proudly say that they already hold the laws necessary to explain and predict what happens in the physical world, except for events taking place immediately after the Big Bang or under extreme conditions that are far beyond the experience of the earthlings. Macroscopically, everything seems to be deterministic, just like what Leibniz pointed out in *Von dem Verhängnisse*: "Given knowledge of present state of the universe, we would see the future in the present as in a mirror."

This is an enticing remark and people have been investigating its validity ever since then. Mathematically, this is done by solving differential equations. The earliest attempts were devoted to obtaining explicit expressions in terms of known functions or quadratures. People had been devising various transformations and introducing and studying more and more special functions. Still, in many cases, they could not get what they wanted and tended to attribute the failure to their lack of cleverness in finding the appropriate transformation that could settle the problem.

The French mathematician Henry Poincaré broke the religion and gave new life to the old subject. In his study of celestial mechanics [202], Poincaré found that the equations of motion of heavenly bodies were in general not integrable, i.e. no smooth transformation existed to reduce the problem to a quadrature. In this sense, exact solutions of some equations are not possible. Instead, Poincaré suggested the qualitative method to study differential equations. An equation can be viewed as a dynamical system associated with a phase space, the orbit structure of which gives the qualitative properties of solutions of the equation. Geometrical and topological methods can then be invoked to study the phase space itself. This led Poincaré to his discovery of many important theorems in the theory of ordinary differential equations and chaos in celestial mechanics.

It was not until 1963 when Lorenz discovered chaotic strange attractor [162] in the atmospheric study that the chaotic dynamical systems started to attract attention of both mathematicians and scientists in general. Lorenz found that the solution of a simple 3-d dynamical system depends on the initial condition so sensitively that any small discrepancy will grow quickly to cover the whole attractor and make the system behavior totally unpredictable in the long run. This fact was later ascribed the term "butterfly effect". Researchers soon discovered that chaos is ubiquitous and accounts for various dynamical phenomena.

From then on, dynamical systems become a hot research area and its content has been extended from ordinary differential equations (ODEs) to partial differential equations (PDEs) [245, 113] and differentiable mappings [62, 41]. The development of digital computer boosted the research greatly with new fields opened to scientists like cellular automata [273] and lattice field theory [44]. Today, research on dynamical systems is rapidly expanding and rewarding in both theory and applications. It leads to many new concepts and methods but raises even more problems and conjectures awaiting an answer. First we review briefly the notions and techniques commonly used in dynamical sytem theory and later use these concepts to illuminate the way in our study of turbulence.

1.1.2 Different approaches to dynamical systems

Analytical manipulation is dear to most scientists for solving differential equations. If a differential equation is reducible to finitely many algebraic equations, even though the algebraic equations may not be explicitly solvable, the problem is considered to be solved since the global structure of solutions is known in principle and specific solutions can be calculated to any accuracy in the whole domain of definition [134, 137, 247, 123]. $n-1$ first integrals yield a full solution of an n-dimensional system. Although the direct integration or series expansion is most effective to linear systems, various technique have been devised to test the integrability of nonlinear equations, like the Painléve [134, 123, 270, 268, 43] and inverse scattering method [1]. Generally, integrability only exist in highly simplied models, but its discussion providing the starting point for studying more complex behavior.

The qualitative theory that combines algebra, analysis and geometry is the main tool to study the behavior of general differential equations. We care most about the long-term dynamics which concentrates on a small subset of the phase space in a dissipative system [199, 168]. To understand the asymptotic behavior of a system, we only need to

identify the subset, and study the dynamics around it [106, 271, 110, 111]. The Banach's contraction mapping principle [112, 118, 226] plays a central role in discussing the existence and analytical properties of solutions. It identifies the dominant features and orders the approximates to the solutions, with fine corrections introduced successively. We will use the technique to analyze the solutions of the complex Ginzburg-Landau equation (CGLe) in chapter 4.

In all this study, symmetry considerations and Lie group theory have been gaining more and more attention [196, 1, 186, 154]. Interestingly, sometimes the precise form of the differential equation is not important for interpreting desired properties of a dynamical system. All that we need to know is the symmetry group associated with the system [100, 14, 45]. The continuity condition of solutions imposes severe constraints on the global topology.Through the construction of certain topological invariants, much can be deduced about the structure of the phase space [42, 180, 218, 183, 96].

In dissipative chaotic systems, the complicated asymptotic dynamics takes place on a compact subset which is not a manifold but has a fractal structure [162, 165], called a strange invariant set (SIS). Various fractal dimensions are introduced to characterize the size and geometric layout of the SIS [73, 223], and Chaoticity of the dynamics is shown by the biggest Lyapunov exponent [106, 223]. Statistical behavior of solutions depends heavily on the ergodic or mixing property of the system, the discussion of which constitutes a lively research direction itself [227]. The statistical properties are also investigated by introducing linear opearators, such as the Perron-Frobenius operator, and by studying their spectra. We will see how the periodic orbit theory is used to calculate the spectra later on.

The above program is carried out analytically only in a small number of systems. In most cases, numerical calculations are needed to assist analysis. Nowadays, with increasing power of digital computers, it is possible to carry out direct numerical simulation of more and more complex nonlinear problems. Numerical computation has become an indispensable tool for the exploration and application of dynamical systems. The computer generated figures provide intuitive pictures and stimulate inspiration for developing analytical methods [277]. Furthermore, numerical calculation with controlled error is an important tool for computer-assisted proofs of theorems [179]. Numerical procedures are also used to produce approximate invariant manifolds [126, 84, 26] which are used as the framework for qualitative discussion of the long-time behavior. Apart from equilibrium points, the simplest and most easily obtainable objects of a chaotic system are unstable periodic orbits (UPOs).

1.2 Periodic orbits: theory and numerics

One of the earliest observations of a dynamical system made by human beings is the periodic motion, *e.g.*, the circular motion of the heavenly bodies. Next discovery was the quasi-periodic motion, motion in which an orbit never retraces itself exactly but is decomposable to a finite set of components with incommensurate frequencies. It was natural to think that the most general form of bounded motion is the quasi-periodic oneb but the discovery of chaos shattered that belief. The chaotic flow has infinitely many UPOs with incommensurate frequencies, and its sensitive dependence on initial conditions precludes the possibility of quasi-periodic motion, even with infinitely many frequencies. It is a new form of motion,

with a distinct nature. Today, it is believed that chaos is the rule in general dynamical systems, and considerable amount of research efforts are devoted to it.

Although the set of UPOs has a zero Lesbegue measure on a SIS, its central importance was realized already by Poincaré [202]. In the early sixties, in order to explain the generation of a SIS, Smale [230] proposed the horseshoe mechanism. Loosely speaking, the SIS results from local stretching and squeezing and global bending and squashing. A SIS is usually a fractal set which is self-similar and covered densely by UPOs. If it is compact, maximal, hyperbolic and indecomposable [106], a Markov partition exists and a finite symbolic set could be defined such that the dynamics on the SIS is topologically equivalent to a subshift of finite type in the symbol space, and every periodic sequence corresponds to a UPO [106]. In general, the SIS has a much more complicated structure and infinitely many symbols are needed to characterize the set and the dynamics.

1.2.0.1 Dynamics and UPOs

The creation or destruction of UPOs under parameter changes indicates bifurcations. How is a periodic orbit generated? In general, there are two ways - through a local bifurcation or through a global bifurcation. Locally, a Hopf bifurcation is the commonly encountered way of producing a periodic orbit. When a complex pair of eigenvalues of the Jacobian matrix of a fixed point cross transversely the imaginary axis, Hopf bifurcation takes place, and the resulting periodic orbit inherits the stability of the fixed point [106]. Globally, a homoclinic bifurcation is frequently associated with appearance or disappearance of UPOs. Horseshoes are often generated by a homoclinic explosion like in the Lorenz system [232, 163], a special form of the homoclinic bifurcation, which results in a infinity of UPOs. Global saddle-node or pitchfork bifurcation are also common for the annhilation or creation of one or two UPOs.

The UPOs form the skeleton of a SIS [50, 49]. The closure of the set of UPOs is the SIS itself and the dynamics on it is a walk through the space of these UPOs. Various physically interesting quantities, like topological entropy, fractal dimension, correlation length and escape rate, can be calculated via spectral determinants or dynamical zeta functions [50], expressed as a convergent sum over the set of UPOs. If a complete symbolic dynamics exists, cycle expansions [9] give exponential (or super-exponential) convergence rate relative to the topological lengths of the UPOs.

We can give a geometrical picture of the role played by the UPOs in the SIS. Every UPO has a linearized neighborhood in which the dynamics is well approximated. Phase space is then partitioned into these neighborhoods. The more UPOs we have, the finer is the partition, the more accurate is the representation. In a hyperbolic system with complete symbolic dynamics, long orbits are shadowed by short ones, leaving only fast decaying curvature contributions. Cycle expansions on spectral determinants (dynamical zeta functions) are a systematic way of piecing the information together for calculating dynamical averages on a SIS.

1.2.0.2 UPOs and numerics

The very existence of UPOs tells us much about the dynamics. Sometimes, several shortest UPOs are enough to set up a frame for discussing qualitive properties of a dynamical system [50, 141]. If all the UPOs up to a given length are found, we may consider using trace formula to evaluate physical averages. It is, therefore, a crucial part of the periodic orbit theory to locate the requested UPOs with given accuracy. Analytical methods have very limited use in this context, so numerical integration is the only choice. Due to the sensitive dependence of solutions on initial conditions in a chaotic dynamical system, it is impossible to follow a typical orbit for arbitrarily long time with reasonable accuracy. To locate a UPO, however, requires only calculation on a finite orbit segment, which can be done with great accuracy [262]. If a UPO is hyperbolic, then it is the maximal invariant set in a small neighborhood of itself and persists under small perturbations, being either small changes of system parameters or numerical noise. So, a hyperbolic UPO is robust and numerically obtainable.

We are mainly concerned with UPOs on a SIS, and many different numerical methods have been developed to locate them. Basically, finding periodic orbits is a boundary value problem on the time axis. If a Poincaré section is chosen in phase space, simple shooting is often used for searching the shortest UPOs. In very chaotic system or to locate long UPOs, multipoint shooting is more stable [50, 238]. Variational methods [156, 148, 119] are useful for complicated or high-dimensional systems, which put a guessed loop in the phase space and then drive it to the desired periodic orbit by some extremization principle. To find periodic orbits in the discrete time series data from an experiment, time series analysis and embeddings are needed. In application of all these methods, it is very important to establish symbolic dynamics. In many systems, short UPOs can be found directly and used to establish symbolic dynamics which gives an upper bound of the number of the UPOs with a given length and helps predict the location of the longer orbits. Ideally no orbit is missing or over-counting. The construction is always possible if a Poincaré map of the SIS is hyperbolic.

1.3 Turbulence:brief notes

1.3.1 Historical perspective

Turbulence has long been one of the natural phenomena which receive most attention of the humankind. From soft breezes to violent hurricane, from boiling water to tsunami, from colorful chemical oscillation to magnificent solar magnetic explosion, everywhere, turbulence is present and has great influence on our life. It is among the most studied subjects but still quite poorly understood because of its extremely rich and complicated behavior, even though the underlying natural laws are clear. Navier-Stokes equation, for example, is a sufficiently good model for the fluid motion in many cases, and is regarded as containing necessary ingredients to explain most turbulent behavior of fluids. But lack of mathematical tools prevents us from fully understanding the nature of its solutions.

With the accumulation of mathematical techniques and experimental facts, study on turbulence made steady progress, though somewhat slowly. Twilight shone from Kolmogorov's work in 1941 [146, 88], a classic in establishing phenomelogical models of turbulence. In addition to the Navier-Stokes equation, two universal assumptions were proposed to explain the experimentally observed two-thirds law and energy dissipation law. Landau questioned the universality and later proposed that turbulence is generated by sequence of Hopf bifurcations which activate infinitely many degrees of freedom with incommensurate frequencies [158]. Although the proposal was known to be incorrect later, Landau's emphasis on the investigation of the origin of turbulence is appreciated by many scientists.

After Lorenz's rediscovery of chaos in 1963, the stochastic motion in deterministic systems was recognized and studied. In 1971, Ruelle and Takens showed that quasi-periodic motion is not generic in general vector fields and the chaotic (strange) attractors occur more often than the high-dimensional tori. The argument was strong and thus made many people believe that chaotic dynamics is somehow closely related to the creation of turbulence. After that, different routes to turbulence were proposed and tested [88, 116, 48].

Experimentally, well-controlled fluid systems were devised and studied to check the various instabilities that lead to sequentially more complex motion. The discovery of coherent structures claimed the inadequacy of statistical description. Large-scale correlation is an significant part of turbulent motion in real fluids. Theoretically, models of various complexity are constructed and investigated in order to account for experimental observations and to extract essential elements of turbulence dynamics.

Nowadays, turbulence has become a general concept, familiar to many scientists in different areas. If a system possesses infinitely many degrees of freedom and the couplings between them are nonlinear, turbulence is likely to occur when control parameters cross certain critical values. Chemical turbulence, acoustic turbulence, optical turbulence and so on are named and studied, and new experimental techniques continue to be developed to test theoretical models and provide facts of turbulence. In extended systems, the study of turbulence is just as important as the study of regular motion due to its universality and genericity.

1.3.2 Main lines of approach

Kolmogorov's statistical model incorporates the symmetry consideration of the fluid system and is based on a multi-scale analysis: the average flow induces pulsations with largest size. Energy is transmitted to smaller and smaller scales in a hierarchical order via nonlinear interaction between modes of different scales. As a consequence, Small pulsations move in the background created by larger ones and have a smaller characteristic time. On the other hand, small scale motions induce extra dissipation and diffusion in an averaged way to the motion in large scales. The inspiration and the ideas contained in this model still influence current turbulence research [231, 89].

The ever improving experimental techniques keep revealing new quantitative features of turbulence which is a source of puzzles as well as inspirations. More subtle modeling is needed to give detailed description of turbulence and explain the observed experimental

facts, like various coherent structures. Recently Numerical simulations achieve considerable success as the digital computer acquires stunning computing power. It is possible to directly evolve Navier-Stokes equation and do various manipulations that cannot be done in an experiment. But physical insights and physical consideration are still needed to make sense of the numerical calculation.

On the other hand, the development of dynamical system theory opened the door for establishing rigorous tools for investigating turbulence. In a finite system, At the onset of spatiotemporal complexity, a series of low-dimensional bifurcations take place which destroy the symmetries of the system steadily [124]. With more and more modes aroused, the spatial structure of the system becomes more and more complicated until the system reaches the spatiotemporal chaotic regime where the dynamics can be roughly viewed as a replica of building blocks juxposed to pave the spatial stretch and all the symmetries are restored in a statistical sense.

Various reduction schemes are used in the dymcial systems approach. P. Holmes *et al.* noticed that the spatial interaction is local and try to build local models to account for the coherent structures [124]. From the consideration of different space time scales, much can be achieved through the construction of amplitude or phase equations [256, 45, 187, 152]. About half a century ago, E. Hopf remarked that the turbulence motion in a finite space region really concentrates on a finite-dimensional manifold in the infinite-dimensional phase space of an extended system [129]. To embrace the idea, the concept of inertial manild is proposed and applied as a extension of the center manifold. On this manifold, the original partial differential equation (PDE) is equivalent to a finite set of ordinary differential equations (ODE).

Most theoretical investigation is based on the NSe which is a sufficiently good model of real fluid turbulence. The NSe has a bunch of symmetries [88], including space and time translational invariance, reflection and scaling invariance. If any model of turbulence is proposed, these symmetries should in a way be accomodated. Except for possible external force, a fluid particle receives action from its neighbors only, which means the coupling term in the NSe has a local nature. All the couplings between fluid particles have the same functional form and are the source of turbulent motion. So, as a dynamical system the NSe has many specific features. Similar is true for most other spatially extended systems. Their solutions should therefore exhibit these internal features. The coherent structures observed in many experiments and numerical simulations are characteristic of solutions and should be explainable from the structures of equations of motion. We will consider the coherent structures both from their origin and from their roles in the formation of spatiotemporal chaos.

1.4 Periodic orbit theory on spatiotemporal chaos

Practically, if the existence of solutions of the NSe is taken for granted, convenient function spaces can be chosen, e.g., the set of smooth periodic functions are good for our investigations. With the chosen basis, the NSe converts to a countable set of coupled ODEs. The task is then to study to what extent the finite(low)-dimensional dynamical system theory,

can be applied to infinite-dimensional systems, and what happens during the transition to a turbulent state.

There is strong indication that a finite-dimensional phase space is enough to give rather complete description of the fluid dynamics. In either numerical simulations or experimental observations, every so often, we catch a glimse of familiar patterns in the ever-evolving turbulent systems. These patterns are the aforementioned coherent structures and more importantly the dynamics is recurrent like a walk through a finite set of spatial patterns. In analogy to low-dimensional chaotic system, the typical motion follows a UPO for a while and then another one, then the next...Mathematically, we always deal with a finite set of excited modes and the rest infinitely many modes are entrained by these active ones. In the presence of viscous dissipation, a typical phase point is often attracted to a strange set of very low dimension. For finite resolution, a finite number of periodic orbits are sufficient to approximate the strange set and the asymptotic dynamics in the whole phase space.

The primary goal of this thesis is to identify the coherent structures and investigate their dynamics from a periodic theory point of view. Analytically, we studied the first instability of the CGLe and proved the existence of modulated amplitude waves (MAWs) which constitute basic building blocks for later spatiotemporal dynamics. We analyzed the structure of steady solutions of the KSe, identified the most importane ones and emphasized their role in organing the phase space dynamics. Numerically, we devised a novel variational technique to locate all the short UPOs in a spatiotemporally chaotic system. Using the set of UPOs, we systematically reconstructed the strange set, deduced the symbolic dynamics and thus calculated statistical averages of various physical quantities. Though the strange set is usually nonhyperbolic, with infinite bifurcations taking place even for the slightest changes of parameter values, the coarse structure of the strange set changes continuously. It is well shadowed by the finite set of periodic orbits the study of which will shed light on the wake of turbulence.

Until now, work has been concentrating on the simplest models which exhibit spatiotemporal chaos, the complex Ginzburg-Landau equation (CGLe) and Kuramoto-Sivashinsky equation (KSe). As a starting try, all the calculation done here may well be view as preliminary, but the techniques and intuition developed will hopefully be extended to real world systems like the NSe, or other field equations.

CHAPTER II

PERIODIC ORBIT THEORY

The theme of the whole thesis is the periodic orbit theory applied to the study of spatiotemporal dynamics of extended systems. Even in low-dimensional dynamical systems, the theory is still under development although the main ingredients are ready. In this chapter, we will review the theory and point out open problems (obstacles in applications) in the end. After reviewing the basic properties and symbolic dynamics description of a dynamical system in sect. 2.1, we discuss the space and time averages and introduce operator formulation of invariant measures in sect. 2.2. In sect. 2.3, the main object in the periodic orbit theory - trace formula, spectral determinant, dynamical zeta functions are derived and their physical interpretation is given. The calculation of physical averages through cycle expansions is discussed in sect. 2.4. Finally, we point out the difficulties and open problems of the periodic orbit theory in sect. 2.5. A comprehensive presentation of the theory is given in [50].

2.1 Dynamical systems

A deterministic dynamical system maps a point in its phase space $\mathcal{M}$ to another point in a discrete (maps) or continous (flows) manner. In this dissertation, we restrict our attention to the dynamical systems with the phase space $\mathcal{M}$ being Euclidean, *i.e.*, $\mathcal{M} \subset \mathbb{R}^n\,, n \in \mathbb{N}$. Let $x \in \mathcal{M}$, then the phase space dynamics consists of a family of continuous mappings

$$f^t : x \to f^t(x)\,,\ t \in \mathcal{S}\,, \tag{1}$$

where $\mathcal{S} \subseteq \mathbb{N}$ or $\mathbb{R}$ is the domain of the evolution parameter t, satisfying: $(1) f^0(x) = x\,; (2) f^{t_2} \circ f^{t_1}(x) = f^{t_1+t_2}(x)\,, \forall t_1\,, t_2 > 0$. If these mappings are homeomorphisms, then they form a group; otherwise, a semigroup. An invariant set $V \subset \mathcal{M}$ is a set that satisfies $f^t(V) = V\,, \forall t$. An orbit is a subset of $\mathcal{M}$ defined as $\iota = \{f^t(x) \in \mathcal{M} : t \in \mathcal{S}\,,$ for any fixed $x \in \mathcal{M}\}$. An orbit is an invariant set and a general invariant set is a collection of orbits.

In chaotic dynamical systems, sensitive dependence on initial conditions precludes the long-time prediction of system behavior, and any open set on the SIS spreads over the whole SIS in finite time. If the dynamics takes place in a compact subset (the SIS) of the phase space, then there is an upper bound over distances between any two points on the SIS, so trajectories have to bend back and mix with each other. Local instability and global mixing creates very complex dynamics. For example, a (typical) point can visit neighborhood of any point infinitely many times. We say that the dynamics is topologically transitive. Specifically, a point can visit its own neighborhood arbitrarily often, which is the recurrence property proved first in Hamiltonian systems by Poincaré. It is natural to ask whether there are points whose orbit actually comes back to itself exactly and forms a periodic orbit. For

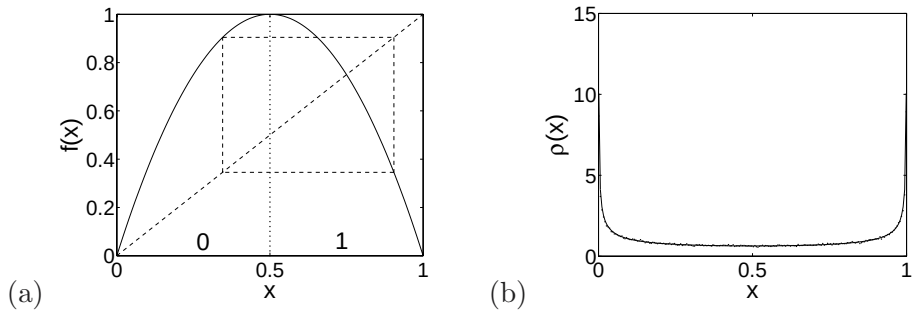

Figure 1: The Ulam map $f(x) = 4x(1-x)$ on the unit interval. (a) The graph of the map with its symbolic regions denoted by 0 and 1. (b) The invariant measure: analytic result is depicted by the solid line; numerical result by the dots.

a typical chaotic system, there are infinitely many such orbits (closing lemma [206]). They cover the SIS densely. A good knowledge of their properties reveals the system dynamics in a hierarchical way.

Though in a chaotic system, the asymptotic dynamics is complicated and unpredictable in the long run, symbolic dynamics is a good description at the global level which encodes all the possible orbits and their topological layout. It is an invariant characterization of the dynamics, independent of the underlying coordinate system. To build a symbolic dynamics, we partition the SIS into units and assign a symbol to each partitioning unit such that a trajectory is uniquely associated with a symbol sequence called itinerary according to the units it visited. A good partition insures that two different trajectories have distinct itineraries. It is possible that no trajectory corresponds to certain symbol sequence, and we then say that there exist pruning rules. A phase point corresponds to the itinerary of its trajectory and the dynamics is described by a shift of the symbols. Periodic orbits correspond to itineraries with repeating symbol blocks. This symbolic dynamics description of a chaotic system is extremely convenient and reveals much about the dynamics of the original system although it takes time and effort to find a good partition in a general dynamical system.

Consider the Ulam map

$$f(x) = 4x(1-x)\,,\ x \in [0,1]\,. \tag{2}$$

This is a quadratic map with the critical point sitting at $x = 0.5$. The non-wandering set is the whole unit interval and the symbolic dynamics of the system is a full shift on two symbols, say $\Sigma = \{0,1\}$, with 0 corresponding to the subinterval on the left and 1 to that on the right of the critical point $x = \frac{1}{2}$, respectively (see figure **??**). According to its itinerary, any orbit correponds uniquely to an infinite sequence $s_1 s_2 s_3 \cdots$, with $s_i \in \Sigma$, and vice versa. A periodic orbit is given by a periodic sequence. For example, the period two orbit in figure **??**(a) is described by the sequence $010101\cdots$, which may be denoted by $\overline{01}$. The *topological length* of this orbit is 2, as its symbol sequence is a repeat of two symbols. A prime cycle is a periodic orbit that can not be decomposed to shorter ones. For example, $\overline{0101}$ is not a prime cycle as it is a repeat of $\overline{01}$.

In applications, often instead of the detailed dynamics averages of physical quantities are the only thing we care about. Due to the vastly different time scales, our observation

or measurement is usually time average of the physical quantity under check. In gas dynamics, the pressure is just the average collision force exerted by the gas molecules on the container wall. In quantum mechanics, the only measurable quantities are the averages of observables. In fluid mechanics, a good many statistical quantities are used to characterize a turbulent flow. They are determined by the system control parameters and reproducible in observations. Usually, statistical models are proposed to explain the experimental observations. Though they capture ingradients of essential dynamics, their extra assumptions may severely restrict the applicability. In the following, we discuss how to use periodic orbits to do these calculations from first principles.

2.2 Physical averages in a dynamical system

2.2.1 Space, time averages and ergodicity

In classical or semiclassical mechanics, observables are (scalar, vector or tensor) functions $a(x)$ defined in $\mathcal{M}$. The integrated quantity $A^t(x_0)$ on an orbit segment is defined as

$$A^t(x_0) = \sum_{k=0}^{t} a(f^k(x_0))\,. \tag{3}$$

This limit may not exist for all $x_0 \in \mathcal{M}$, but it does exist for almost all x_0 as the distribution of orbits from these points approach a definite limit. For flows the summation is replaced by integration over time. The time average of the observable a along a trajectory is

$$\bar{a}(x_0) = \lim_{t\to\infty} \frac{1}{t} A^t(x_0)\,. \tag{4}$$

Specifically, on a periodic orbit p, we may define

$$A_p = A^{T_p}(x_0)\,,\ a_p = \frac{1}{T_p} A_p\,,$$

where T_p is the period of the periodic orbit. Notice that $A_p\,, a_p$ does not depend on the starting point x_0 on the periodic orbit. The space average of $a(x)$ on a ensemble of phase points is

$$\langle a(t)\rangle = \int_{\mathcal{M}} dx\, \omega(x) a(f^t(x))\,, \tag{5}$$

where $\omega(x)$ is the initial distribution of these phase points and normalized such that

$$\int_{\mathcal{M}} dx\, \omega(x) = 1\,.$$

If the dynamics is ergodic, then for almost all $x_0 \in \mathcal{M}$, $\bar{a}(x_0)$ exists and *equals* to a constant value (independent of x_0). This is easily understood from a symbolic dynamics point of view. Suppose that the phase space is partitioned into m regions and the dynamics is a full shift of m symbols. in each region the observable has a value, so A is determined by the number (frequency) of each symbol but not their order in the symbol sequence of a trajectory. The itineraries with the m symbols occuring almost equally frequently dominate, which means

that the corresponding phase points dominate and will have equal $\bar{a}$. To exclude the effect of the zero-measure bad set, we may take the space average of the time average and thus define the expectation value

$$\langle a \rangle = \lim_{t\to\infty} \frac{1}{t} \int_{\mathcal{M}} dx\, A^t(x)\,. \tag{6}$$

The space-time averaging is linear functional of the observale, since $\langle c_1 a + c_2 b\rangle = c_1\langle a\rangle + c_2\langle b\rangle$. If the system is ergodic [227, 73], there exists a measure $\rho(x)$ defined on $\mathcal{M}$ such that

$$\langle a \rangle = \int_{\mathcal{M}} dx\, \rho(x) a(x)\,. \tag{7}$$

In this way, the typical time average becomes a space average with a particular weight function $\rho(x)$. In a chaotic system, $\rho(x)$ is usually a non-differentiable function supported on a fractal set. The example given in figure 1 is an exceptional case where $\rho(x)$ is a smooth function defined on $(0,1)$,

$$\rho(x) = \frac{1}{\pi x\sqrt{1-x}}\,. \tag{8}$$

The profile of (8) is depicted in figure 1(b) in solid line. The dots in the graph represent the approximation of $\rho(x)$ obtained from numerical evolution of a typical phase point for 10^5 steps. From (8), it is easy to get the moments

$$\langle x^n \rangle = \frac{B(n+1/2,1/2)}{\pi} = \frac{(2n-1)!!}{2^n n!}\,,$$

where $B(n+1/2,1/2)$ is the Beta function. In particular, we get $\langle x\rangle = 1/2\,, \langle x^2\rangle = 3/8$.

Though the existence of $\rho(x)$ is easy to prove, its exact form is hard to obtain. Like in equilibrium statistical thermodynamics, we can conveniently define a generating functional such that all the statistical information of a particular dynamical variable is contained in it. Let's define

$$s(\beta) = \lim_{t\to\infty} \frac{1}{t} \ln\langle e^{\beta A^t}\rangle\,, \tag{9}$$

where β is an auxilliary variable and the ln is used to normalize the measure. The averaged quantity $\exp \beta A^t$ is multiplicative along an orbit, which is essential to the formulation below. Due to ergodicity, any smooth measure can be used in (9) to take the space average. For example, the uniform distribution will be used later. It is easy to see that

$$\begin{aligned} \langle a\rangle &= \lim_{t\to\infty}\frac{1}{t}\langle A^t\rangle = \left.\frac{\partial s}{\partial\beta}\right|_{\beta=0} \\ \langle a^2\rangle - \langle a\rangle^2 &= \lim_{t\to\infty}\frac{1}{t^2}(\langle A^t A^t\rangle - \langle A^t\rangle\langle A^t\rangle) = \left.\frac{\partial^2 s}{\partial\beta^2}\right|_{\beta=0}\,. \end{aligned} \tag{10}$$

Any moment of a is obtainable by taking derivatives of S.

2.2.2 Evolution operators and invariant measures

In the dynamical system (1), a time evolution operator $\mathcal{L}^t$ can be defined for continuous function $h(x)$ on $\mathcal{M}$,

$$\mathcal{L}^t \circ h(x) = \int_{\mathcal{M}} dy\, \delta(x - f^t(y)) e^{\beta A^t} h(y)\,. \tag{11}$$

Physically, the evolution can be viewed as a passive transport of some quantity $h(x)$ attached to each phase point. The function

$$\mathcal{L}^t(x,y) = \delta(x - f^t(y))e^{\beta A^t} \tag{12}$$

is called the kernel of the evolution operator $\mathcal{L}^t$. It depends on the integrated quantity A^t. The delta function collects points y which evolves to x in time t. The usual evolution operator depends only on the flow, for example, when $\beta = 0$, $\mathcal{L}^t(x,y)$ reduces to the familiar Frobenius-Perron kernel. Note that the evolution operator has semigroup property for a general flow, *i.e.*,

$$\mathcal{L}^{t_1} \circ \mathcal{L}^{t_2} \circ h(x) = \mathcal{L}^{t_1+t_2} \circ h(x)\,, t_1, t_2 \in \mathbb{R}^+\,.$$

If the original dynamics f^t is a diffeomorphism, then the above relation holds for any $t_1, t_2 \in \mathbb{R}$ and thus the set of operators $\mathcal{L}^t$ form an Abelian group.

In a closed system, the Frobenius-Perron operator $\mathcal{L}^t|_{\beta=0}$ does not change the average of the function $h(x)$, since

$$\int_{\mathcal{M}} dx\, \mathcal{L}^t|_{\beta=0} \circ h(x) = \int_{\mathcal{M}} dx \int_{\mathcal{M}} dy\, \delta(x - f^t(y))h(y) = \int_{\mathcal{M}} dy\, h(y)\,.$$

Furthermore, if the system is autonomous, for any smooth function $a(x)$, $\langle a \rangle$ is independent of time, so $\rho(x)$ is invariant in time,

$$\mathcal{L}^t|_{\beta=0} \circ \rho(x) = \rho(x)\,. \tag{13}$$

We call $\rho(x)$ an invariant measure of dynamical system (1). For the Ulam map, (13) becomes

$$\frac{\rho(\frac{1+\sqrt{1-x}}{2})}{4\sqrt{1-x}} + \frac{\rho(\frac{1-\sqrt{1-x}}{2})}{4\sqrt{1-x}} = \rho(x)\,.$$

It is a functional equation which can be used to determine $\rho(x)$ if it is unknown. In a chaotic system, infinitely many invariant measures can exist. For example, the delta measure defined on a compact invariant set is an invariant measure. $\rho(x)$ discussed above is the one most relevant to the dynamics. Any smooth distributions will evolve asymptotically to $\rho(x)$. If a typical phase point is evolved for a long time on the computer, the phase space density of the points on its trajectory is proportional to $\rho(x)$. In the following, we will analyze the invariant measure $\rho(x)$ in the neighborhood of any periodic orbit and use the trace formula to piece together the useful information. The ensuing spectral determinants and dynamical zeta functions then provide basis for fast-convergent calculations - cycle expansions.

2.3 Trace formula, spectral determinant and dynamical zeta function

2.3.1 Trace formula

In terms of the evolution operator, we may write

$$\langle e^{\beta A^t} \rangle = \langle \mathcal{L}^t \circ \mathcal{I}(x) \rangle\,,$$

where $\mathcal{I}(x) \equiv 1$ is the identity function. According to (6), we mainly care about the long (infinite) time behavior of $\mathcal{L}^t$. In view of the semi-group property and linearity of $\mathcal{L}^t$, it is clear that the asymptotic state is dominated by the eigenstate of the "differential" of $\mathcal{L}^t$ that has the maximum eigenvalue. Under quite general assumptions, we may take the ansatz (for flows)

$$\mathcal{L}^t = e^{t\mathcal{A}}\,,$$

where $\mathcal{A}$ is called the generator of the evolution operator $\mathcal{L}^t$ and is the "differential" just mentioned. It is a linear operator independent of t and its spectrum determines the property of $\mathcal{L}^t$. Why is it so? Let's suppose that the eigenvalues and the eigenfunction of $\mathcal{A}$ are ordered as following (assume no degeneracy exists),

$$\begin{array}{ccccccc} s_0 & , & s_1 & , & s_2 & , & \cdots \\ \phi_0 & , & \phi_1 & , & \phi_2 & , & \cdots \end{array}$$

where $Re(s_k) > Re(s_{k+1})$, such that $\mathcal{A} \circ \phi_k = s_k \phi_k$. If we expand the identity function $\mathcal{I}(x)$ in terms of the eigenfunctions

$$\mathcal{I} = \sum_k I_k \phi_k\,,$$

then

$$\langle e^{\beta\, A^t} \rangle = \langle \mathcal{L}^t \circ \mathcal{I} \rangle = \langle \sum_k I_K e^{t\, s_k} \phi_k \rangle\,. \tag{14}$$

So, $\langle e^{\beta\, A^t} \rangle \sim e^{t\, s_0}$, for $t \to \infty$. The average is dominated by the maximum eigenvalue in the large time limit. In the following, we will study how to extract the spectrum of $\mathcal{A}$ from the set of periodic orbits. We will derive the formula for maps and write out the formula for flows directly.

For maps, we may write $\mathcal{L} = \exp(\mathcal{A})$. The notation is consistent as $\mathcal{L} = \mathcal{L}^1$. In analogy to the matrix calculation, the spectrum of the linear operator $\mathcal{L}$ is determined by solving the determinant equation $\det(\mathbb{1} - z\mathcal{L}) = 0$. But how to compute the determinant of an operator? Note the following identity in the matrix algebra

$$\det(M) = \exp(\mathrm{tr} \ln M)\,, \tag{15}$$

where M is an arbitrary square matrix and tr takes the trace of a matrix. Using (15), we can write

$$\begin{aligned} \det(\mathbb{1} - z\mathcal{L}) &= \exp(\mathrm{tr} \ln(\mathbb{1} - z\mathcal{L})) \\ &= \exp(-\sum_{k=1}^{\infty} \frac{z^k}{k} \mathrm{tr}(\mathcal{L}^k))\,, \end{aligned} \tag{16}$$

where we have used the Taylor expansion of the logrithmic function. This determinant is called spectral determinant as its zeros give the spectrum of the operator. So, in order to get the spectrum of the operator $\mathcal{L}$, we only need to calculate the trace $\mathrm{tr}(\mathcal{L}^k))\,, \forall k \in \mathbb{N}$. If we know the spectrum $\{s_m\}_{m \in \mathbb{Z}^+}$ of $\mathcal{L}$, then the trace

$$\mathrm{tr}(\mathcal{L}^k) = \sum_m e^{k s^m} \sim e^{k s_0}\,, k \to \infty\,,$$

increases exponentially if s_0 is the largest eigenvalue of $\mathcal{L}$.

The trace of an operator is defined in analogy with the marix case as the sum of diagonal terms, *i.e.*,

$$\begin{aligned} \mathrm{tr}(\mathcal{L}^k) &= \int_{\mathcal{M}} dx \int_{\mathcal{M}} dz\, \delta(z-x) \int_{\mathcal{M}} dy\, \delta(z-f^k(y)) e^{\beta A^k} \delta(y-x) \\ &= \int_{\mathcal{M}} dx\ \delta(x-f^k(x)) e^{\beta A^k}\,. \end{aligned} \tag{17}$$

Here, delta functions are used as the basis functions to calculate the trace. Sometimes, *i.e.*, like in the intermittency case this is not well defined as we we will explain. We may now directly integrate the delta function to get the trace. Notice that every time $f^k(x) = x$, *i.e.*, x is a periodic point of period k, the delta function contributes a term. So, we write the trace as a summation over periodic points

$$\mathrm{tr}(\mathcal{L}^k) = \sum_{f^k(x_i)=x_i} \frac{e^{\beta A^k(x_i)}}{|\det\left(1-J_k(x_i)\right)|}\,, \tag{18}$$

where $J_k(x_i)$ is the Jacobian matrix of f^k evaluated at x_i. Notice that (18) only holds for hyperbolic periodic orbits. If a neutral direction exists for the Jacobian, then $|\det(1-J_k(x_i))| = 0$ and (18) has a zero denominator. This intermittency case even invalidates (17) since the delta function is not defined at degenerate zeros of function $x - f^k(x)$. With special care, the trace of the evolution operator is still computable but found to depend on powers of k. [10] We may now write the following generating functional for the trace

$$\begin{aligned} \mathrm{tr}\frac{z\mathcal{L}}{1-z\mathcal{L}} &= \sum_{k=1}^{\infty} z^k \mathrm{tr}(\mathcal{L}^k) \\ &= \sum_p n_p \sum_{r=1}^{\infty} z^{rn_p} \frac{e^{\beta A_p}}{|\det\left(1-J_p^r\right)|}\,, \end{aligned} \tag{19}$$

where the summation has been decomposed into summation over prime cycles p and their repeats. A_p, J_p are the integrated quantity and the Jacobian along the prime cycle p, and $A_p, \det(1-J_k(x_i))$ depend only on the cycle but not the starting point on the cycle. (19) may be viewed as a generating function for the trace $\mathrm{tr}(\mathcal{L}^k)$. The spectral determinant is now easily calculated to be

$$\det(\mathbb{1}-z\mathcal{L}) = \exp\left[-\sum_p \sum_{r=1}^{\infty} \frac{z^{rn_p}}{r} \frac{e^{\beta A_p}}{|\det\left(1-J_p^r\right)|}\right]. \tag{20}$$

The trace formula for flows is derived as [52]

$$\mathrm{tr}\mathcal{L}^t = \sum_p T_p \sum_{r=1}^{\infty} \frac{e^{r\beta\cdot A_p}}{|\det\left(1-J_p^r\right)|} \delta(t-rT_p)\,, \tag{21}$$

where T_p is the period of the period orbit p. Now we have a continuous family of operators. So, to obtain the corresponding generating function we have to use integration instead of summation,

$$\int_{0^+}^{\infty} dt\, e^{-st} \mathrm{tr}\mathcal{L}^t = \mathrm{tr}\frac{1}{s-\mathcal{A}} = \sum_p T_p \sum_{r=1}^{\infty} \frac{e^{r(\beta\cdot A_p - sT_p)}}{|\det\left(1-J_p^r\right)|}\,, \tag{22}$$

where J_p is the restriction on a transverse section of the monodromy matrix associated with the orbit p. The neutral direction along the cycle is excluded. In Appendix **??**, it is shown that the eigenvalues of J_p does not depend on the choice of the section. The spectral determinant is

$$F(s) = \det(s - \mathcal{A}) = \exp\left[-\sum_p \sum_{r=1}^{\infty} \frac{1}{r} \frac{e^{\beta \cdot A_p - sT_p}}{|\det(1 - J_p^r)|}\right] . \tag{23}$$

It is easy to check that

$$\mathrm{tr}\frac{1}{s-\mathcal{A}} = \frac{d}{ds} \ln\det(s-\mathcal{A}) = \frac{d}{ds} \ln F(s) .$$

Note that the spectral determinants for maps and flows are very similar. Under the substitution

$$z \to e^{-s} , \; n_p \to T_p$$

(20) becomes (23). In fact, in all the general expressions related to the spectral properties of the evolution operator, this substitution relates the map version to the flow version.

Very often, we are only interested in the leading eigenvalue of the evolution operator. In this case, only the dominant asymptotic behavior is of interest. If the flow is hyperbolic, a further simplification is possible,

$$\frac{1}{|\det(1 - J_p^r)|} \approx \frac{1}{|\Lambda_p|^r} , \tag{24}$$

where $\Lambda_p = \Pi_e \Lambda_{p,e}$ is a product of expanding eigenvalues $\{\Lambda_{p,e}\}_e$ of the matrix J_p. With $r \to \infty$, the relative difference between the two sides of (24) becomes exponentially small, and (20) leads to the dynamical zeta function

$$\frac{1}{\xi(z)} = \exp\left(-\sum_p \sum_{r=1}^{\infty} \frac{1}{r} t_p^r\right) = \prod_p (1 - t_p) , \tag{25}$$

where $t_p = z^{n_p} \exp(\beta A_p)/|\Lambda_p|$. In practice, the spectral determinant (20) has better convergence properties [50] and if we need more eigenvalues other than the leading one, the spectral determinant gives the correct result.

2.3.2 Geometrical interpretation

We now give an intuitive explanation to (25) from a geometrical point of view. Consider the set $\mathcal{P}_n = \{p_{i,n} : f^n(p_{i,n}) = p_{i,n}\}$ of fixed points of f^n and assume that there are m of them. The SIS in the phase space is partitioned by the neighborhoods $\{\mathcal{M}_{i,n}\}$ of these periodic points. For simplicity, suppose that each of the neighborhoods $\mathcal{M}_{i,n}$ expands to cover the whole SIS in a one-to-one manner under the map f^n. So, if $n \to \infty$, the size of each $\mathcal{M}_{i,n}$, denoted by $V(\mathcal{M}_{i,n})$ goes to zero exponentially. If n is large, then $V(\mathcal{M}_{i,n}) \propto 1/\Lambda_{i,n}$, where $\Lambda_{i,n}$ is the product of expanding eigenvalues of $Df^n(p_{i,n})$, and to a high accuracy f^n can be treated as linear in each $\mathcal{M}_{i,n}$. The SIS has each component $\mathcal{M}_{i,n}$ as a preimage, so f^n will map m different pieces to $\mathcal{M}_{i,n}, \forall i$, one piece from each $\mathcal{M}_{j,n}, j = 1, \cdots, m$.

Put a uniform density defined by $\mathcal{I}(x)$ on the SIS. After the action by f^n, we see that *mass* contained in $\mathcal{M}_{i,n}$ (the integral of $\mathcal{I}(x)$ over $\mathcal{M}_{i,n}$) is proportional to its size $V(\mathcal{M}_{i,n})$ because the mass contained in each of its m preimages is proportional to the size of the preimage in the corresponding $\mathcal{M}_{j,n}$. We know that $\mathcal{I}^n(x) = \mathcal{L}^n \circ \mathcal{I}(x)$ tends to the natural invariant measure $\rho(x)$ for large n, so

$$\begin{aligned} \langle a \rangle &= \int_{\mathcal{M}} dx\, \rho(x) a(x) \approx \int_{\mathcal{M}} dx\, \mathcal{I}^n(x) a(x) \\ &\approx C \sum_{i=1}^{m} \frac{a(x_i)}{\Lambda_{i,n}}, \end{aligned}$$

where C is a constant and $x_i \in \mathcal{M}_{i,n}$ is a representative point. The deviation comes from the non-uniform expansion of f^n and non-constancy of $a(x)$ inside each $\mathcal{M}_{i,n}$, which become vanishingly small when n is large. So, we may interpret (25) as the natural weight of each periodic point. The trace formula (18) is just a weighted summation over the linear neighborhood of all the periodic points. The weight is given by (24), and it is an invariant quantity determined by the dynamics f, independent of the choice of coordinate system.

2.3.3 Correlation functions

We know that the largest eigenvalue of the evolution operator dominates $s(\beta)$, thus determines the statistical properties of an observable. What is the physical significance of the rest eigenvalues? Below, we will see that they determine the correlation of two or more observables.

The *time correlation function* $C_{ab}(t)$ of two observables a and b along the trajectory $x(t) = f^t(x_0)$ is defined as

$$C_{ab}(t; x_0) = \lim_{T\to\infty} \frac{1}{T} \int_0^T d\tau a(x(\tau + t)) b(x(\tau)), \qquad x_0 = x(0). \tag{26}$$

If the system is ergodic [267], with invariant continuous measure $\rho(x)$, then correlation functions do not depend on x_0 (apart from a set of zero measure), and may be computed by a space average as well

$$C_{ab}(t) = \int_{\mathcal{M}} dx_0\, \rho(x_0) a(f^t(x_0)) b(x_0). \tag{27}$$

For a chaotic system we expect that time evolution will lose the information contained in the initial conditions, so that $C_{ab}(t)$ will approach the *uncorrelated* limit $\langle a \rangle \langle b \rangle$. As a matter of fact, the asymptotic decay of correlation functions

$$\hat{C}_{ab} := C_{ab} - \langle a \rangle \langle b \rangle \tag{28}$$

for any pair of observables coincides with the definition of *mixing*, a fundamental property in ergodic theory. We now assume $\langle b \rangle = 0$ (otherwise we may define a new observable by $b(x) - \langle b \rangle$). Our purpose is now to connect the asymptotic behavior of correlation functions with the spectrum of $\mathcal{L}$. We can write (27) as

$$C_{ab}(t) = \int_{\mathcal{M}} dx \int_{\mathcal{M}} dy\, a(y) b(x) \rho(x) \delta(y - f^t(x)),$$

and recover the evolution operator

$$C_{ab}(t) = \int_{\mathcal{M}} dx \int_{\mathcal{M}} dy\, a(y)\mathcal{L}^t(y,x)|_{\beta=0} b(x)\rho(x)$$

We showed that $\rho(x)$ is the eigenvector of $\mathcal{L}$ corresponding to probability conservation

$$\int_{\mathcal{M}} dy\, \mathcal{L}^t(x,y)\rho(y) = \rho(x)\,.$$

The corresponding leading eigenvalue is 0. Now, we can expand the x dependent part in terms of the eigenbasis of $\mathcal{L}$:

$$b(x)\rho(x) = \sum_{\alpha=0}^{\infty} c_\alpha \phi_\alpha(x),$$

where $\phi_0 = \rho(x)$. Let $\mathcal{L}^t(y,x)|_{\beta=0\,,t\to\infty}$ acts on both sides. The average of the left hand side is zero since the evolution operator does not change the average. The average of the right hand side is equal to c_0, since other eigenmodes decay exponentially during the evolution as their eigenvalues are smaller than zero. So $c_0 = 0$ and the action of $\mathcal{L}$ then can be written as

$$C_{ab}(t) = \sum_{m\neq 0} e^{s_m t} c_\alpha \int_{\mathcal{M}} dy\, a(y)\phi_k(y). \tag{29}$$

We see immediately that if the spectrum has a *gap*, that is the second largest leading eigenvalue is isolated from the largest eigenvalue ($s_0 = 0$) then (29) implies an *exponential* decay of correlations

$$C_{ab}(t) \sim e^{\nu t}.$$

The correlation decay rate $\nu = s_1$ then depends only on intrinsic properties of the dynamical system (the position of the next-to-leading eigenvalue of the Perron-Frobenius operator), while the choice of particular observables determines the prefactor.

Correlation functions are important because they are often accessible from time series measurable in laboratory experiments and numerical simulations: moreover they are linked to transport exponents.

2.4 Cycle expansions

The spectral determinant (20) and (23) or the dynamical zeta function (25) are just formal infinite product expressions, and a effective way to evaluate them has to be presented in practice. To achieve this goal, in this section the cycle expansion method will be introduced and discussed. It reexpresses the formal product in terms of a convergent sum over periodic orbits ordered with a hierarchical way with contributions from long cycles decaying rapidly.

It is easiest to illustrate the cycle expansion by the dynamical zeta function. Consider the dynamical zeta function for a system whose symbolic dynamics is a full shift on two symbols $\{0,1\}$:

$$\frac{1}{\xi(x)} = (1-t_0)(1-t_1)(1-t_{01})(1-t_{001})(1-t_{011})(1-t_{0001})(1-t_{0011})(1-t_{0111})\cdots\,.$$

Expanded into a sum over cycles of increasing total length this becomes:

$$\begin{aligned}\frac{1}{\xi(z)} &= 1 - t_0 - t_1 - t_{01} - t_{001} - t_{011} - \cdots \\ &\quad + t_0 t_1 + t_0 t_{01} + t_1 t_{01} + t_0 t_{001} + \cdots \\ &\quad - t_0 t_1 t_{01} - t_0 t_1 t_{001} - \cdots , \end{aligned} \tag{30}$$

where the products of t_*'s are called pseudocyles, *e.g.*, $t_0 t_1\,, t_0 t_1 t_{001}$ are pseudocycles. Such series representation of a dynamical zata function or spectral derterminant, expanded as a sum over pseudocycles and ordered by increasing cycle length and instability, is called *cycle expansion*. In a uniformly hyperbolic map like the Ulam map (quadratic map) or tent map (piecewise linear map), $|t_p|\rangle C/\Lambda^n$, where $C > 0$ and $\Lambda > 1$ are constants, and n is the length of the cycle. Let

$$F_1 = |t_0| + |t_1| + |t_{01}| + |t_{001}| + |t_{011}| + \cdots . \tag{31}$$

As the number of prime cycles of period n is less than $2^n/n$, the series in (31) converges and F_1 can be made to be smaller than 1 if z in t_p is chosen sufficiently small. It follows that

$$\left|\frac{1}{\xi(z)}\right| < 1 + F_1 + F_1^2 + F_1^3 + \cdots = \frac{1}{1 - F_1} . \tag{32}$$

From (32), we see that the dynamical zeta function $1/\xi(z)$ is well defined and is an analytic function of z for z sufficiently small. $1/\xi(z)$ may be extended to bigger domains in the complex plane by analytic continuation. This proof of convergence can be easily extended to general hyperbolic systems with more complex symbolic dynamics or higher phase space dimensions.

While we proved the convergence of (30), the summation scheme used in the proof is not the best. A better one is to regroup the terms into the dominant *fundamental* contributions t_f and the decreasing *curvature* corrections c_n:

$$\begin{aligned}\frac{1}{\xi(z)} &= 1 - t_0 - t_1 - [t_{01} - t_0 t_1] - [t_{001} - t_0 t_{01} + t_{011} - t_{01} t_1] - \cdots \\ &= 1 - \sum_f t_f - \sum_n c_n . \end{aligned} \tag{33}$$

We refer such regrouped series as *curvature expansion*. The fundamental contribution originates from the symbolic dynamics partition and reflects the qualitative dynamics of the system at the coarsest level. The curvature correction is due to the non-uniform expansion of the map. Longer cycles correspond to finer partitions of the phase space, and the curvature corrections are the difference between locally linear approximations of f^t in the coarse and the fine partitions. For example, the curvature term $[t_{01} - t_0 t_1]$ in (33) accounts for the difference of weights between the partitions of unit interval into two parts (centered around periodic points $p_0\,, p_1$) and into four parts (centered around $p_0\,, p_1\,, p_{01}\,, p_{10}$) [56]. For uniformly hyperbolic systems, the curvature corrections decay exponentially fast with the cycle length, with convergence controled by the second derivatives (curvatures) of f^t. In this case, we say that that the long cycles are *shadowed* by shorter ones. Shadowing is an important observation to justify the numerical calculation when the dynamics is chaotic [106, 102]. Here, shadowing between periodic orbits is an intrinsic property and reveals the existence

of the underlying hierarchical structure in the dynamical system. For the tent map (Eq. (**??**) in Chapter 3), the curvature corrections c_n are identically zero as its expansion rate is uniform everywhere.

If we write out (33) in a polynomial series of z, it is clear that the terms which have the same powers of z are grouped. Here z can be viewed as a kind of topological index, the powers of which indicate the topological length of cycles or psudocycles. By applying the same technique to the spectral determinant, we group terms of same powers of z in the cumulant expansion of the exponential in (20). In the flow case, we need to introduce some topological length (integers) to each cycle p. For example, the flow may be viewed as a map on some Poincaré section and we assign the topological length of a cycle in the map to its correspondent in the flow. Usually, this is simultaneously done with the symbolic dynamics established on the Poincaré section. One example is the 3-disk billiard [50], every collision of the billiard with a disk increases the topological length by one. Once the topological length of each cycle is known, we may encode this information to the spectral determinant (23) by adding an auxiliary variable z such that (23) becomes

$$F(s) = \exp\left[-\sum_p \sum_{r=1}^{\infty} \frac{1}{r} \frac{z^{rn_p} e^{r\beta A_p - sT_p}}{|\det\left(1 - J_p^r\right)|}\right], \tag{34}$$

where n_p is the topological length of the prime cycle p. The symbolic dynamics as well as the topological length assignment is no way unique. A good choice should exhibit maximal shadowing and thus lead to a fast convergence of the curvature expansion. After the curvature expansion is implemented, we may set $z = 1$ and solve $F(s) = 0$ for the eigenvalues s of the evolution operator.

2.4.1 Cycle formula for dynamical averages

In view of (14) and (9), we have

$$s(\beta) = s_0(\beta)\,,$$

where $s_0(\beta)$ is the largest eigenvalue of $\mathcal{L}$ (or $\mathcal{A}$ for the flow) and depends on the parameter β. Here we have assumed that $s_0(\beta)$ is seperated from other eigenvalues by a finite gap. In general, there is no analytic expression for $s(\beta)$, and all calculations have to be carried out numerically. Once we calculate $s_0(\beta)$, the corresponding dynamical averages are obtained through (10). The computation requires taking derivatives of $s_0(\beta)$ with respect to β, which inevitably lowers the accuracy of the calculation if numerical differentiation is used. Moreover several $s_0(\beta)$ values have to be calculated for different β's near $\beta = 0$.

Such numerical derivatives are not needed, as we can use the spectral determinant or dynamical zeta function directly to compute the derivatives. In both formulations, $s_0(\beta)$ satisfies equations of the form $G(\beta, s(\beta)) = 0$. The first and second derivative of $G(\beta, s(\beta)) = 0$ yields respectively

$$\frac{\partial s}{\partial \beta} = -\frac{\partial G/\partial \beta}{\partial G/\partial s} \tag{35}$$

$$\frac{\partial^2 s}{\partial \beta^2} = -\left[\frac{\partial^2 G}{\partial \beta^2} + 2\frac{\partial^2 G}{\partial \beta \partial s}\frac{\partial s}{\partial \beta} + \frac{\partial^2 G}{\partial s^2}\left(\frac{\partial s}{\partial \beta}\right)^2\right] \Big/ \frac{\partial G}{\partial s}\,, \tag{36}$$

where all the terms are evaluated at $s = s_0(\beta = 0)$. Note that all the quantities on the right hand side can be calculated directly through the spectral determinant or the dynamical zeta function. So, the accuracy of the evaluation is not lost and only $s_0(\beta = 0)$ has to be solved for.

2.5 Summary

One advantage of the periodic orbit theory is that all the eigenvalues of an evolution operator are obtained without explicitly constructing the singular eigenfunctions defined on a fractal set. Second, only short UPOs are needed for any finite precision calculation. Furthermore, UPOs and their stabilites are intrinsic properties of a dynamical system. They are independent of the representation coordinates, *i.e.*, invariant under smooth conjugacies [62]. We may choose the best representation that meets our needs. Third, if the chaotic system is uniformly hyperbolic, cycle expansions converge exponentially fast. If in addition a Markov partition [106] exists, the cycle expansion converges super-exponentially.

There are also many open problems in this periodic orbit approach. Establishing and controling the rate of convergence of cycle expansions remains the biggest problem. What is proven in literature is that cycle expansions are convergent if the nonlinear system is uniformly hyperbolic. Most physical systems we encounter are not uniformly hyperbolic, indeed they are almost never purely hyperbolic. Though cycle expansions are a useful tool in many cases, they fail (converge extremely slowly) on other occasions. The failure is mainly due to the bad shadowing of certain long cycles by the short ones. Some procedures have been proposed to improve the convergence, for example, a symbolic dynamics of infinite alphabet has been used in the $1 - d$ intermittent map [10], or special ordering is used to do the grouping and truncation [61]. The problem is far from solved. For example, we still do not know how to treat the intermittency in general high-dimensional systems, how to give correct weights to each component in a mixed phase space, or have trace formulas for invariant sets other than the perodic orbits, like the invariant tori.

Another problem is associated with the complexity of the phase space structure. In all cycle expansion calculations, the UPOs have to be classified and ordered in a hierarchical way, so the establishment of a symbolic dynamics is necessary. Unfortunately, only one- or two-dimensional maps can be treated fairly completely [50, 117]. Little has been done to deal with the high-dimensional case. For example, in the applications discussed in this thesis we never know whether all the periodic orbits up to some given length are found. Even one omitted short orbit could undermine the accuracy considerably [50]. The hope for which we offer some evidence in what follows, is that we may use UPOs and other invariant sets like equilibria or heteroclinic orbits to unfold the structure of the phase space level by level.

Except for a few exceptional cases, the theory requires efficient numerical determination of the shortest periodic orbits in a given nonlinear system. If the system is strongly chaotic or has a high-dimensional phase space, many existing methods either fail or are inefficient. Development of reliable and efficient numerical schemes for locating periodic orbits is a big challenge in the application of periodic orbit theory. In the next chapter, we will

introduce a new set of numerical methods for detecting UPOs, taylored to high (and infinite-) dimensional dynamical flows.

CHAPTER III

PERIODIC ORBITS AND HOW TO FIND THEM

In the previous chapter, we have emphasized the crucial role of UPOs in studying a dynamical system and suggested application of the periodic orbit theory to spatiotemporal chaos. The successful implementation of these ideas depends heavily on efficient numerical techniques for finding UPOs. Various methods have been developed to find UPOs in low-dimensional chaotic systems, either discrete or continous [50], while efficient methods are still called upon in high-dimensional systems. In this chapter, we will review common techniques and then introduce a novel variational scheme for finding periodic orbits. Finally, further developments of the method and some possible applications are proposed.

3.1 Review of known techniques for locating UPOs

In essence, any method for numerically finding periodic orbits is based on devising a new dynamical system which possesses the desired orbit as an attracting fixed point with a sizable basin of attraction. Beyond that, there is much freedom in constructing such systems. In the following, several techniques are briefly reviewed with their advantages and disadvantages being mentioned.

3.1.1 Inverse iteration and anti-integral limit method

The inverse iteration is most easily described in the $1-d$ map and can be generalized to higher-dimensional cases under certain cercumstances. The anti-integral limit method is closely related to the inverse iteration. Both of them enjoy direct and heuristic applications of symbolic dynamics.

To find a prime cycle with a given symbol sequence in the unimodal map, we read the symbol sequence backward, pick up a point in the subinterval corresponding to the last symbol, and then start the inverse iteration. A point has two preimages and only one of them is picked up according to the reversed symbol sequence. As $f(x)$ is expanding, the inverse iteration is contracting. The resulting orbit point will approach the desired periodic orbit exponentially fast since the discrepancy shrinks exponentially under the contractive inverse map.

In higher dimensions, maps or flows usually have both contracting and expanding directions. Inverse iteration does not apply directly. If in the contracting directions, the SIS is thin enough to be treated approximately as an zero-dimensional object - a finite set of points (actually a fractal set with a dimension between 0 and 1; by "thin", we mean that the dimension is close to 0), we are able to build a non-invertible expanding map by

projecting the original map onto the unstable manifolds and investigate the simplied model system. As there are only expanding directions now, inverse iteration may be invoked again to give periodic orbits of the model system. These orbits are often quite close to the true UPOs of the original system, and are profitably used as the starting guesses for other UPO determining methods. The anti-integral limit [11] is a good example in this direction [237].

In spirit, the anti-integrable limit is similar to the slaving function [245] for flows. Consider a smooth flow

$$\dot{x} = f(x, y)\,,\ \dot{y} = \frac{-y}{\epsilon} + g(x, y)\,, \tag{37}$$

where $x, f \in \mathbb{R}^d; y, g \in \mathbb{R}^m$, and ϵ is a small parameter. If we consider the motion in a bounded neighborhood $\mathcal{N}$ of the origin, in the limit $\epsilon \to 0$, we may set $y = 0$ due to the strong contraction term $-y/\epsilon$ in the second equation of (37). To the zeroth order in ϵ, $y = 0$ defines a slaving function of the motion, putting geometrical constraints on the asymptotic dynamics which is determined by the first equation of (37). When ϵ assumes a small but finite value, the motion is not strictly confined though very close to the slaving manifold. Hyperbolic motion on the manifold at $\epsilon = 0$ can easily be continued to motion at $\epsilon > 0$. Alternatively, we may multiply the second equation by ϵ and ignore the time evolution term on the left hand side due to the smallness of ϵ. The idea can be conveniently carried over to a continuous family of maps $x_{k+1} = f_\epsilon(x_k)$ with $x, f \in \mathbb{R}^d, \epsilon \in \mathbb{R}$, which can be written as

$$\epsilon f_1(x_{k+1}, x_k) + f_2(x_{k+1}, x_k) = 0.$$

In the anti-integrable limit $\epsilon \to 0$, we have the geometrical constraints $f_2(x_{k+1}, x_k) = 0$, rendering a new map hopefully less complex than the original one. In particular, when f_2 only involves x_k, the constraints $f_2(x_k) = 0$ give a countable (usually finite) collection of fixed points. If we assign a symbol to each of these points, the map reduces to arbitrary transitions among these points and can be conveniently described by a symbolic dynamics. Under quite general assumptions, the orbits, especially the UPOs, prescibed by the symbolic dynamics can be uniquely continued to the orbit for $\epsilon \neq 0$ [237].

We now see an example. Consider the circle map

$$x_{i+1} = x_i + \alpha + k \sin x_i\,, \tag{38}$$

which is equivalent to

$$\sin x_i - \epsilon(x_{i+1} - x_i - \alpha) = 0\,,$$

with $\epsilon = 1/k$. In the anti-integral limit, $\epsilon \to 0$, the dynamical system becomes implicit and defined by the equation

$$sinx_i = 0$$

which yields the points $x_i = m_i\pi\,, m_i \in \mathbb{Z}$. So the dynamics of (38) for large k is coded by an infinite sequence of symbols. On a circle, x_i is defined up to multiples of 2π, the symbol sequence reduces to two symbols. See [11] for more examples.

In both the anti-integrable limit or the inverse iteration, the deterministic nature of maps is lost as the current state cannot uniquely determine the future state. We need a symbol sequence to make the map uniquely defined. The current position in the expanding direction is determined by the future itinerary and in the contracting direction determined

by the past itinerary. Even the crudest description - the symbolic dynamics will determine the position accurately. So, the topology prescribed by the symbolic dynamics is robust and very constraining. In this sense, the symbolic dynamics and the stability eigenvalues give a detailed intrinsic description of the phase dynamics on the SIS and define an abstract dynamical object. How to embed this object to a specific phase space is a geometrical problem determined by the specific dynamical system.

3.1.2 Phase-space partition method and cyles from long time series

Very often, we have a long discrete time series extracted from either experimental measurements or numerical simulations on a chaotic system. To find embedded UPOs, we have to depend on near recurrences, having in mind the ergodic property of chaotic systems. We prefix a positive integer n as the period of the periodic orbits under search and start to compare all data pairs that are separated by $n-1$ intermediate points. If the data in a pair are close to each other, it is likely that they are close to a periodic orbit of period n. These pairs can be used as a starting point for further calculations. In this way, sets of periodic orbits and their stability eigenvalues can be calculated quite accurately [12].

When the phase space is known or reconstructed from time series, we may do a little bit better. One natural way to approximate the chaotic dynamics on a compact invariant set is to partition the phase space (or Poincaré section) into a set of controllable cells and study mappings among these cells. If a cell contains a fixed point, then it must map to itself. To reduce workload, a coarse partition is used at the beginning and the mappings of the cells are checked. Refinements are made only with those which contain themselves in their images. In ref. [122], linearized maps are used to approximate the nonlinear map near the lattice points and successive refinements locate the fixed points quite accurately.

The good part of this global searching method is that it only needs evaluation of the map on the lattice points, which avoids the usual time-consuming calculation of the Jacobian of the map. There are two disadvantages. If the phase space dimension is high, it requires a good many cells to cover the SIS and this may make the program very slow. Secondly, if a long cycle is under search, the linear region of the repeated map is so small that the partition has to be very fine to capture the essential dynamics, which of course could tremendously increase the computation load and lower numerical accuracy.

3.1.3 Shooting method

If we have a good guess of the position of one or more points on a periodic orbit, simple or multipoint shooting [238, 50] is a nice method to apply. They are variants of Newton's root-searching scheme and retain its quadratic convergence when the guess is close to a true solution.

Consider a map $f : \mathbb{R}^d \to \mathbb{R}^d$. We are trying to find one of its fixed points, say $\bar{x} : f(\bar{x}) = \bar{x}$, starting from the present guess x_k. Assume that x_k is close to $\bar{x}$, that is to say, $\bar{x} = x_k + \delta x_k$ with $|\delta x_k|$ small. From the fixed point condition, we have

$$x_k + \delta x_k = f(x_k + \delta x_k) \approx f(x_k) + \delta x_k \cdot \nabla f(x_k)\,.$$

Solving for δx_k and replacing x_k by $x_{k+1} = x_k + \delta x_k$ result in Newton-Raphson iteration,

$$x_{k+1} = x_k + (1 - \nabla f(x_k))^{-1} \cdot (f(x_k) - x_k)\,, \tag{39}$$

which is a widely employed method for finding roots of nonlinear equations.

Small modifications easily adapt the method to treating flows. Consider a flow $f^t : \mathbb{R} \times \mathbb{R}^d \to \mathbb{R}^d$. A Poincaré section $\mathcal{P} = \{x \in \mathbb{R}^d : a \cdot x = 0\}$, where $a \in \mathbb{R}^d$ is given, will produce a map out of the flow if orbits of the flow intersect $\mathcal{P}$ transversely. Fixed points on $\mathcal{P}$ are periodic orbits for the flow. Suppose that we have a guess of x_k on $\mathcal{P}$ and the return time t_k at a cycle $\bar{x} = x_k + \delta x_k$ with the return time $\bar{t} = t_k + \delta t_k$. From the periodicity condition and the assumption that $\delta x_k, \delta t_k$ are small, we have

$$\begin{aligned} x_k + \delta x_k &= f^{t_k + \delta t_k}(x_k + \delta x_k) \\ &\approx f^{t_k}(x_k) + \mathbb{J}_k \cdot \delta x_k + v_k \delta t_k\,, \end{aligned} \tag{40}$$

where

$$v_k = \frac{\partial f^{t_k}}{\partial t}(x_k)\,,\ J_k = \frac{\partial f^{t_k}}{\partial x}(x_k)\,.$$

In matrix form, we have

$$\begin{pmatrix} 1 - J_k & -v_k \\ a & 0 \end{pmatrix} \begin{pmatrix} \delta x_k \\ \delta t_k \end{pmatrix} = \begin{pmatrix} f^{t_k}(x_k) - x_k \end{pmatrix}\,, \tag{41}$$

where the last row keeps the coordinates on the Poincaré section. Solving (41) gives the corrections δx_k and δt_k. For very long or very unstable orbits, multipoint shooting replaces the simple shooting to make each of the shooting segments controllable, thus leading to a more stable numerical procedure [238].

Since the multipoint shooting only involves a local orbit segment, it is very adaptive. An example is associated with the development of automatic differentiation [104]. By applying the method, the local orbit segment is conveniently expressed in terms of polynomials of the time variable from the truncated Taylor series. For finding UPOs, a set of points are sprinkled along the initial guessed orbit positions. The polynomials give local solution curves through each point. Matching values of the polynomials and their derivatives at intermediate points leads to the location of true periodic orbits [107].

3.1.4 Variational and relaxation approach

If the equations of motion in a dynamical system are associated with a variational principle, extremization techniques can be invoked to produce periodic orbits. For example, in a classical mechanical system, with Lagrangian $\mathcal{L}(q, \dot{q}, t)$, where $q \in \mathbb{R}^d$, the equations of motion are determined by the action principle

$$\delta R[q] = \delta \int_{t_1}^{t_2} dt\, \mathcal{L}(q, \dot{q}, t) = 0\,. \tag{42}$$

Euler-Langrian equation is a consequence of (42) if the initial configuration at t_1 and the final configuration at t_2 are fixed. The action principle can also be used directly for searching periodic orbits. Creating a loop, a smooth closed curve $q(t)$ with $q(t+T) = q(t)$ as the initial guess and extremizing (42) leads to a periodic orbit. This can be done in either Fourier space (in view of the periodicity) or configuration space. The advantage of this approach is that cycles are produced with a given topology since the initial guess is not a point but a whole loop and the topological feature of the targeting cycle is very robust.

In Lagrangian maps, orbits can also be expressed as extrema of a variational principle. Periodic orbits are stationary points of a finite set of ODEs [147, 80, 249]. Even when the map is not area-preserving, sometimes it is still possible to find a variational principle for the orbits. For example, Biham and Wenzel [18] proposed a fictitious time τ "Hamiltonian"

$$H = \frac{1}{2}\Sigma_k\, b^{-k}\left(\frac{dx_k}{dt}\right)^2 + (-b)^{-k}\left[x_k(x_{k+1}-x_{k-1}) - (b^{-1}+1)\left(ax_k - \frac{1}{3}x_k^3\right)\right] \tag{43}$$

whose stationary points are orbits of the Hénon map

$$x_{k+1} = a - x_k^2 + by_k\,,\ y_{k+1} = x_k\,. \tag{44}$$

The fictitious time flow toward a guessed n-point cycle is governed by

$$\frac{dx_k}{dt} = s_k F_k\,,\ k = 1, \cdots, n\,, \tag{45}$$

where $F_k = (-b)^{-k}(b^{-1}+1)[-x_{k+1}+a-x_k^2+bx_{k-1}]$, $s_k = \pm 1$ and $x_{n+1} = x_1$. The stationary points of (45) correspond to the period n cycles of (44). If an equilibrium is stable, it attracts the corresponding cycle guess in its basin of attraction. In general, a stationary point can be an attractor, a repeller or a saddle point, and in Biham-Wenzel approach a stationary point of (45) is made stable with appropriate choice of prefactors s_k. Depending on the a, b values, almost all admissible periodic orbits up to some length are found if 2^n different choices of $\{s_k\}_{k=1}^n$ are tried. However, K. T. Hansen pointed out that the method fails to converge for some cycles [114]. In ref. [101], it is shown that the method might fail in two ways: the search ends up with a limit cycle of (45), or two different sequences of $\{s_k\}$ result in the same orbit. Later, in another paper [19], the authors extended the method to cycle search on the complex plane. There, all the 2^n cycles (including the complex ones) of length n are found.

The idea of changing stability of orbits was further pursued in refs. [60, 63, 201, 200, 221]. Suppose that we have a map $f : \mathbb{R}^d \to \mathbb{R}^d$. The fixed points are obtained by designing a new map

$$L_n :\ x_{k+1} = x_k + S_n[f(x_k) - x_k]\,, \tag{46}$$

where S_n is a constant invertible matrix. Fixed points of L_n are by construction also the fixed points of f. It is expected that by multiplying with an appropriate S_n the desired periodic orbit becomes stable for L_n, and with other choices of S_n's, L_n converges to other cycles. The advantage of the approach is that an explicit analytical expression for the map is not necessary. Problems of such approaches are similar to those mentioned above for the Biham-Wenzel's method for the Hénon map, and .

In sect. 3.2, we will devise a variational method for searching periodic orbits in a general flow. Our method combines the robustness of the relaxation approach with the fast

convergence of the Newton-Raphson method when the search is sufficiently close to a true UPO. The idea of our method is to make an informed rough guess of what the desired cycle looks like globally, and then use a variational method to drive the initial guess toward the exact solution. For robustness, we replace the guess of a single orbit point by a guess of an entire orbit. For numerical safety we replace the Newton-Raphson iteration by the "Newton descent", a differential flow that minimizes monotonically a cost function computed as deviation of the approximate flow from the true flow along a smooth loop approximation to a cycle.

3.2 The Newton descent method in loop space

The multipoint shooting method eliminates the long-time exponential instability of unstable orbits by splitting an orbit into a number of short segments, each with a controllable expansion rate. Combined with the Newton-Raphson root-seaching technique it is an efficient tool for locating periodic orbits of maps [37]. A search for periodic orbits of a continuous time flow can be reduced to a multiple shooting search for periodic orbits of a set of maps by constructing a set of phase space Poincaré sections such that an orbit leaving one section reaches the next one in a qualitatively predictable manner, without traversing other sections along the way. In turbulent, high-dimensional flows such sequences of sections are hard to come by. One solution might be a large set of Poincaré sections, with the intervening flight segments short and controllable.

Here we follow a different strategy, and discard Poincaré sections altogether; we replace maps between spatially fixed Poincaré sections, by maps induced by discretizing the time evolution into small time steps. For sufficiently small time steps such maps are small deformations of identity. We distribute many points along a smooth loop L, our initial guess of a cycle location and its topological layout. If both the time steps and the loop deformations are taken infinitesimal, a partial differential equation governs the "Newton descent", a fictitious time flow of a trial loop L into a genuine cycle p, with exponential convergence in the fictitious time variable. We then use methods developed for solving PDEs to get the solution.

In this section we derive the partial differential equation which governs the evolution of an initial guess loop toward a cycle and the corresponding cost function. An extension of the method to Hamiltonian systems and systems with higher time derivatives is presented in sect. 3.3. Simplifications due to symmetries and details of our numerical implementation of the method are discussed in sect. 3.4. In sect. 3.5 we test the method on the Hénon-Heiles system, the restricted three body problem, and a weakly turbulent Kuramoto-Sivashinsky system. We summarize our results and discuss possible improvements of the method in sect. 3.6.

3.2.1 A variational equation for the loop evolution

A periodic orbit is a solution (x, T), $x \in \mathbb{R}^d$, $T \in \mathbb{R}$ of the *periodic orbit condition*

$$f^T(x) = x\,, \qquad T > 0 \tag{47}$$

for a given flow or discrete time mapping $x \mapsto f^t(x)$. Our goal is to determine periodic orbits of flows defined by first order ODEs

$$\frac{dx}{dt} = v(x)\,, \qquad x \in \mathcal{M} \subset \mathbb{R}^d\,, \qquad (x,v) \in \mathbf{T}\mathcal{M} \tag{48}$$

in many (even infinitely many) dimensions d. Here $\mathcal{M}$ is the phase space (or state space) in which evolution takes place, $\mathbf{T}\mathcal{M}$ is the tangent bundle [8], and the vector field $v(x)$ is assumed to be smooth (sufficiently differentiable) almost everywhere.

We make our initial guess at the shape and the location of a cycle p by drawing a loop L, a smooth, differentiable closed curve $\tilde{x}(s) \in L \subset \mathcal{M}$, where s is a loop parameter. As the loop is periodic, we find it convenient to restrict s to $[0, 2\pi]$, with the periodic condition $\tilde{x}(s) = \tilde{x}(s + 2\pi)$. Assume that L is close to the true cycle p, pick N pairs of nearby points along the loop and along the cycle

$$\begin{aligned} \tilde{x}_n &= \tilde{x}(s_n)\,, \qquad 0 \le s_1 < \ldots < s_N < 2\pi\,, \\ x_n &= x(t_n)\,, \qquad 0 \le t_1 < \ldots < t_N < T_p\,, \end{aligned} \tag{49}$$

and denote by $\delta\tilde{x}_n$ the deviation of a point x_n on the periodic orbit p from the nearby point $\tilde{x}_n$,

$$x_n = \tilde{x}_n + \delta\tilde{x}_n\,.$$

The deviations $\delta\tilde{x}$ are assumed small, vanishing as L approaches p.

The orientation of the s-velocity vector tangent to the loop L

$$\tilde{v}(\tilde{x}) = \frac{d\tilde{x}}{ds}$$

is intrinsic to the loop, but its magnitude depends on the (still to be specified) parametrization s of the loop.

At each loop point $\tilde{x}_n \in L$ we thus have two vectors, the loop tangent $\tilde{v}_n = \tilde{v}(\tilde{x}_n)$ and the flow velocity $v_n = v(\tilde{x}_n)$. Our goal is to deform L until the directions of $\tilde{v}_n$ and v_n coincide for all $n = 1, \ldots, N$, $N \to \infty$, that is $L = p$. To match their magnitude, we introduce a local time scaling factor

$$\lambda(s_n) \equiv \Delta t_n / \Delta s_n\,, \tag{50}$$

where $\Delta s_n = s_{n+1} - s_n, n = 1, \ldots, N-1\,, \Delta s_N = 2\pi - (s_N - s_1)$, and likewise for Δt_n. The scaling factor $\lambda(s_n)$ ensures that the loop increment Δs_n is proportional to its counterpart $\Delta t_n + \delta t_n$ on the cycle when the loop L is close to the cycle p, with $\delta t_n \to 0$ as $L \to p$.

Let $x(t) = f^t(x)$ be the state of the system at time t obtained by integrating (48) with initial state x, and $\mathbf{J}(x,t) = dx(t)/dx$ be the corresponding Jacobian matrix obtained by integrating

$$\frac{d\mathbf{J}}{dt} = A\mathbf{J}\,, \quad A_{ij} = \frac{\partial v_i}{\partial x_j}\,, \qquad \text{with } \mathbf{J}(x,0) = \mathbb{1}\,. \tag{51}$$

Since the point $x_n = \tilde{x}_n + \delta\tilde{x}_n$ is on the cycle,

$$f^{\Delta t_n + \delta t_n}(\tilde{x}_n + \delta\tilde{x}_n) = \tilde{x}_{n+1} + \delta\tilde{x}_{n+1}\,. \tag{52}$$

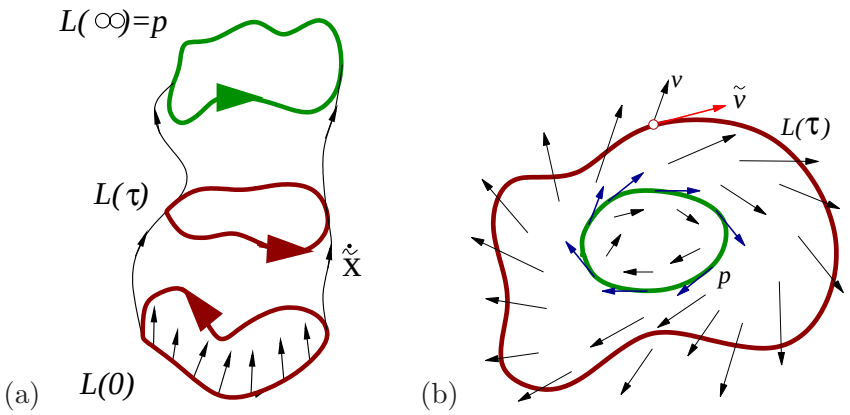

Figure 2: (a) An annulus $L(\tau)$ swept by the Newton descent flow $d\tilde{x}/d\tau$, connecting smoothly the initial loop $L(0)$ to the periodic orbit $p = L(\infty)$. (b) In general the loop velocity field $\tilde{v}(\tilde{x})$ does not coincide with $\lambda v(\tilde{x})$; for a periodic orbit p, it does so at every $x \in p$.

Linearization

$$f^{\delta t}(x) \approx x + v(x)\delta t\,, \qquad f^t(x+\delta x) \approx x(t) + \mathbf{J}(x,t)\delta x\,,$$

of (52) about the loop point $\tilde{x}_n$ and the time interval Δt_n to the next cycle point leads to the multiple shooting Newton-Raphson equation, for any step size Δt_n:

$$\delta\tilde{x}_{n+1} - \mathbf{J}(\tilde{x}_n, \Delta t_n)\delta\tilde{x}_n - v_{n+1}\delta t_n = f^{\Delta t_n}(\tilde{x}_n) - \tilde{x}_{n+1}\,. \tag{53}$$

Provided that the initial guess is sufficiently good, the Newton-Raphson iteration of (53) generates a sequence of loops L with a decreasing cost function [55]

$$F^2(\tilde{x}) \equiv \frac{N}{(2\pi)^2}\sum_{i=1}^{N}(f^{\Delta t_n}(\tilde{x}_n) - \tilde{x}_{n+1})^2, \qquad \tilde{x}_{N+1} = \tilde{x}_1\,. \tag{54}$$

The prefactor $N/(2\pi)^2$ makes the definition of F^2 consistent with (59) in the $N \to \infty$ limit. If the flow is locally strongly unstable, the neighborhood in which the linearization is valid could be so small that the full Newton step would overshoot, rendering F^2 bigger rather than smaller. In this case the step-reduced, damped Newton method is needed. As proved in ref. [142], under conditions satisfied here, F^2 decreases monotonically if appropriate step size is taken. If infinitesimal steps are taken, decrease of F^2 is ensured. We parametrize such continuous deformations of the loop by a *fictitious time* τ.

We fix Δs_n and proceed by $\delta\tau$ each step of the iteration, that is, multiply the right hand side of (53) by $\delta\tau$. According to (50), the change of Δt_n with respect to τ is equal to $\delta t_n = \frac{\partial\lambda}{\partial\tau}(s_n,\tau)\delta\tau\Delta s_n$. As $\delta\tilde{x}_n = \frac{\partial}{\partial\tau}\tilde{x}(s_n,\tau)\delta\tau$, dividing both sides of (53) by $\delta\tau$ yields

$$\frac{d\tilde{x}_{n+1}}{d\tau} - \mathbf{J}(\tilde{x}_n,\Delta t_n)\frac{d\tilde{x}_n}{d\tau} - v_{n+1}\frac{\partial\lambda}{\partial\tau}(s_n,\tau)\Delta s_n = f^{\Delta t_n}(\tilde{x}_n) - \tilde{x}_{n+1}\,. \tag{55}$$

In the $N \to \infty$ limit, the step sizes $\Delta s_n, \Delta t_n = O(1/N) \to 0$, and we have

$$\begin{aligned} v_{n+1} &\approx v_n\,, & \tilde{x}_{n+1} &\approx \tilde{x}_n + \tilde{v}_n\Delta s_n\,,\\ \mathbf{J}(\tilde{x}_n,\Delta t_n) &\approx 1 + A(\tilde{x}_n)\Delta t_n\,, & f^{\Delta t_n}(\tilde{x}_n) &\approx \tilde{x}_n + v_n\Delta t_n\,. \end{aligned}$$

Substituting into (55) and using the scaling relation (50), we obtain

$$\frac{\partial^2 \tilde{x}}{\partial s \partial \tau} - \lambda A \frac{\partial \tilde{x}}{\partial \tau} - v \frac{\partial \lambda}{\partial \tau} = \lambda v - \tilde{v}. \tag{56}$$

This PDE, which describes the evolution of a loop $L(\tau)$ toward a periodic orbit p, is our central result. The family of loops so generated is parametrized by $\tilde{x} = \tilde{x}(s,\tau) \in L(\tau)$, where s denotes the position along the loop, and the fictitious time τ parametrizes the deformation of the loop, see figure 2(a). We refer to this infinitesimal step version of the damped Newton-Raphson method as the "Newton descent".

The important feature of this equation is that a decreasing cost functional exists. Rewriting (56) as

$$\frac{\partial}{\partial \tau}(\tilde{v} - \lambda v) = -(\tilde{v} - \lambda v)\,, \tag{57}$$

we have

$$\tilde{v} - \lambda v = e^{-\tau}(\tilde{v} - \lambda v)|_{\tau=0}\,, \tag{58}$$

so the fictitious time τ flow decreases the cost functional

$$F^2[\tilde{x}] = \frac{1}{2\pi} \oint_{L(\tau)} ds\ (\tilde{v}(\tilde{x}) - \lambda v(\tilde{x}))^2 \tag{59}$$

monotonically as the loop evolves toward the cycle.

At each iteration step the differences of the loop tangent velocities and the dynamical flow velocities are reduced by the Newton descent. As $\tau \to \infty$, the fictitious time flow aligns the loop tangent $\tilde{v}$ with the dynamical flow vector $\tilde{v} = \lambda v$, and the loop $\tilde{x}(s,\tau) \in L(\tau)$, see figure 2(b), converges to a genuine periodic orbit $p = L(\infty)$ of the dynamical flow $\dot{x} = v(x)$. Once the cycle p is reached, by (50), $\lambda(s,\infty) = \frac{dt}{ds}(\tilde{x}(s,\infty))$, and the cycle period is given by

$$T_p = \int_0^{2\pi} \lambda(\tilde{x}(s,\infty)) ds\,.$$

Of course, as at this stage we have already identified the cycle, we may pick instead an initial point on p and calculate the period by a direct integration of the dynamical equations (48).

3.2.2 Marginal directions and accumulation of loop points

Numerically, two perils lurk in a direct implementation of the Newton descent (56).

First, when a cycle is reached, it remains a cycle under a cyclic permutation of the representative points, so on the cycle the operator

$$\bar{A} = \frac{\partial}{\partial s} - \lambda A$$

has a marginal eigenvector $v(\tilde{x}(s))$ with eigenvalue 0. If λ is fixed, as the loop approaches the cycle, (56) approaches its limit

$$\bar{A}\,\frac{\partial x}{\partial \tau} = 0\,.$$

Therefore, on the cycle, the operator $\bar{A}^{-1}$ becomes singular and the numerical woes arise.

The second potential peril hides in the freedom of choosing the loop (re-)parametrization. Since s is related to the time t by the yet unspecified factor $\lambda(s,\tau)$, uneven distributions of the sampling points over the loop L could arise, with the numerical discretization points $\tilde{x}_n$ clumping densely along some segments of L and leaving big gaps elsewhere, thus degrading the numerical smoothness of the loop.

We remedy these difficulties by imposing constraints on (56). In our calculation for Kuramoto-Sivashinsky system of sect. 3.5, the first difficulty is dealt with by introducing one Poincaré section, for example, by fixing one coordinate of one of the sampling points, $\tilde{x}_1(s_2,\tau) = const$. This breaks the translational invariance along the cycle. Other types of constraints might be better suited to a specific problem at hand. For example, we can demand that the average displacement of the sampling points along the loop vanishes, thus avoiding a spiraling descent toward the desired cycle.

We deal with the second potential difficulty by choosing a particularly simple loop parametrization. So far, the parametrization s is arbitrary and there is much freedom in choosing the best one for our purposes. We pick $s-$independent constant scaling $\lambda(s,\tau) = \lambda(\tau)$. With uniform grid size $\Delta s_n = \Delta s$ and fixed λ (in s), the loop parameter $s = t/\lambda$ is proportional to time t, and the discretization (56) distributes the sampling points along the loop evenly in time. As the loop approaches a cycle, $\frac{\partial \tilde{x}}{\partial \tau}$ is numerically obtainable from (56), and on the cycle the period is given by $T_p = 2\pi\lambda$.

Even though here we concentrate on searching for periodic orbits, the Newton descent is a general method. With appropriate modifications of boundary conditions and scaling of time, (56) can be adapted to determination of homoclinic or heteroclinic orbits between equilibrium points or periodic orbits of a flow, or more general boundary value problems. Applied to 2-point boundary value problems, Newton descent is similar to the quasilinearization [238] but has the advantage that the free parameters $\lambda(s,\tau)$ are available for adjusting scales in the problem and that searches can be restricted to phase space submanifolds of interest. A simple example of a restriction to a submanifold are searches for cycles of a given energy, constrained to the $H(q,p) = E$ energy shell in the phase space of a Hamiltonian system. Furthermore, as we shall show now, the symplectic structure of Hamilton's equations greatly reduces the dimensionality of the submanifold that we need to consider.

3.3 Extensions of Newton descent

As mentioned above, in classical mechanics particle trajectories are also solutions of a variational principle, the Hamilton's variational principle. For example, variational methods are the key ingredient of the Aubry-Mather theory of area-preserving twist maps, discrete-time Hamiltonian dynamical systems particularly suited to explorations of the K.A.M. theorem. Proofs of the Aubry-Mather theorem [170] on existence of quasi-periodic solutions are variational. It was quickly realized that the variational methods can also yield reliable, high precision computations of long periodic orbits of twist map models in 2 or more dimensions, needed for K.A.M. renormalization studies [148].

A fictitious time gradient flow for orbits of mappings, similar to the one discussed in ref. [55], was introduced by Anegent [2] for twist maps, and used by Gole [98] in his proof of the Aubry-Mather theorem. Mathematical bounds on the regions of stability of K.A.M. tori are notoriously restrictive compared to the numerical indications, and de la Llave, Falcolini and Tompaidis [80, 249] have found the gradient flow formulation advantageous both in studies of the analyticity domains of the K.A.M. stability, as well as proving the Aubry-Mather theorem for extended systems.

As far as we know, all numerical applications so far have been to low-dimensional Hamiltonian maps, not to continuous time flows. Instead of attempting to implement the least-action variational principle as loop dynamics in a fictitious time, here we shall implement our Newton descent as a flow that again minimizes a cost function, this time one that penalizes misalignment of accelerations, the true one and the one computed on the loop approximation to a cycle. We discuss the merits of the two kinds of variational principles in Appendix B.

To motivate what follows on level of everyday intuition, consider how the least action periodic orbit search works for a billiard: Connect points by a rubber band with a desired topology, and then move the points along the billiard walls until the length (that is, the action) of the rubber band is extremal (maximal or minimal under infinitesimal changes of the boundary points). Note that the extremization of action requires only D configuration coordinate variations, not the full $2D$-dimensional phase space variations.

Can we exploit this property of the Newtonian mechanics to reduce the dimensionality of our variational calculations? The answer is yes, and easiest to understand in terms of the Hamilton's variational principle which states that classical trajectories are extrema of the Hamilton's principal function (or, for fixed energy E, the action $S = R + Et$)

$$R(q_1, t_1; q_0, t_0) = \int_{t_0}^{t_1} dt\, \mathcal{L}(q(t), \dot{q}(t), t)\,,$$

where $\mathcal{L}(q, \dot{q}, t)$ is the Lagrangian. Given a loop $L(\tau)$ we can compute not only the tangent "velocity" vector $\tilde{v}$, but also the local loop curvature or "acceleration" vector

$$\tilde{a} = \frac{\partial^2 \tilde{x}}{\partial s^2}\,,$$

and indeed, as many s derivatives as needed. Matching the dynamical acceleration $a(\tilde{x})$ (assumed to be functions of $\tilde{x}$ and $v(\tilde{x})$) with the loop "acceleration" $\tilde{a}(\tilde{x})$ results in a new cost function and the corresponding PDE (57) for the evolution of the loop

$$\frac{\partial}{\partial \tau}(\tilde{a} - \lambda^2 a) = -(\tilde{a} - \lambda^2 a)\,.$$

We use λ^2 instead of λ in order to keep the notation consistent with (50), that is $t = \lambda\, s$. Expressed in terms of the loop variables $\tilde{x}(s)$, the above equation becomes

$$\frac{\partial^3 \tilde{x}}{\partial^2 s \partial \tau} - \lambda \frac{\partial a}{\partial v}\frac{\partial^2 \tilde{x}}{\partial s \partial \tau} - \lambda^2 \frac{\partial a}{\partial \tilde{x}}\frac{\partial \tilde{x}}{\partial \tau} + \left(\frac{\partial a}{\partial v}\frac{\partial \tilde{x}}{\partial s} - 2\lambda a\right)\frac{\partial \lambda}{\partial \tau} = \lambda^2 a - \tilde{a}\,, \tag{60}$$

where $v = \frac{\partial \tilde{x}}{\lambda \partial s}$. Although (60) looks more complicated than (56), in numerical fictitious time integrations, we are rewarded by having to keep only half of the phase space variables.

More generally, if a differential equation has the form:

$$x^{(m)} = f(x, x^{(1)}, \cdots, x^{(m-1)}) , \tag{61}$$

where $x^{(k)} = \frac{d^k x}{dt^k}$, $k = 1, \cdots, m$ and $x \in \mathbb{R}^d$, the same technique can be used to match the highest derivatives $\lambda^m x^{(m)}$ and $\tilde{x}^{(m)}$,

$$\frac{\partial}{\partial \tau}(\tilde{x}^{(m)} - \lambda^m x^{(m)}) = -(\tilde{x}^{(m)} - \lambda^m x^{(m)}) ,$$

with $\tilde{x}^{(m)} = \frac{\partial^m}{\partial s^m}\tilde{x}(s)$ calculated directly from $\tilde{x}(s)$ on the loop by differentiation. In loop variables $\tilde{x}(s)$ we have,

$$\begin{aligned} \frac{\partial^{m+1}\tilde{x}}{\partial s^m \partial \tau} - \lambda^m \sum_{k=0}^{m} \frac{\partial f}{\partial x^{(k)}} \cdot \frac{\partial}{\partial \tau} \frac{\partial^k \tilde{x}}{\lambda^k \partial s^k} - m\lambda^{m-1}\tilde{x}^{(m)} \frac{\partial \lambda}{\partial \tau} \\ = \lambda^m x^{(m)} - \tilde{x}^{(m)} , \end{aligned} \tag{62}$$

where $x^{(0)} = x$ and $x^{(k)} = \frac{\partial^k \tilde{x}}{\lambda^k \partial^k s}$, $k = 1, \cdots, m-1$ are assumed. Conventionally, (61) is converted to a system of md first order differential equations, whose discretized derivative (see (63) below) are banded matrices with band width of $5md$. Using (62), we only need d equations and for the same accuracy the corresponding band width is $(m+4)d$. The computing load has been greatly reduced, the more so the larger m is. Nevertheless, choice of a good initial loop guess and visualization of the dynamics are always aided by a plot of the orbit in the full md-dimensional phase space, where loops cannot self-intersect and topological features of the flow are exhibited more clearly.

3.4 Implementation of Newton descent

As the loop points satisfy a periodic boundary condition, it is natural to employ truncated discrete Fast Fourier Transforms (FFT) in numerical integrations of (56). Since we are interested only in the final, stationary cycle p, the accuracy of the fictitious time integration is not crucial; all we have to ensure is the smoothness of the loop throughout the integration. The Euler integration with fairly large fictitious time steps $\delta\tau$ suffices. The computationally most onerous step in implementation of the Newton descent is the inversion of the large matrix $\bar{A}$ in (56). When the dimension of the dynamical phase space of (48) is high, the inversion of $\bar{A}$ needed to get $\frac{\partial \tilde{x}}{\partial \tau}$ takes most of the integration time, making the evolution extremely slow. This problem is partially solved if the finite difference methods are used. The large matrix $\bar{A}$ then becomes sparse and the inversion can be done far more quickly.

3.4.1 Numerical implementation

In a discretization of a loop, numerical stability requires accurate discretization of loop derivatives such as

$$\tilde{v}_n \equiv \left.\frac{\partial \tilde{x}}{\partial s}\right|_{\tilde{x}=\tilde{x}(s_n)} \approx (\hat{D}\tilde{x})_n .$$

In our numerical work we use the four-point approximation [24],

$$\hat{D} = \frac{1}{12h} \begin{pmatrix} 0 & 8 & -1 & & & & & & 1 & -8 \\ -8 & 0 & 8 & -1 & & & & & & 1 \\ 1 & -8 & 0 & 8 & -1 & & & & & \\ & & & & & \cdots & & & & \\ & & & & & & 1 & -8 & 0 & 8 & -1 \\ -1 & & & & & & & 1 & -8 & 0 & 8 \\ 8 & -1 & & & & & & & 1 & -8 & 0 \end{pmatrix} \tag{63}$$

where $h = 2\pi/N$. Here, each entry represents a $[d\times d]$ matrix, $8 \to 8\mathbb{1}$, *etc.*, with blank spaces filled with zeros. The two $[2d\times 2d]$ matrices

$$M_1 = \begin{pmatrix} \mathbb{1} & -8\mathbb{1} \\ 0 & \mathbb{1} \end{pmatrix}, \qquad M_2 = \begin{pmatrix} -\mathbb{1} & 0 \\ 8\mathbb{1} & -\mathbb{1} \end{pmatrix},$$

located at the top-right and bottom-left corners take care of the periodic boundary condition.

The discretized version of (56) with a fictitious time Euler step $\delta\tau$ is

$$\begin{pmatrix} \hat{A} & -\hat{v} \\ \hat{a} & 0 \end{pmatrix} \begin{pmatrix} \delta\hat{x} \\ \delta\lambda \end{pmatrix} = \delta\tau \begin{pmatrix} \lambda\hat{v} - \hat{\tilde{v}} \\ 0 \end{pmatrix}, \tag{64}$$

where

$$\hat{A} \;=\; \hat{D} - \lambda\, \mathrm{diag}[A_1, A_2, \cdots, A_N]\,,$$

with $A_n = A(\tilde{x}(s_n))$ defined in (51), and

$$\begin{aligned} \hat{v} &= (v_1, v_2, \cdots, v_N)^t\,, \qquad \text{with } v_n = v(\tilde{x}(s_n))\,, \\ \hat{\tilde{v}} &= (\tilde{v}_1, \tilde{v}_2, \cdots, \tilde{v}_N)^t\,, \qquad \text{with } \tilde{v}_n = \tilde{v}(\tilde{x}(s_n))\,, \end{aligned}$$

are the two column vectors that we want to match during the evolution of the loop. $\hat{a}$ is an Nd dimensional row vector which imposes the constraint on the coordinate variations $\delta\hat{x} = (\delta\tilde{x}_1, \delta\tilde{x}_2, \cdots, \delta\tilde{x}_N)$. The discretized Newton descent (64) is an infinitesimal time step variant of the multipoint (Poincaré section) shooting equation for flows(53). In formulating a variational method for periodic orbit searches in a 3-d generalized standard map, Tompaidis [249] also derived an expression similar to (64). In order to solve for the deformation of the loop coordinates and period, $\delta\hat{x}$ and $\delta\lambda$, we need to invert the $[(N\,d+1)\times(N\,d+1)]$ matrix on the left hand side of (64).

In our numerical work, this matrix is inverted using the banded LU decomposition on the embedded band-diagonal matrix, and the Woodbury formula [205] on the cyclic and border terms. The LU decomposition takes most of the computation time and considerably slows down the fictitious time integration. We speed up the integration by a new inversion scheme which relies on the smoothness of the flow in the loop space. It goes as follows. Once we have the LU decomposition at one step, we use it to approximately invert the matrix in the next step, with accurate inversion achieved by the iterative approximate inversions [205]. In our applications we find that a single LU decomposition can be used for many $\delta\tau$ evolution steps. The further we go, the more iterations at each step are needed to implement the

inversion. After the number of such iterations exceeds some given fixed maximum number, we perform another LU decomposition and proceed as before. The number of integration steps following one decomposition is an indication of the smoothness of the evolution, and we adjust accordingly the integration step size $\delta\tau$: the greater the number, the bigger the step size. As the loop approaches a cycle, the evolution becomes so smooth that the step size can be brought all the way up to $\delta\tau = 1$, the full undamped Newton-Raphson iteration step. In practice, one can start with a small but reasonable number of points, in order to get a coarse solution of relatively low accuracy. After achieving that, the refined guess loop can be constructed by interpolating more points, and can be processed with a more accurate calculation in which $\delta\tau$ can be set as large as the full Newton step $\delta\tau = 1$, recovering the rapid quadratic convergence of the Newton-Raphson method.

It is essential that the smoothness of the loop is maintained throughout the calculation. We monitor the smoothness by checking the Fourier spectrum of $\tilde{x}(\cdot, \tau)$. An unstable difference scheme for loop derivatives might lead to unbounded sawtooth oscillations [248]. An empirical local linear stability analysis (described in [212]) indicates that our scheme is stable, and that the high frequency components do not generate instabilities.

3.4.2 Initialization and convergence

As in any other method, a qualitative understanding of the dynamics is a prerequisite to successful cycle searches. We start by numerical integration with the dynamical system (48). Numerical experiments reveal regions where a trajectory spends most of its life, giving us the first hunch as to how to initialize a loop. We take the FFT of some nearly recurred orbit segment and keep only the lowest frequency components. The inverse Fourier transform back to the phase space yields a smooth loop that we use as our initial guess. Since any generic orbit segment is not closed and might exhibit large gaps, the Gibbs phenomenon can take the initial loop so constructed quite far away from the region of interest. We deal with this problem by manually deforming the orbit segment into a closed loop before performing the FFT. Searching for longer cycles with multiple circuits requires more delicate initial conditions. The hope is that a few short cycles can help us establish an approximate symbolic dynamics, and guess for longer cycles can be constructed by cutting and gluing the short, known ones. For low dimensional systems, such methods yield quite good systematic initial guesses for longer cycles [36].

An alternative way to initialize the search is by utilizing adiabatic deformations of dynamics, or the homotopy evolution [42]. If the dynamical system (48) depends on a parameter μ, short cycles might survive as μ varies passing through a family of dynamical systems, giving in the process birth to new cycles through sequences of bifurcations. Most short unstable cycles vary little for small changes of μ. So, a cycle existing for parameter value μ_1 can be chosen as the initial trial loop for a nearby cycle surviving a small change $\mu_1 \to \mu_2$. In practice, one or two iterations often suffice to find the new cycle.

A good choice of the initial loop significantly expedites the computation, but there are more reasons why good initial loops are crucial. First of all, if we break the translational invariance by imposing a constraint such as $\tilde{x}_1(s_2, \tau) = c$, we have to make sure that both the initial loop and the desired cycle intersects this Poincaré plane. Hence, the initial

loop cannot be wildly different from the desired cycle. Second, in view of (58), the loop always evolves toward a local minimum of the cost functional (59), with discretization points moving along the $\tilde{v} - \lambda v$ fixed direction, determined by the initial condition. If the local minimum corresponds to a zero of the cost functional, we obtain a true cycle of the dynamical flow (48). However, if the value of cost functional is not equal to zero at the minimum while the gradient is zero, (64) yields a singular matrix $\hat{A}$. In such cases the search has to be abandoned and restarted with a new initial loop guess. In the periodic orbit searches of sect. 3.5 starting with blind initial guesses (guesses unaided by a symbolic dynamics partition), such local minima were encountered in about 30% of cases.

3.4.3 Symmetry considerations

The system under consideration often possesses certain symmetries. If this is the case, the symmetry should be both be feared for possible marginal eigendirections, and be embraced as a guide to potential simplifications of the numerical calculation.

If the dynamical system equations (48) are invariant under a discrete symmetry, the concept of fundamental domain [53, 50] can be utilized to reduce the length of the initial loop when searching for a cycle of a given symmetry. In this case, we need to discretize only an irreducible segment of the loop, decreasing significantly the dimensionality of the loop representation. Other parts of the loop are replicated by symmetry operations, with the full loop tiled by copies of the fundamental domain segment. The boundary conditions are no longer periodic, but all that we need to do is modify the cyclic terms. Instead of using M_1 and M_2 in (63), we use $M_1 Q$ and $M_2 Q^{-1}$, where Q is the relevant symmetry operation that maps the fundamental segment to the neighbor that precedes it. In this way, a fraction of the points represent the cycle with the same accuracy, speeding up the search considerably.

If a continuous symmetry is present, it may complicate the situation at first glance but becomes something that we can take advantage of after careful checking. For example, for a Hamiltonian system unstable cycles may form continuous families [120, 224], with one or more members of a family belonging to a given constant energy surface. In order to cope with the marginal eigendirection associated with such continuous family, we search for a cycle on a particular energy surface by replacing the last row of equation (64) by an energy shell constraint [37]. We put one point of the loop, say $\tilde{x}_2$, on the constant energy surface $H(\tilde{x}) = E$, and impose the constraint $\bigtriangledown H(\tilde{x}_2) \cdot \delta\tilde{x}_2 = 0$, so as to keep $\tilde{x}_2$ on the surface for all τ. The integration of (56) then automatically brings all other loop points to the same energy surface. Alternatively, we can look for a cycle of given fixed period T by fixing λ and dropping the constraint in the bottom line of (64). These two approaches are conjugate to each other, both needed in applications. In most cases, they are equivalent. One exception is the harmonic oscillator for which the oscillations have identical period but different energy. Note that in both cases the translational invariance is restored, as we have discarded the Poincaré section condition of sect. 3.2.2. As explained in [262], this causes no trouble in numerical calculations.

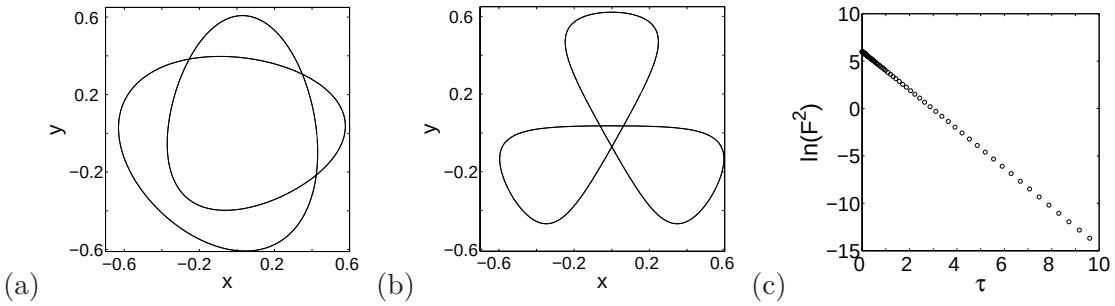

Figure 3: The Hénon-Heiles system in a chaotic region: (a) An initial loop $L(0)$, and (b) the unstable periodic orbit p of period $T = 13.1947$ reached by the Newton descent (60). (c) The exponential decrease of the cost function, $\ln(F^2) \approx -2.0502\,\tau + 6.0214$.

3.5 Applications

We have checked that the iteration of (64) yields quickly and robustly the short unstable cycles for standard models of low-dimensional dissipative flows such as the Rössler system [210]. A more daunting challenge are searches for cycles in Hamiltonian flows, and searches for spatio-temporally periodic solutions of PDEs. In all numerical examples that follow, the convergence criterion is $F^2 < 10^{-5}$.

3.5.1 Hénon-Heiles system and restricted three-body problem

First, we test the Hamiltonian version of the Newton descent derived in Sect. 3.3 by applying the method to two Hamiltonian systems, both with two degrees of freedom. In both cases, our initial loop guesses are rather arbitrary combinations of trigonometric functions. Nevertheless, the observed convergence is fast.

The Hénon-Heiles system [121] is a standard model in celestial mechanics, described by the Hamiltonian

$$H = \frac{1}{2}(p_x^2 + p_y^2 + x^2 + y^2) + x^2 y - \frac{y^3}{3}\,. \tag{65}$$

It has a time reversal symmetry and a three-fold discrete spatial symmetry. Figure 3 shows a typical application of (60), with the Newton descent search restricted to the configuration space. The initial loop, figure 3(a), is a rather coarse initial guess. We fix arbitrarily the scaling $\lambda = 2.1$, that is, we search for a cycle p of the fixed period $T_p = 13.1947$, with no constraint on the energy. Figure 3(b) shows the cycle found by the Newton descent, with energy $E = 0.1794$, and the full discrete symmetry of the Hamiltonian. This cycle persists adiabatically for a small range of values of λ; with λ changed much, the Newton descent takes the same initial loop into other cycles. Figure 3(c) verifies that the cost functional F^2 decreases exponentially with slope -2 throughout the $\tau = [0, 10]$ integration interval, as predicted by (58). The points get more and more sparse as τ increases, because our numerical implementation adaptively chooses bigger and bigger step sizes $\delta\tau$.

In the Hénon-Heiles case, the accelerations a_x, a_y depend only on the configuration variables x, y. More generally, the accelerations could also depend on $\dot{x}, \dot{y}$. Consider as an

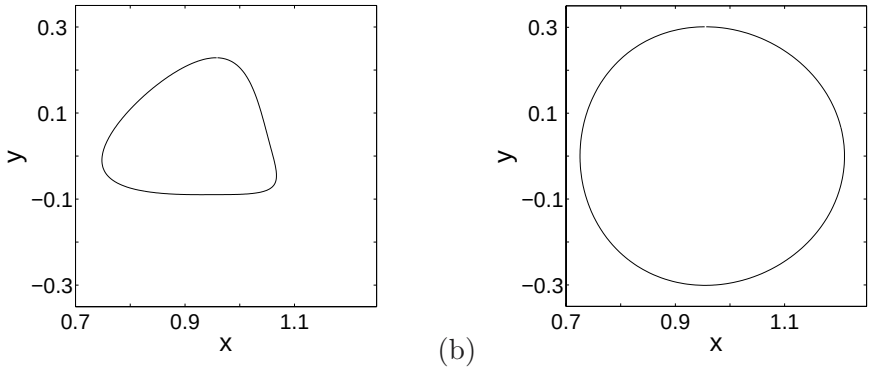

Figure 4: (a) An initial loop $L(0)$, and (b) the unstable periodic orbit p of period $T_p = 2.7365$ reached by the Newton descent (60), the restricted three body problem (66) in the chaotic regime, $\mu = 0.04$.

example the equations of motion for the restricted three-body problem [242],

$$\begin{aligned} \ddot{x} &= 2\dot{y} + x - (1-\mu)\frac{x+\mu}{r_1^3} - \mu\frac{x-1+\mu}{r_2^3}\,, \\ \ddot{y} &= -2\dot{x} + y - (1-\mu)\frac{y}{r_1^3} - \mu\frac{y}{r_2^3}\,, \end{aligned} \tag{66}$$

where $r_1 = \sqrt{(x+\mu)^2 + y^2}$, $r_2 = \sqrt{(x-1+\mu)^2 + y^2}$. These equations describe the motion of a test particle in a rotating frame under the influence of the gravitational force of two heavy bodies with masses 1 and $\mu \ll 1$ fixed at $(-\mu, 0)$ and $(1-\mu, 0)$ in the (x, y) coordinate frame. The stationary solutions of (66) are called the Lagrange points, corresponding to a circular motion of the test particle in phase with the rotation of the heavy bodies. The periodic solutions in the rotating frame correspond to periodic or quasi-periodic motion of the test particle in the inertial frame. Figure 4 shows an initial loop and the cycle to which it converges, in the rotating frame. Although the cycle looks simple, the Newton descent requires advancing in small $\delta\tau$ steps in order for the initial loop to converge to it.

In order to successfully apply the Hamiltonian version of the Newton descent (60), we have to ensure that the test particle keeps a finite distance from the origin. If a cycle passes very close to one of the heavy bodies, the acceleration can become so large that our scheme of uniformly distributing the loop points in time might fail to represent the loop faithfully. Another distribution scheme is required in this case, for example, making the density of points proportional to the magnitude of acceleration.

3.5.2 Periodic orbits of Kuramoto-Sivashinsky system

The Kuramoto-Sivashinsky equation arises as an amplitude equation for interfacial instability in a variety of contexts [153, 228]. In 1-dimensional space, it reads

$$u_t = (u^2)_x - u_{xx} - \nu u_{xxxx}, \tag{67}$$

where ν is a "super-viscosity" parameter which controls the rate of dissipation and $(u^2)_x$ is the nonlinear convection term. As ν decreases, the system undergoes a series of bifurcations, leading to increasingly turbulent, spatio-temporally chaotic dynamics.

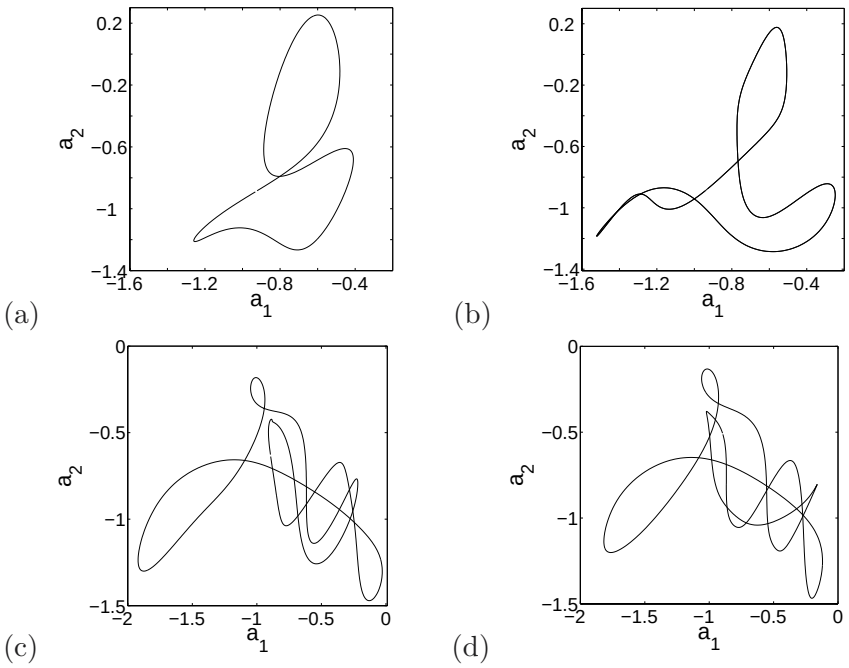

Figure 5: The Kuramoto-Sivashinsky system in a spatio-temporally turbulent regime (viscosity parameter $\nu = 0.015$, $d = 32$ Fourier modes truncation). (a) An initial guess L_1, and (b) the periodic orbit p_1 of period $T_1 = 0.744892$ reached by the Newton descent. (c) Another initial guess L_2, and (d) the resulting periodic orbit p_2 of period $T_2 = 1.184668$.

If we impose the periodic boundary condition $u(t, x+2\pi) = u(t, x)$ and choose to study only the odd solutions $u(-x, t) = -u(x, t)$, $u(x, t)$ can be expanded in a discrete spatial Fourier series [36],

$$u(x,t) = i \sum_{k=-\infty}^{\infty} a_k(t) e^{ikx}, \tag{68}$$

where $a_{-k} = -a_k \in \mathbb{R}$. In terms of the Fourier components, PDE (133) becomes an infinite ladder of ODEs,

$$\dot{a_k} = (k^2 - \nu k^4) a_k - k \sum_{m=-\infty}^{\infty} a_m a_{k-m} \,. \tag{69}$$

In numerical simulations we work with the Galerkin truncations of the Fourier series since in the neighborhood of the strange attractor the magnitude of a_k decreases very fast with k, high frequency modes playing a negligible role in the asymptotic dynamics [192]. In this way Galerkin truncations reduce the dynamics to a finite but large number of ODEs. We work with $d = 32$ dimensions in our numerical calculations. In ref. [36], multipoint shooting has been successfully applied to obtain periodic orbits close to the onset of spatiotemporal chaos ($\nu = 0.03$). In this regime, our method is so stable that big time steps $\delta\tau$ can be employed even at the initial guesses, leading to extremely fast convergence. We attribute this robustness to the simplicity of the structure of the attractor at high viscosity values.

The challenge comes with decreasing ν, with the dynamics turning more and more turbulent. Already at $\nu = 0.015$, the system is moderately turbulent and the phase space portraits of the dynamics reveal a complex labyrinth of "eddies" of different scales and

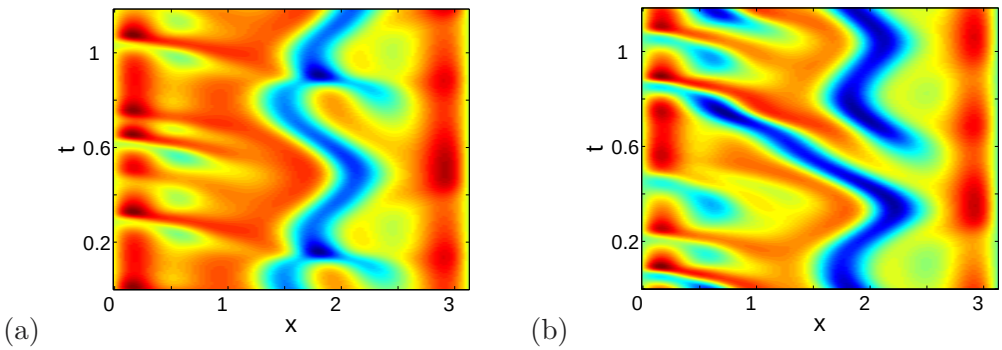

Figure 6: Level plot of the space-time evolution $u(x,t)$ for the two spatio-temporally periodic solutions of figure 5: (a) the evolution of p_1, with start of a repeat after the cycle period $T_1 = 0.744892$, and (b) one full period $T_2 = 1.184668$ in the evolution of p_2.

orientations. While the highly unstable nature of orbits and intricate structure of the invariant set hinder applications of conventional cycle-search routines, in this setting our variational method shines through. We design rather arbitrary initial loops from numerical trajectory segments, and the calculation proceeds as before, except that now a small $\delta\tau$ has to be used initially to ensure numerical stability. Topologically different loops are very likely to result in different cycles, while some initial loop guesses may lead to local nonzero minima of the cost functional F^2. As explained in Sect. 3.4, in such cases the method diverges, and the search is restarted with a new initial loop guess.

Two initial loop guesses are displayed in figure 5, along with the two periodic orbits detected by the Newton descent. In discretization of the initial loops, each point has to be specified in all d dimensions; here the coordinates $\{a_1, a_2\}$ are picked so that topological similarity between initial and final loops is visually easy to identify. Other projections from $d = 32$ dimensions to subsets of 2 coordinates appear to make the identification harder, if not impossible. In both calculations, we molded segments of typical trajectories into smooth closed loops by the Fourier filtering method of Sect. 3.4. As the desired orbit becomes longer and more complex, more sampling points are needed to represent the loop. We use $N = 512$ points to represent the loop in the (a)-(b) case and $N = 1024$ points in the (c)-(d) case. The space-time evolution of $u(x,t)$ for these two unstable spatio-temporally periodic solutions is displayed in figure 6. As $u(x,t)$ is antisymmetric on $[-\pi, \pi]$, it suffices to display the solutions on the $x \in [0, \pi]$ interval.

3.6 Summary

In order to cope with the difficulty of finding periodic orbits in high-dimensional chaotic flows, we have devised the *Newton descent method*, an infinitesimal step variant of the damped Newton-Raphson method. Our main result is the PDE (56) which solves the variational problem of minimizing the cost functional (59). This equation describes the fictitious time τ flow in the space of loops which decreases the cost functional at uniform exponential rate, see (58). Variants of the method are presented for special classes of systems, such as the Hamiltonian systems. An efficient integration scheme for the PDE is devised and tested on the Kuramoto-Sivashinsky system, the Hénon-Heiles system and the

restricted three-body problem.

Our method uses information from a large number of points in phase space, with the global topology of the desired cycle protected by insistence on smoothness and a uniform discretization of the loop. The method is quite robust in practice.

The numerical results presented here are only a proof of principle. We do not know to what periodic orbit the flow (56) will evolve for a given dynamical system and a given initial loop. Empirically, the flow goes toward the "nearest" periodic orbit, with the largest topological resemblance. Each particular application requires much work in order to elucidate and enumerate the relevant topological structures. The hope is that the short spatiotemporally periodic solutions revealed by the Newton descent searches will serve as the basic building blocks for systematic investigations of chaotic and perhaps even "turbulent" dynamics.

CHAPTER IV

COMPLEX GINZBURG-LANDAU EQUATION

From this chapter on, we will study pattern formation in $1-d$ spatially extended systems from a periodic orbit theory point of view. The Kuramoto-Sivashinsky equation (KSe) and the complex Ginzburg-Landau equation (CGLe) are the prototyped equations in this investigation. In this chapter, we emphasiz the important role played by coherent structures in the dynamics of the CGLe which can be defined as the steady or traveling wave solutions. Basic properties of the CGLe are reviewed in sect. 4.1, and various coherent structures are defined and their importance is discussed in sect. 4.2. A new formulation of the steady solutions of the CGLe is presented in sect. 4.3 by which we proved the existence of the modulated-amplitude waves (MAWs) near the onset of instability. We compare the obtained analytical expression with the numerical calculation and discuss their stability as well in sect. 4.5.

4.1 Review

4.1.1 Introduction

The complex Ginzburg-Landau equation (CGLe) is a generic amplitude equation describing Hopf bifurcation in spatially extended systems, *i.e.*, I_o systems [45], with reflection symmetry [135, 222, 256]. It is of great interest due to its genericity and applications to onset of wave pattern-forming instabilities [45] in various physical systems such as fluid dynamics, optics, chemistry and biology. It exhibits rich dynamics and has become a paradigm for studying transitions to spatiotemporal chaos.

Consider the $1-d$ CGLe for the complex amplitude field $A(x,t)$:

$$A_t = \mu A + (1+i\alpha)A_{xx} - (1+i\beta)|A|^2 A\,, \tag{70}$$

where $A(x,t) : \mathbb{R}^2 \mapsto \mathbb{C}$, and $\mu, \alpha, \beta \in \mathbb{R}$, $x \in \mathcal{D}$. $\mathcal{D}$ is the spatial domain on which the equation is defined. A_t, A_{xx} denote repectively the first temporal derivative and the second spatial derivative of A. Interesting domains for us are either the whole real axis or a finite box of length L with periodic boundary conditions. μ is the control parameter. Only $\mu > 0$ is considered as we study the supercritical Ginzburg-Landau equation; one could set $\mu = 1$ by appropriate rescaling of the time, space and amplitude, but we keep it as a parameter for closer connection with experimental results and literature. Coefficients α and β parametrize the linear and nonlinear dispersion.

If both α and β are set to 0, we recover the real Ginzburg-Landau equation (GLe) in which only the diffusion term and the stabilizing cubic term compete with each other and

with the linear term. A Lyapunov functional exists in that case [45] and the GLe behaves like a gradient system. Another limit — the nonlinear Schrödinger equation — results from setting $\alpha, \beta \to \infty$; we then have an integrable nonlinear PDE with infinitely many conserved quantity. For parameter values in the intermediate range, the CGLe inherits partial properties of the gradient system and the conserved system, and long-time behavior of the CGLe can vary from stationary to periodic and to spatiotemporal chaos [225]. We will concentrate on the stationary solutions of the CGLe in a finite box of length L with periodic boundary conditions, and the case $\alpha \neq \beta$. Stationary solutions are the simplest non-trivial solutions, related to propagating solutions by a change of frame of reference $(x,t) \mapsto (x - vt, t)$ with fixed $v \in \mathbb{R}$.

4.1.2 Symmetries and Bekki-Nozaki solutions

Equation (70) is invariant under temporal and spatial translations. Moreover, it is invariant under a global gauge transformation $A \to A\exp(i\phi)$, where $\phi \in \mathbb{R}$, and under $x \to -x$ reflection. As a consequence, it preserves the parity of A, i.e., if $A(-x,0) = \pm A(x,0)$, then $A(-x,t) = \pm A(x,t)$ for any later time $t > 0$. If $A(x,t)$ has no parity, then $A(-x,t)$ gives another solution.

For a spatially infinite system there exists a continuous family of traveling holes - the Bekki-Nozaki solution [15]. If we set $\xi = x - ct$, the position in the moving frame (c is the velocity to be determined later), then the Bekki-Nazakisolution is

$$A = \frac{b_1 e^{\kappa\xi} + b_2 e^{-\kappa\xi}}{e^{\kappa\xi} + e^{-\kappa\xi}} \exp\left(\frac{i}{2}\int_0^\xi (\kappa_+ + \kappa_- \tanh\kappa s)\, ds - i\Omega t\right), \tag{71}$$

where

$$\begin{aligned}
&\Omega = \alpha\mu - c\frac{\kappa_1\kappa_2}{\sqrt{\mu}}, \quad c = (\kappa_1+\kappa_2)(\alpha-\beta),\\
&\kappa_\pm = \kappa_1 \pm \kappa_2, \quad \kappa = -\frac{\kappa_-}{2\alpha}; \quad |b_j|^2 = \mu - \kappa_j^2, \text{ for } j = 1,2,\\
&\sigma \equiv \arg(\frac{b_2}{b_1}) = -\arctan\left(2\kappa_+\kappa_- \frac{p(\alpha-\beta) - \frac{1}{p}(1+\alpha\beta)}{(1+\beta^2)\kappa_+^2 - (p^2+p^{-2})(1+\alpha^2)\kappa_-^2}\right),\\
&p = -q \pm (2+q^2)^{\frac{1}{2}}, \quad q = -\frac{3}{2}\frac{1+\alpha\beta}{\alpha-\beta}.
\end{aligned}$$

The asymptotic wave-numbers (at $|\kappa\xi| \gg 1)\kappa_1$ and κ_2 satisfy

$$\frac{(\kappa_1+\kappa_2)^2}{a_1^2} + \frac{(\kappa_1-\kappa_2)^2}{a_2^2} = 1,$$

where

$$a_1^2 = 4\mu\left(1 - \frac{3p(1+\beta^2)}{(\alpha-\beta)(1+p^2)}\right)^{-1}, \quad a_2^2 = 4\mu\left(1 - \frac{3(1+\alpha^2)}{p(\alpha-\beta}\right)^{-1}.$$

A branch of p should be chosen so as to make a_1^2 and a_2^2 to be positive. The solution is highly unstable for α, β values we are considering here.

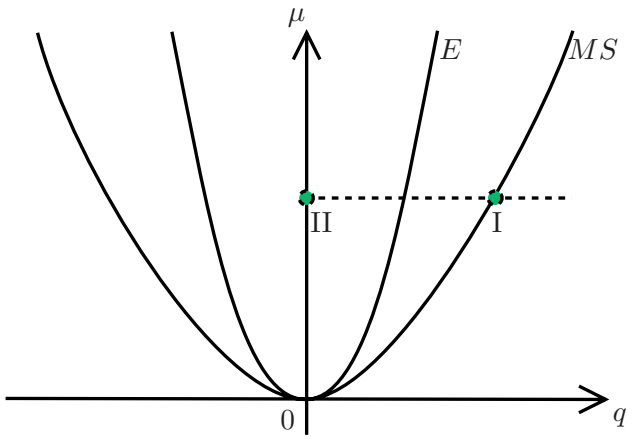

Figure 7: Marginal stability curve (MS) and Eckhaus instability curve (E) defining regions where plane waves solutions exist in the CGLe (inside (MS)), and are stable when $1+\alpha\beta > 0$ (inside (E)). Case I corresponds to the wave of maximal possible wavenumber and Case II to the wave with $q = 0$ and the maximal amplitude.

The one-parameter family of the hole solutions strongly suggest the existence of a hidden symmetry in the CGLe [259]. Inclusion of higher order terms, such as a quintic term $\delta|A|^4A$ eliminates this family of solutions [67]. So, the family is structurally unstable, and the hidden symmetry appears specific to the cubic CGLe. In the stationary case, the existence of the solitory solution and more complicated solutions can be inferred by an application of the counting argument associated with the reflection symmetry [14].

4.1.3 Stokes solutions and their stability

The global phase invariance implies that the CGLe has nonlinear plane wave solutions of the form

$$A(x,t) = R_0 \exp(i(qx - \omega t)) \,, \tag{72}$$

where $R_0^2 = \mu - q^2$ is the square of the amplitude, $\omega = \mu\beta + (\alpha - \beta)q^2$ is the frequency, and $q \in \mathbb{R}$ with $q^2 \leq \mu$ is the wavenumber. They are called Stokes solutions [3] and are parametrized by the wavenumber q. The two limit cases of interest to us are highlighted on figure 7: a plane wave of wavenumber $\mu^{1/2}$ and of vanishing amplitude (case I), and the wave with zero wavenumber and maximum amplitude μ (case II). In case II, the solution oscillates uniformly in space; we call it the homogeneously oscillating state (HOS).

For the infinite system, the Benjamin-Feir-Newell [187] criterion states that all plane wave solutions are unstable with respect to long wavelength perturbations, *i.e.*, of wavenumber $k \to 0$) if $1+\alpha\beta < 0$. If $1+\alpha\beta > 0$, we have to consider the Eckhaus stability criterion which states that only a band of wavenumbers are stable against long wavelength perturbations:

$$q^2 < q_{\rm E}^2 \equiv \frac{(1+\alpha\beta)\mu}{3+\alpha\beta+2\beta^2} \,. \tag{73}$$

For a finite periodic system the wavenumbers for both the original states and the perturbations are quantized. In this context, the above criteria were re-examined by Matkowsky and Volpert using linear stability analysis [171].

4.1.4 Low-dimensional behavior of the CGLe

The CGLe describes a dynamical system with infinitely many degrees of freedom. But in either experiments or numerical simulations, only a finite number of patterns play a role in the long-time dynamics. For the CGLe in a periodic box, a global attracting set exist towards which all the solutions approach in a finite time. An upper bound on the number of Fourier modes needed to give a complete knowledge of the asymptotic dynamics is derived in ref. [69]. The rest of the infinitely many modes are determined by geometric constraints that define the finite-dimensional inertial manifold in the phase space. Thus, the global attractor which lies on the inertial manifold also has a finite dimension. By estimating the Lyapunov exponents on the asymptotic trajectory, similar result was also claimed in ref. [95]. In the even solution space, the magnitude of the Mth mode of the global attractor decays faster than any algebraic order of M^{-1} [66].

Though the above analytic results provide a rigorous justification for simulating the CGLe dynamics with finite Gälerkin truncations, these estimated bounds on the number of effective modes are usually much higher than what is needed for actual numerical calculations. In practice, we always try to use the smallest number of modes, sufficient to capture the dynamics of interest. Near the onset of chaotic behavior, just a few modes are important and enough to give a complete description of bifurcation sequences [66, 163]. In the chaotic region, a common approach to select the optimal basis is the Karhunen-Loeve or proper orthogonal decomposition (POD) which orders the orthogonal linear basis according to their relative importance [209] by checking the 2-point correlation matrix on the strange attractor. This method does not utilize geometrical information about the layout of inertial manifold, and is inadequate for our purposes.

In a periodic box, we can clearly see how the destabilization of low wavenumber modes leads to spatiotemporal chaos. When the size L is small, homogeneous oscillatory state (HOS) is stable. The first instability generates stationary modulated amplitude waves (MAWs). They partially break the space translational symmetry but retain the parity. The ensueing pitchpork bifurcation breaks the parity of $|A|$ and sets the whole profile moving. As the system size increases further, spatiotemporal chaos arises and both the amplitude and phase of A fluctuate irregularly. Bifurcations in the even solution space have been studied in great detail [66, 163]. Similarly to the Lorenz attractor [232], the first strange attractor is generated through a homoclinic explosion [163].

4.1.5 Phase chaos versus defect chaos

In the infinite domain all the plane waves become unstable above the Benjamin-Feir (BF) line ($1 + \alpha\beta < 0$) [22], and the system becomes chaotic. There are two types of chaos in the chaotic region: phase chaos and defect (or amplitude) chaos. In the phase chaos, the

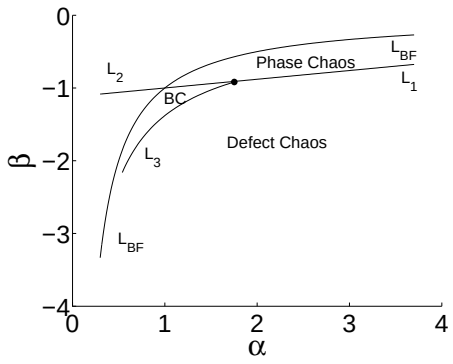

Figure 8: Phase diagram of the CGLe. The line L_{BF} is the locus of the Benjamin-Feir instability. L_1, L_2 and L_3 intersect at the point C^*. Below L_1 and L_3, only defect chaos is observed. The region enclosed by L_2, L_3 and L_{BF} is a bichaotic region (marked BC). Note that L_2 crosses L_{BF}.

amplitude of A is bounded away from zero, while in the defect chaos $|A|$ reaches zero at isolated space-time points. When $|A(x,t)| = 0$, we say that a defect forms; at the defect point the phase of A is not defined. The Bekki-Nozaki solutions are believed to play an important role in the defect chaos. Two characteristics can be used to distinguish phase chaos and defect chaos [250, 182, 252]: the defect density n_d which is the space-time average of the number of defects that appear in the system, and the phase winding number

$$\nu = \frac{1}{2\pi} \int_0^L \partial_x \phi(x,t)\, dx$$

which represents the phase change of A over the interval. In the defect chaotic region, $n_d \neq 0$ and $\nu = 0$ but in the phase chaotic one $n_d = 0$ and $\nu \neq 0$. There exists a line in the α, β parameter space below which only defect chaos is present [225] (see figure 8). The line consists of two parts: L_1 and L_3 (we use the notation of ref. [225]). Across L_1 the transition is continuous [225, 76]. Near L_3, there is a bichaotic region, where both the phase chaos and the defect chaos are metastable and they may transform to each other by finite-amplitude perturbations. The L_1 line can be continued to L_2 which crosses the BF line. A spatiotemporal intermittency region [34] lies below the L_2 line where the metastable states are plane waves and defect chaos.

Near the BF line in the phase chaotic region, the states result from a Hopf bifurction of the HOS when the long-wavelength components become linearly unstable. As the interaction between different modes is very weak, each mode can be viewed as an independent oscillator with the amplitude entrained to the phase (see sect. 5.1 in Chapter 5), and thus phase equations can be developed to describe the evolution of the system [152]. The most commonly used one is the Kuramoto-Sivashinsky equation (KSe) [153, 228]. In the defect chaos region, the interaction between modes are so strong that $|A|$ is brought down to zero at discrete space-time points where the winding number changes through phase-slip process. In this case, the defect dynamics sets in and phase equation fails [219].

4.2 Coherent structures and MAWs

In extended systems, chaotic states are usually a juxtapostion of patches of regular patterns called "coherent structures" (CS) [259]. The CS play a very important role in the study of pattern formation and dynamical properties of the CGLe. In the laminar case, the CS includes uniform states, plane waves, pulses, fronts, holes. In the chaotic case, the overall pattern consists of near-regular patches connected by localized defects or interfaces. After doing the following substitution in (70),

$$A(x,t) \to A(x-ct,t)e^{i(kx-\omega t)}\,,$$

we get

$$A_t = (\mu - k^2 + i\omega)A + (c+2ik)A_x + (1+i\alpha)A_{xx} - (1+i\beta)|A|^2 A\,. \tag{74}$$

The coherent structures we will discuss below are the steady solutions of (74), *i.e.*, $A_t = 0$. There exists a similarity transformation which maps steady states to each other for different $\alpha\,,\beta$ values in the parameter space along the constant C-curve

$$C = \frac{\alpha-\beta}{1+\alpha\beta}\,.$$

$k\,,c\,,A$ and ω have to change accordingly during the process while the shape of the magnitude profile of A does not change.

In the steady equation, if we use polar coordinates,

$$A(x,t) = R(x)e^{i\phi(x)}\,,$$

a 3-D nonlinear dynamical system is obtained [259]

$$\begin{aligned}
R_x &= \psi \\
\psi_x &= R\kappa^2 + \frac{1+\alpha\beta}{1+\alpha^2}R^3 + (2kR - \frac{c\alpha}{1+\alpha^2})\kappa - \frac{c}{1+\alpha^2}\psi + \frac{k^2+\alpha^2k^2-\mu-\alpha\omega}{1+\alpha^2}R \\
\kappa_x &= \frac{\beta-\alpha}{1+\alpha^2}R^2 + \frac{\alpha\mu-\omega}{1+\alpha^2}(\frac{c\alpha}{1+\alpha^2} - 2k)\frac{\psi}{R} - \frac{2\kappa\psi}{R} - \frac{c}{1+\alpha^2}\kappa\,,
\end{aligned} \tag{75}$$

where $\psi = R_x$ is the gradient of R and $\kappa = \phi_x$ is the local wavenumber. By redefining ω and κ, the parameter k can be set to zero. There are essentially two free parameters: the frequency ω and the group velocity c. when $c = 0$, (75) becomes an equation for the stationary solution of the CGLe and is invariant under the transformation $(R,\psi,\kappa,x) \to (R,-\psi,-\kappa,-x)$.

The equilibrium points of (75) are plane waves described in sect. 4.1.3. The homoclinic [253] and heteroclinic [259] connections between equilibria correspond to localized coherent structures. The Nozaki-Bekki solutions [15] belong to this category; they connect asymptotic plane waves with different wavenumbers. In large domain numerical simulations, near-coherent structures are frequently observed in the intermittency or chaotic regimes [225, 257, 259, 34, 4, 254, 255, 193, 15] and play an essential role in the pattern formation process.

Recent numerical studies reveal another kind of coherent structure: modulated amplitude waves (MAWs) for the CGLe [30]. They correspond to limit cycles of (75). When

$c = 0$, MAWs are stationary. The formation of MAWs is the first instability encountered when a plane wave state crosses the Eckhaus or Benjamin-Feir stability line. The MAW structure is frequently observed in experiments [136, 94], and is considered a key to interpretation of patterns and bifurcations exhibited during the system's transition to spatiotemporal chaos [28, 27, 30].

In the following, we reformulate the equation for steady solutions, and prove the existence of MAWs for case I and II. The stability analysis indicates that the MAWs arising in case I are unstable but the MAWs in case II are stable. By comparing with numerical calculations, we find that the later ones are indeed the stationary waves observed after the first bifurcation.

4.3 Reformulation of the problem

Since we are only interested in the steady solutions of the CGLe, we substitute the ansatz

$$A(x,t) = R(x)\exp(i\phi(x) - i\omega t), \qquad (R,\phi) \in \mathbb{R}^2 \tag{76}$$

into (70). We then have

$$(1+\alpha^2)G_x = K \equiv (\beta-\alpha)R^4 - (\omega-\mu\alpha)R^2 \tag{77}$$

$$(1+\alpha^2)G^2 = M \equiv (1+\alpha^2)R^3R_{xx} + (\alpha\omega+\mu)R^4 - (1+\alpha\beta)R^6\,. \tag{78}$$

where $G \equiv \phi_x R^2$ is reminiscent of "angular momentum". Note that if $\alpha = \beta$, this "angular momentum" is conserved — it is constant in space — provided that $\omega = \mu\alpha$. In that case, (78) can be solved in terms of elliptic functions [160]. We will only consider the case $\alpha \neq \beta$ in the following. Equations (77) and (78) are invariant under $(G,x,R) \to (-G,-x,\pm R)$. Note that for plane waves, $K = 0$ and G is a constant. If K is not always zero, differentiating (78) and dividing the result by (77) gives

$$2G = M_x/K\,, \tag{79}$$

and by (78)

$$M = \frac{1+\alpha^2}{4}\frac{M_x^2}{K^2}\,. \tag{80}$$

Furthermore, we can factorize R^2 from M_x and K and write $M_x = R^2N$ and $K = R^2P$, where

$$\begin{aligned} N &\equiv (1+\alpha^2)\frac{1}{2}(R^2)_{xxx} + (\alpha\omega+\mu)2(R^2)_x - (1+\alpha\beta)3R^2(R^2)_x \\ P &\equiv (\beta-\alpha)R^2 - (\omega-\mu\alpha)\,. \end{aligned} \tag{81}$$

The last relation can be used to express R^2 in terms of P:

$$R^2 = \frac{(\omega-\mu\alpha)+P}{\beta-\alpha} = e + dP = R_0^2 + \frac{P}{\beta-\alpha}\,, \tag{82}$$

where $d \equiv 1/(\beta - \alpha)$ and $e \equiv (\omega - \mu\alpha)/(\beta - \alpha)$.

Note that $e = R_0^2$ is the square of the homogeneous amplitude $R_0(q, \omega)$ of the Stokes plane wave solution (72) of frequency ω and wavevector $q(\omega)$. P then appears as the modulation of the amplitude squared with respect to the Stokes solution, and so it is an appropriate variable to describe a MAW.

Substituting K and M_x into (80), we have

$$\frac{1+\alpha^2}{4}\frac{N^2}{P^2} = M\,. \tag{83}$$

If $P \neq 0$ (83) is equivalent to (77) and (78). It is easy to check that if we regard (79) as a definition of G, and use K, M, N, P expressed in terms of R, equation (77) and (78) will be recovered as a result of (80) and (83). Differentiating both sides of (83) results in

$$\frac{1+\alpha^2}{2}(PN_x - NP_x) = R^2P^3\,. \tag{84}$$

In this step we have extended the solution set of (83), because as we integrate (84) back, we get

$$\frac{1+\alpha^2}{4}\frac{N^2}{P^2} = M + \mathcal{C}\,, \tag{85}$$

where $\mathcal{C}$ is an integration constant. Only for $\mathcal{C} = 0$ a solution of (84) is a solution of (83). For this reason, when obtaining solutions of (84), we have to check the *consistency condition*

$$\frac{1+\alpha^2}{4}\frac{N^2}{P^2} - M = 0 \tag{86}$$

to make sure that we have a solution of (83), thus a solution of (77) and (78). Note that if K vanishes identically we have to go back to (77) and (78), since in that case (83) is not well defined. Let us rewrite N in terms of P:

$$N = \frac{2}{1+\alpha^2}\left(aP_{xxx} + bP_x + cPP_x\right)\,, \tag{87}$$

where a, b, c are constants

$$\begin{aligned} a &\equiv \frac{(1+\alpha^2)^2}{4(\beta-\alpha)} \\ b &\equiv \frac{1+\alpha^2}{2}\left(\frac{2(\alpha\omega+\mu)}{\beta-\alpha} - \frac{3(1+\alpha\beta)(\omega-\mu\alpha)}{(\beta-\alpha)^2}\right) \\ c &\equiv -\frac{3(1+\alpha\beta)(1+\alpha^2)}{2(\beta-\alpha)^2}\,. \end{aligned} \tag{88}$$

We use (87) and (82) to rewrite (84) using only P and its spatial derivatives:

$$P(aP_{xxx} + bP_x + cPP_x)_x - P_x(aP_{xxx} + bP_x + cPP_x) = (dP + e)P^3 \tag{89}$$

Note that this equation contains even numbers of derivatives of P in each term on the left hand side, and also that the powers of P increase while the derivatives decrease. We now

rewrite the equation in a form which takes advantage of this structure. For example, the following equation is equivalent to (89) for any real λ:

$$P(aP_{xxx}+bP_x+(c+\lambda)PP_x)_x - P_x(aP_{xxx}+bP_x+(c+\lambda)PP_x) \\ = P^2(\lambda P_{xx}+dP^2+eP)\,,$$

or, put in another form and introducing another real parameter k:

$$\left(\frac{(aP_{xx}+bP+\frac{c+\lambda}{2}P^2)_x}{P}\right)_x = \lambda P_{xx}+dP^2+\tilde{e}P+\frac{a}{\lambda}kP\,,$$

where we have written $\tilde{e}+\frac{a}{\lambda}k=e$.

In this equation, we have three free parameters: besides ω, introduced by the ansatz (76) as the carrier frequency of the solution, we have introduced free parameters λ and k. We now fix λ by imposing the condition

$$\frac{a}{\lambda}=\frac{b}{\tilde{e}}=\frac{c+\lambda}{2d}\,, \tag{90}$$

which allows us to write the equation in a more suggestive form:

$$\left(\frac{(\lambda P_{xx}+dP^2+\tilde{e}P)_x}{P}\right)_x = \frac{\lambda}{a}(\lambda P_{xx}+dP^2+\tilde{e}P)+kP\,,$$

or more concisely,

$$\left(\frac{\tilde{M}_x}{P}\right)_x = \frac{\lambda}{a}\tilde{M}+kP\,, \qquad \text{where } \tilde{M}\equiv\lambda P_{xx}+dP^2+\tilde{e}P\,. \tag{91}$$

This equation will lead to the 4-D ODE of section 4.4.

λ is determined by (90):

$$\lambda^2+c\lambda-2ad=0\,. \tag{92}$$

The discriminant of (92) is

$$\begin{aligned}\Delta &= c^2+8ad \\ &= \left(\frac{1+\alpha^2}{2(\beta-\alpha)}\right)^2\left(\frac{9(1+\alpha\beta)^2}{(\beta-\alpha)^2}+8\right)\,.\end{aligned}$$

So $\Delta>0$ for any real values of α and β, and the quadratic equation (92) always has two real roots

$$\lambda=\frac{3(1+\alpha\beta)(1+\alpha^2)}{4\,(\beta-\alpha)^2}\pm\frac{1+\alpha^2}{4(\beta-\alpha)^2}\sqrt{9(1+\alpha\beta)^2+8(\beta-\alpha)^2} \tag{93}$$

Note that λ is a function of α and β only. In some applications [204], the two values of λ correspond to two distinct solutions of the CGLe. In our case, λ is an intermediate variable used in the derivation and the proofs, but our solutions to the CGLe do not distinguish the two values of λ.

4.4 4-D dynamical system and the existence of periodic solutions

Let us take τ as the spatial variable, $P = P(\tau)$ in (81), and rewrite (91) as a system of first order equations in τ. With $\tilde{N} = \tilde{M}_\tau / P$ and $Q = P_\tau$, from (91) we have

$$\left\{ \begin{array}{rcl} \dot{\tilde{M}} & = & \tilde{N} P \\ \dot{\tilde{N}} & = & \frac{\lambda}{a}\tilde{M} + kP \\ \dot{P} & = & Q \\ \dot{Q} & = & \frac{1}{\lambda}(\tilde{M} - dP^2 - \tilde{e}P) \end{array} \right. , \tag{94}$$

where the dot represents the derivative with respect to the spatial variable τ.

It is easy to check that $P \equiv 0$ is a solution of the original equations (77) and (78), corresponding to the plane wave solution of the CGLe with frequency ω. We will study the behavior near $P = 0$ and prove the existence of periodic solutions for small P. In the CGLe, this corresponds to a weakly modulated amplitude wave which bifurcates from a plane wave solution. If $P \sim \epsilon$, where ϵ is a small parameter, so are $\tilde{M}, \tilde{N}, Q$ by their definitions. Write

$$(\tilde{M}, \tilde{N}, P, Q) = (\epsilon x, \epsilon y, \epsilon z, \epsilon w)$$

and set $k = k_1 + \epsilon k_2$. Substituting these into the 4-D system, we have

$$\frac{d}{d\tau}\begin{pmatrix} x \\ y \\ z \\ w \end{pmatrix} = A \begin{pmatrix} x \\ y \\ z \\ w \end{pmatrix} + \epsilon \begin{pmatrix} y\,z \\ k_2\,z \\ 0 \\ -\frac{d}{\lambda}z^2 \end{pmatrix}, \text{ where } A = \begin{pmatrix} 0 & 0 & 0 & 0 \\ \frac{\lambda}{a} & 0 & k_1 & 0 \\ 0 & 0 & 0 & 1 \\ \frac{1}{\lambda} & 0 & \frac{-\tilde{e}}{\lambda} & 0 \end{pmatrix}.$$

The linear part A describes the behavior of the system in the neighborhood of the trivial fixed point $(0,0,0,0)$. Note that the system is invariant under $(t, y, w) \to -(t, y, w)$. We will use this property to simplify our analysis. Moreover, this system defines an incompressible flow since $\nabla \cdot \vec{X} = 0$, where $\vec{X} = (x, y, z, w)$. It follows from (85) that the system has one integration constant $\mathcal{C}$. This constant induces a foliation of the phase space into three-dimensional manifolds. Physical solutions, i.e., the solutions of the original CGLe, are restricted to $\mathcal{C} = 0$, the manifold that satisfies the *consistency condition* (86).

These properties strongly restrict the possible distributions of eigenvalues of A. We restrict our analysis to the case $\tilde{e}/\lambda > 0$. In that case, A has eigenvalues $\{0, 0, i\omega_1, -i\omega_1\}$ with $\omega_1 = \sqrt{\tilde{e}/\lambda}$, and periodic solutions or MAWs can exist, as we will prove in the following. The evolution of the system respects the constant $\mathcal{C}$ foliation: if the solution is on a constant $\mathcal{C}$ manifold at initial time, it remains there for any later time.

We now discuss the condition $\tilde{e}/\lambda > 0$ in terms of an instability of the underlying plane wave. We can rewrite $\tilde{e}/\lambda$ using (88) and (90). Assuming that the solution we are searching for is close to a plane wave, we can use the wavenumber q instead of the frequency ω, using the dispersion relation (72) for plane waves:

$$\begin{aligned} \frac{\tilde{e}}{\lambda} = \frac{b}{a} &= \frac{2}{1+\alpha^2}\left[2(\alpha\omega + \mu) - \frac{3(1+\alpha\beta)(\omega - \mu\alpha)}{\beta - \alpha}\right] \\ &= \frac{2}{1+\alpha^2}\left[(3 + \alpha\beta + 2\alpha^2)q^2 - (1+\alpha\beta)\mu\right]. \end{aligned} \tag{95}$$

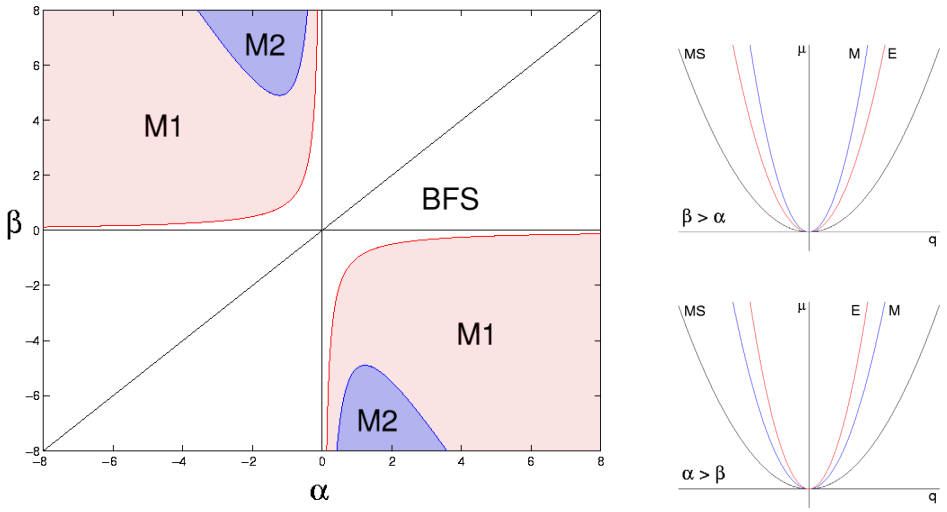

Figure 9: Left: wavenumber distribution of stationary MAWs in the (α, β) plane. In (BFS), MAWs exist if $q^2 > q_{\rm M}^2$. In (M1), MAWs exist $\forall q$. In (M2), MAWs exist if $q^2 < q_{\rm M}^2$. Right: regions of existence of MAWs in the (q, μ) plane in the Benjamin-Feir-Newell stable regime ((BFS) region). (MS) is the marginal stability curve, (E) is the Eckhaus instability curve and (M) is existence curve defined by (96). Stationary MAWs exist outside (M).

If we write

$$q_{\rm M}^2 \equiv \frac{(1+\alpha\beta)\mu}{3+\alpha\beta+2\alpha^2}\,, \tag{96}$$

we have

$$\frac{\tilde{e}}{\lambda} > 0 \quad \Leftrightarrow \quad \left| \begin{array}{rll} q^2 > q_{\rm M}^2 & \text{if} & (1+\alpha\beta) > 0 \\ q^2 < q_{\rm M}^2 & \text{if} & (1+\alpha\beta) < -2(1+\alpha^2) \\ \forall q \in [-\sqrt{\mu}, \sqrt{\mu}] & \text{if} & -2(1+\alpha^2) < 1+\alpha\beta < 0 \end{array} \right. . \tag{97}$$

The corresponding regions are illustrated on Fig. 9. Note that $q_{\rm M}(\alpha,\beta,\mu) = q_{\rm E}(\beta,\alpha,\mu)$. If $|\alpha| = |\beta|$, the positivity of $\tilde{e}/\lambda$ is assured when the corresponding plane wave is Eckhaus unstable. If $|\alpha| \neq |\beta|$, the positivity does not coincide anymore with the Eckhaus criterion; this is not surprising considering that we do not restrict our analysis to long wavelength perturbations of plane waves, but that the solutions we are seeking may have any wavenumber.

In the following we distinguish two cases. In the first case eigenvalue 0 has a simple elementary divisor, *i.e.*, has two distinct eigenvectors [112]. This coincides with case I: the MAW solution bifurcates from the $A = 0$ state, with $\omega \sim \mu\alpha$ and hence $\tilde{e}/\lambda \sim 4\mu > 0$, for $\mu > 0$. In the second case, eigenvalue 0 has only one eigenvector. This coincides with case II: the MAW is superimposed over a plane wave with $\omega \simeq \mu\beta$, so $q \simeq 0$, and

$$\frac{\tilde{e}}{\lambda} \simeq -\frac{2\mu(1+\alpha\beta)}{1+\alpha^2} > 0,$$

where the positivity is insured if the system is Benjamin-Feir-Newell unstable, $(1+\alpha\beta) < 0$.

In terms of $\tilde{M}, \tilde{N}, P, Q$, the *consistency condition* (86) can be written as

$$(1+\alpha^2)M = \left(\frac{a}{\lambda}\tilde{N} - \lambda Q\right)^2 \tag{98}$$

where in new variables

$$M = \frac{d(1+\alpha^2)}{2\lambda}(d\,P+e)(\tilde{M}-d\,P^2-\tilde{e}\,P)-\frac{d^2(1+\alpha^2)}{4}\,Q^2+ (\alpha\omega+\mu)(d\,P+e)^2-(1+\alpha\,\beta)(d\,P+e)^3\,.$$

Recalling (78), we may express G by

$$G=\frac{\frac{a}{\lambda}\tilde{N}-\lambda Q}{1+\alpha^2}\,. \tag{99}$$

Here we are allowed to fix the sign of the right hand side expression because of the $(G,x)\mapsto(-G,-x)$ reflection symmetry of (77) and (78).

4.4.1 Case I

We want the eigenvalue 0 to have non-degenerate eigenvectors, for this, we set

$$\frac{\frac{\lambda}{a}}{\frac{1}{\lambda}}=\frac{k_1}{-\frac{\tilde{e}}{\lambda}}\,,\qquad i.e.,\ k_1=-\frac{\lambda\tilde{e}}{a}\,.$$

Consequently, we have

$$e=\tilde{e}+\frac{a}{\lambda}k=\frac{\epsilon a}{\lambda}k_2\,. \tag{100}$$

Notice that $e\sim 0$ to the zeroth order, so $R_0\sim 0$ and $\omega\sim\mu\alpha$, which means that the solution to be considered bifurcates from the zero solution $A=0$, corresponding to a plane wave around the marginal stability curve, with wavenumber $q\sim\pm\mu^{1/2}$. This solution is therefore outside the Eckhaus stability region when $1+\alpha\beta>0$.

The four eigenvectors of A are:

$$\begin{pmatrix}0\\1\\0\\0\end{pmatrix}\quad\begin{pmatrix}\tilde{e}\\0\\1\\0\end{pmatrix}\quad\begin{pmatrix}0\\-ik_1\omega_1^{-1}\\1\\i\omega_1\end{pmatrix}\quad\begin{pmatrix}0\\ik_1\omega_1^{-1}\\1\\-i\omega_1\end{pmatrix}.$$

Let

$$D=\begin{pmatrix}0&\tilde{e}&0&0\\1&0&0&\frac{\lambda^2}{a}\\0&1&1&0\\0&0&0&1\end{pmatrix},\qquad D^{-1}=\begin{pmatrix}0&1&0&-a^{-1}\lambda^2\\\tilde{e}^{-1}&0&0&0\\-\tilde{e}^{-1}&0&1&0\\0&0&0&1\end{pmatrix},$$

and $\vec{\tilde{X}}\equiv(\tilde{x},\tilde{y},\tilde{z},\tilde{w})=D^{-1}\vec{X}$. The dynamical equations for the new variables become

$$\frac{d}{d\tau}\vec{\tilde{X}}=M(\omega_1)\vec{\tilde{X}}+\epsilon\begin{pmatrix}k_2(\tilde{y}+\tilde{z})+\frac{\lambda d}{a}(\tilde{y}+\tilde{z})^2\\\frac{1}{\tilde{e}}(\tilde{x}+\frac{\lambda^2}{a}\tilde{w})(\tilde{y}+\tilde{z})\\-\frac{1}{\tilde{e}}(\tilde{x}+\frac{\lambda^2}{a}\tilde{w})(\tilde{y}+\tilde{z})\\-\frac{d}{\lambda}(\tilde{y}+\tilde{z})^2\end{pmatrix},$$

where

$$M(\omega_1) = D^{-1}AD = \begin{pmatrix} 0 & 0 & 0 & 0 \\ 0 & 0 & 0 & 0 \\ 0 & 0 & 0 & 1 \\ 0 & 0 & -\omega_1^2 & 0 \end{pmatrix} .$$

The angular frequency of the solution Ω should be close to ω_1, $\Omega^2 = \omega_1^2 + \epsilon\gamma$, with the shift γ to be determined later. Next, we change variables to:

$$\begin{cases} \tilde{x} &= x_1 \\ \tilde{y} &= x_2 \\ \tilde{z} &= z_1 \sin\Omega\tau + z_2 \cos\Omega\tau \\ \tilde{w} &= \Omega z_1 \cos\Omega\tau - \Omega z_2 \sin\Omega\tau \end{cases} \tag{101}$$

The 4-D system of equations then takes form:

$$\begin{aligned} \dot{x_1} &= \epsilon\left[k_2(x_2 + z_1\sin\Omega\tau + z_2\cos\Omega\tau) + \frac{\lambda d}{a}(x_2 + z_1\sin\Omega\tau + z_2\cos\Omega\tau)^2\right] \\ \dot{x_2} &= \frac{\epsilon}{\tilde{e}}\left[x_1 + \frac{\Omega\lambda^2}{a}(z_1\cos\Omega\tau - z_2\sin\Omega\tau)\right](x_2 + z_1\sin\Omega\tau + z_2\cos\Omega\tau) \\ \dot{z_1} &= \frac{\epsilon}{\Omega}\left[-\frac{d}{\lambda}(x_2 + z_1\sin\Omega\tau + z_2\cos\Omega\tau)^2\cos\Omega\tau\right. \\ &\quad +\gamma(z_1\sin\Omega\tau + z_2\cos\Omega\tau)\cos\Omega\tau \\ &\quad \left.-\frac{\Omega}{\tilde{e}}\left(x_1 + \frac{\Omega\lambda^2}{a}(z_1\cos\Omega\tau - z_2\sin\Omega\tau)\right)(x_2 + z_1\sin\Omega\tau + z_2\cos\Omega\tau)\sin\Omega\tau\right] \\ \dot{z_2} &= \frac{\epsilon}{\Omega}\left[\frac{d}{\lambda}(x_2 + z_1\sin\Omega\tau + z_2\cos\Omega\tau)^2\sin\Omega\tau\right. \\ &\quad -\gamma(z_1\sin\Omega\tau + z_2\cos\Omega\tau)\sin\Omega\tau \\ &\quad \left.-\frac{\Omega}{\tilde{e}}\left(x_1 + \frac{\Omega\lambda^2}{a}(z_1\cos\Omega\tau - z_2\sin\Omega\tau)\right)(x_2 + z_1\sin\Omega\tau + z_2\cos\Omega\tau)\cos\Omega\tau\right] \end{aligned} \tag{102}$$

The proof of the existence of weak MAWs close to $P = 0$ relies on a series of theorems from J. Hale's monograph [112]. We reproduce the relevant theorems in appendix **??**, and refer to them as the need arises.

Note that the transformation $(\tau, x_1, x_2, z_1, z_2) \to (-\tau, -x_1, x_2, -z_1, z_2)$ leaves the system (102) invariant. So, by definition C.0.1 of appendix **??** the system has the property E with respect to Q, with

$$Q = \mathrm{diag}(-1, 1, -1, 1) .$$

As we are interested only in the solutions with definite parity, we may start the iteration with the vector

$$\vec{X_0} = (0, a_2, 0, a_4) .$$

According to Theorem C.0.4, our solution $z(\tau, \vec{X_0}, \epsilon)$ has the property

$$Qz(-\tau, \vec{X_0}, \epsilon) = z(\tau, \vec{X_0}, \epsilon) ,$$

which means that our solutions are either symmetric or antisymmetric. According to Theorem C.0.5, the second and the fourth determining equations are always zero for this starting vector. For the first and the third determining equations, the zeroth order solution of $\vec{\tilde{X}}$, *i.e.*, $\vec{X}_0$, may be substituted in, and we get

$$k_2 a_2 + \frac{\lambda d}{a}(a_2^2 + \frac{1}{2}a_4^2) = 0 \tag{103}$$

$$\frac{\gamma}{2\Omega}a_4 + \frac{\lambda^2 \Omega a_2 a_4}{2a\tilde{e}} - \frac{d}{\lambda\Omega}\, a_2 a_4 = 0\,. \tag{104}$$

From (104), we have two possibilities: either $a_4 = 0$ or

$$\gamma + a_2\left(\frac{\lambda^2\Omega^2}{a\tilde{e}} - \frac{2d}{\lambda}\right) = 0\,. \tag{105}$$

When $a_4 = 0$, using $\vec{X}_0 = (0, a_2, 0, 0)$ in (102) leads to a trivial constant solution. In the following, we consider only the second case (105). We can solve (103) and (105) for γ and a_4 and prove that the system (102) has periodic solutions. Note that we have three free parameters ϵ, a_2, k_2. But as we will see further, ϵ and a_2 are always combined as ϵa_2 in the first approximation controlling the amplitude and the period of the solution, and the combination will therefore be regarded here as one single free parameter. For general periodic solutions without parity, a_2 can be interpreted as a phase control parameter, *i.e.*, a parameter giving the initial location on the periodic orbit at $\tau = \tau_0$. Here, because we only consider symmetric solutions, the translational symmetry of the autonomous system is broken, and that is the reason why ϵ and a_2 combine into a single parameter. The remaining parameter k_2 can be chosen freely, for example as to satisfy the *consistency condition* (98), which, when the zeroth order solution is substituted, becomes at order (ϵ^2):

$$-\frac{d^2}{4}\,\Omega^2\, a_4^2 + \mu\left(d a_2 + \frac{k_2 a}{\lambda}\right)^2 = 0\,. \tag{106}$$

At zeroth order, $\Omega^2 = \omega_1^2 = 4\mu$ and $\tilde{e} = 4\mu\lambda$. Solving the system of equations (103), (105) and (106), we get

$$\begin{cases} k_2 = -\frac{3\lambda}{a} d a_2 \\ \gamma = \frac{c}{a} a_2 \\ a_4 = \pm 2 a_2 \end{cases}.$$

We can write out the Jacobian for those three equations explicitly:

$$J = \begin{pmatrix} a_2 & 0 & \frac{\lambda d}{a} a_4 \\ 0 & 1 & 0 \\ \frac{2\mu a}{\lambda}(d a_2 + \frac{k_2 a}{\lambda}) & 0 & -\frac{d^2}{2}\Omega^2 a_4 \end{pmatrix}.$$

The determinant of this Jacobian is

$$\det J = \frac{1}{2} d^2 \Omega^2 a_2 a_4 \neq 0\,, \qquad a_2 \neq 0\,.$$

We now invoke theorem C.0.2, reproduced in Appendix A, and conclude our proof that system (77) and (78) has periodic solutions near $P = 0$. We shall show that in this case the periodic solutions contain defects and give their approximate analytic expressions in section 4.5.

4.4.2 Case II

Eigenvalue 0 has only one eigenvector. In this case, we assume that $\frac{\lambda}{a}\tilde{e} + k_1 \neq 0$ to the zeroth order in ϵ, so without loss of generality we can choose $k_2 = 0$. Then $\frac{\lambda}{a}e = \frac{\lambda}{a}\tilde{e} + k_1$. Implementing the transformation $\vec{X} = D\vec{\tilde{X}}$ with

$$D = \begin{pmatrix} 0 & \tilde{e} & 0 & 0 \\ 1 & 0 & 0 & -k_1\omega_1^{-2} \\ 0 & 1 & 1 & 0 \\ 0 & 0 & 0 & 1 \end{pmatrix}$$

we have

$$\frac{d}{d\tau}\vec{\tilde{X}} = M(\omega_1)\vec{\tilde{X}} + \epsilon \begin{pmatrix} -\frac{d}{\tilde{e}}k_1(\tilde{y}+\tilde{z})^2 \\ \frac{1}{\tilde{e}}(\tilde{x} - k_1\frac{\lambda}{\tilde{e}}\tilde{w})(\tilde{y}+\tilde{z}) \\ -\frac{1}{\tilde{e}}(\tilde{x} - k_1\frac{\lambda}{\tilde{e}}\tilde{w})(\tilde{y}+\tilde{z}) \\ -\frac{d}{\lambda}(\tilde{y}+\tilde{z})^2 \end{pmatrix},$$

where

$$M(\omega_1) = D^{-1}AD = \begin{pmatrix} 0 & \frac{\lambda e}{a} & 0 & 0 \\ 0 & 0 & 0 & 0 \\ 0 & 0 & 0 & 1 \\ 0 & 0 & -\omega_1^2 & 0 \end{pmatrix}.$$

As in case I, let $\Omega^2 = \omega_1^2 + \epsilon\gamma$ and perform the same transformation (101) into variables x_1, x_2, z_1, z_2. We then obtain a 4-D system similar to (102). However, in the equation for $\dot{x_1}$, there is an ϵ-free term. In order to use the successive approximation method, further transformations are required. Let $\rho \in \mathbb{R}$ such that $\rho^2 = \epsilon$. With the transformation $x_2 \to \rho x_2, \epsilon \to \rho^2$ we recover the standard form

$$\begin{aligned}
\dot{x_1} &= \frac{\rho\lambda e}{a}x_2 - \rho^2 k_1 \frac{d}{\tilde{e}}(\rho x_2 + z_1\sin\Omega\tau + z_2\cos\Omega\tau)^2 \\
\dot{x_2} &= \frac{\rho}{\tilde{e}}\left[x_1 - k_1\frac{\Omega\lambda}{\tilde{e}}(z_1\cos\Omega\tau - z_2\sin\Omega\tau)\right](\rho x_2 + z_1\sin\Omega\tau + z_2\cos\Omega\tau) \\
\dot{z_1} &= \frac{\rho^2}{\Omega}\left[\frac{-d}{\lambda}(\rho x_2 + z_1\sin\Omega\tau + z_2\cos\Omega\tau)^2\cos\Omega\tau \right. \qquad (107) \\
&\quad +\gamma(z_1\sin\Omega\tau + z_2\cos\Omega\tau)\cos\Omega\tau \qquad (108) \\
&\quad \left. -\frac{\Omega}{\tilde{e}}\left(x_1 - \frac{\Omega\lambda}{\tilde{e}}k_1(z_1\cos\Omega\tau - z_2\sin\Omega\tau)\right)(\rho x_2 + z_1\sin\Omega\tau + z_2\cos\Omega\tau)\sin\Omega\tau\right] \\
\dot{z_2} &= \frac{\rho^2}{\Omega}\left[\frac{d}{\lambda}(\rho x_2 + z_1\sin\Omega\tau + z_2\cos\Omega\tau)^2\sin\Omega\tau \right. \\
&\quad -\gamma(z_1\sin\Omega\tau + z_2\cos\Omega\tau)\sin\Omega\tau \\
&\quad \left. -\frac{\Omega}{\tilde{e}}\left(x_1 - \frac{\Omega\lambda}{\tilde{e}}k_1(z_1\cos\Omega\tau - z_2\sin\Omega\tau)\right)(\rho x_2 + z_1\sin\Omega\tau + z_2\cos\Omega\tau)\cos\Omega\tau\right], \qquad (109)
\end{aligned}$$

The system (108) has the same symmetry as identified in the case I. If we are only interested in solutions with definite parity, we may again start the iteration with $\vec{X_0} = (0, a_2, 0, a_4)$.

To the second order (ρ^2), the determining equations are:

$$a_2\frac{\lambda e}{a} - \rho\frac{da_4^2 k_1}{2\tilde{e}} + O(\rho^3) = 0 \tag{110}$$

$$\rho\frac{\gamma a_4}{2\Omega} - \rho^2\left(\frac{da_2a_4}{\lambda\Omega} + \frac{\lambda\Omega a_2 a_4 k_1}{2\tilde{e}^2}\right) + O(\rho^3) = 0\,. \tag{111}$$

From the second equation we obtain either $a_4 = 0$ (trivial for our purposes, as discussed above) or

$$\gamma - \rho a_2\left(\frac{2d}{\lambda} + \frac{\lambda\Omega^2 k_1}{\tilde{e}^2}\right) + O(\rho^2) = 0\,. \tag{112}$$

If we backtrack the transformations made, it is clear that the *consistency condition* requires that we keep terms up to the fourth order (ρ^4). We find that with the substitution

$$e = \frac{\alpha\omega + \mu}{1+\alpha\beta} + \rho^2(\rho^2\omega_3 - \rho d a_2)\,,$$

where ω_3 is a new parameter, only the fourth or higher order terms are left in the *consistency condition*. From the definition $e = R_0^2 = (\omega - \mu\alpha)/(\beta - \alpha)$ and the above equation, we get $\omega \sim \mu\beta$ and then $e \sim \mu$ to the zeroth order. So $R_0 \sim \sqrt{\mu}$, $q \sim 0$, which means that this solution bifurcates from the HOS $A = \sqrt{\mu}\exp(-i\omega t)$. To the leading order ($\rho^4$), we are allowed to use the following substitutions in the *consistency condition* (98):

$$a_2 \to 0 \quad \omega \to \mu\beta \quad \Omega \to \sqrt{-\frac{2\mu(1+\alpha\beta)}{1+\alpha^2}},$$
$$k_1 \to \frac{\mu\lambda}{a}\left(1 + \frac{2\lambda(1+\alpha\beta)}{1+\alpha^2}\right) \quad \tilde{e} \to -\frac{2\mu\lambda(1+\alpha\beta)}{1+\alpha^2}\,. \tag{113}$$

The resulting equation is of a relatively simple form:

$$a_4^2(-\lambda + d^2(1+\alpha\beta)(1+\alpha^2+\lambda+\lambda\alpha\beta)) + 4(1+\alpha\beta)^2\lambda\mu\omega_3 = 0\,. \tag{114}$$

From (110) it follows that a_2 is of order ρ, and from (112) that $\gamma \sim O(\rho^2)$. After a change of variable $a_2 = \rho\, a_{22}$ and keeping only the highest order for the equations, we can rewrite (110) and (112) as

$$a_{22}\frac{\lambda e}{a} - \frac{k_1 d a_4^2}{2\tilde{e}} = 0\,, \tag{115}$$

$$\gamma = 0. \tag{116}$$

For $e, \tilde{e}, k_1$ we use the values in (113). From (115), (116) and (114), we can solve for a_{22}, γ, ω_3. The Jacobian of those equations is

$$J = \begin{pmatrix} \frac{\lambda e}{a} & 0 & 0 \\ 0 & 1 & 0 \\ 0 & 0 & 4(1+\alpha\beta)^2\lambda\mu \end{pmatrix},$$

So, $\det J = 4(1+\alpha\beta)^2\lambda^2\mu e/a \neq 0$ for $1+\alpha\beta \neq 0$. According to Theorem C.0.2, we have proved that equations (77) and (78) possess periodic solutions.

4.5 Analytic form of periodic solutions, stability analysis and numerical tests

We have proved in the preceding section the existence of symmetric periodic solutions in case I and II. In both cases, a small parameter ϵ or ρ ensures the convergence of successive approximations. However, we did not give a bound on the allowable value of this parameter, nor did we show that the solutions which we obtain are the ones observed in numerical simulations. In this section we give the approximate analytical form of periodic solutions. We compare them with direct numerical integration of the CGLe in case II.

The solutions are shown to be independent of λ to order ϵ in case I and to order ϵ^2 in case II. In addition, these solutions should also satisfy the $3-d$ ODE mentioned in section 4.2 which do not contain λ, so they can be matched with the solutions of the $3-d$ system in a unique way, independent of the value of λ. Hence, we conclude that to all orders the physical solutions are identical for the two values of λ.

The two cases are taken separately. In this section, we reinstate x as the spatial variable, $R = R(x)$.

4.5.1 Case I

Using (82), (99) and the case I calculations of the preceding section, we have after some algebra:

$$\begin{aligned} R^2 &= -2\epsilon d a_2 (1 \pm \cos \Omega x) \\ \phi_x &= -\frac{\epsilon a_2}{2(1+\alpha^2)\Omega} \frac{\sin 2\Omega x \pm 2 \sin \Omega x}{1 \pm \cos \Omega x} . \end{aligned} \tag{117}$$

To the first order of ϵ, R and ϕ_x are independent of λ. The $\pm$ sign selects two solutions which transform into each other by translating a half period. This is reminiscent of the spatial translation invariance in the symmetric solution space. From the definitions of e, Ω and from (100), (95), we get to the first order:

$$\begin{aligned} \omega &= \mu\alpha - 3\epsilon a_2 \\ \omega_1^2 &= 4\mu + \frac{6\epsilon d a_2}{1+\alpha^2}(\alpha\beta + 2\alpha^2 + 3) \\ \Omega &= \omega_1 + \frac{\epsilon\gamma}{2\omega_1} . \end{aligned} \tag{118}$$

We see that ω and Ω are independent of λ. On the other hand, for periodic boundary conditions, we can use Fourier modes directly to transform the PDE (70) to a finite set of approximate ODE's by Galerkin truncation. Then the stationary solution can be obtained by solving a set of nonlinear algebraic equations.

4.5.1.1 Numerical comparison

If we take as an example the following parameter values (previously used in [161]) for which defect chaos is expected (in the thermodynamic limit):

$$\alpha = 1.5, \quad \beta = -1.2$$

and fix the size of the domain to $L = 24$, then at $\mu = 0.072644$, $\omega = 0.097879$, a periodic solution of period $L/2$ is found. This solution has $R_{max} \simeq 0.0750$. On the other hand, if we use the same α, β, μ and search for $R_{max} \simeq 0.075$ by adjusting ϵ (we always keep $a_2 = 1$), we find that

$$\epsilon \sim 0.00380, \quad \omega = 0.097566, \quad \text{period } \frac{2\pi}{\Omega} = 12.0102\,.$$

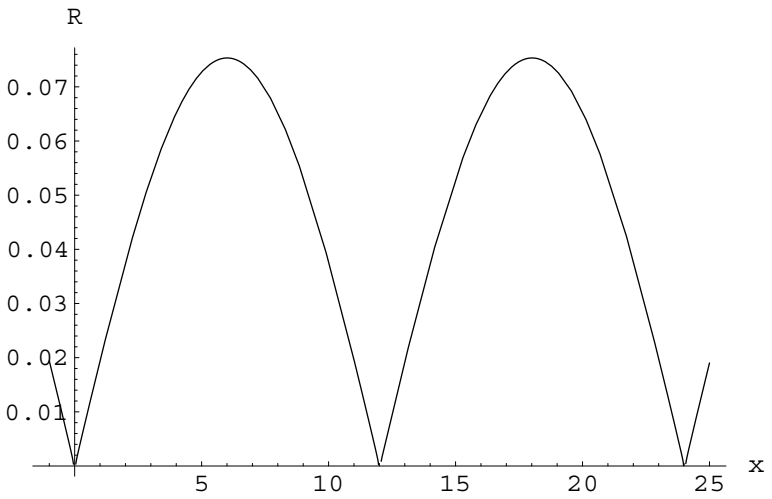

Figure 10: Spatial profile of the amplitude $R(x)$ from (117) at $\mu = 0.07264$, with $R_{\mathsf{max}} = 0.075$.

The approximate analytic solution and the numerical solution of the exact CGLe agree very well. The profile of R from our successive approximation is shown in Fig. 10.

4.5.1.2 Analytic structure near the defect

It is easy to see from (117) that only $\epsilon a_2 > 0$ is the physically interesting combination. However, we may wonder whether it is really true that $R^2 = dP + e$ remains non-negative everywhere while touching zero at isolated points. Fig. 10 and the first equation of (117) suggest a positive answer to this question. But since we have only an approximate solution, further justification is needed. Suppose at some instant x_0, we have $dP + e = 0$ on the periodic orbit. From the *consistency condition* (98), at this transition point

$$\frac{d^2(1+\alpha^2)}{4} Q^2 + \left(\frac{a}{\lambda}\tilde{N} - \lambda Q\right)^2 = 0,$$

so, $Q = \tilde{N} = 0$. According to (94), $\dot{\tilde{M}} = 0$ and $\dot{P} = 0$. Assume that $\dot{Q} = 0$, then $\dot{\tilde{N}} \neq 0$ since the transition point is not an equilibrium. At next instant $x_0 + \delta x$, the *consistency*

condition can not be satisfied as the two sides of (98) have different orders of δx. So we conclude that $\dot{Q} \neq 0$ at the point x_0, which means that $Q(x_0+\delta x)$ has negative sign to that of $Q(x_0-\delta x)$. Thus, after touching the zero value hyper-plane, $dP+e$ returns to the positive half space again. The turning happens exactly on the $dP+e=0$ plane. We claim that $dP+e \geq 0$ always holds and the equality holds periodically for the periodic orbit under consideration. From (117), in the neighborhood of $R=0$ at $x=x_0$ on the periodic orbit, R behaves like

$$R \sim \left(\frac{d\dot{Q}}{2}\right)^{1/2} |x-x_0|\,,$$

and is manifestly a non-analytic function of x.

We do not discuss the stability of the solutions in case I, as this has already been accomplished by Takáč [244] who has proven that these solutions are unstable.

4.5.2 Case II

To the first order of ϵ, the solutions are

$$\begin{cases} x_1 &= -\frac{\epsilon k_1 a_4^2}{8\tilde{e}^2\Omega}(2d\tilde{e}+\lambda k_3)\sin 2\Omega x \\ x_2 &= \epsilon(a_2^2 - \frac{\lambda k_1 a_4^2}{4\tilde{e}^2}\cos 2\Omega x) \\ z_1 &= -\frac{\epsilon a_4^2}{12\tilde{e}^2\lambda\Omega^2}(3(3d\tilde{e}^2+\lambda^2\Omega^2 k_1)\sin\Omega x + (d\tilde{e}^2-\lambda^2\Omega^2 k_1)\sin 3\Omega x) \\ z_2 &= a_4 + \frac{\epsilon a_4^2}{12\tilde{e}^2\lambda\Omega^2}(3(\lambda^2\Omega^2 k_1 - d\tilde{e}^2)\cos\Omega x + (\lambda^2\Omega^2 k_1 - d\tilde{e}^2)\cos 3\Omega x)\,, \end{cases}$$

where $\epsilon=\rho^2>0$, and a_4 is a free parameter. In the following, we will see that ϵ and a_4 always emerge in the combination $\epsilon\, a_4$ for physical quantities. To the second order, ω is

$$\omega = \mu\beta + \frac{\epsilon^2 a_4^2}{4\mu(1+\alpha^2)}\left(\frac{1+\alpha\,\beta}{\beta-\alpha}+\frac{\beta-\alpha}{1+\alpha\,\beta}\right).$$

It is independent of λ, and therefore e, b, Ω are also independent of λ. R and ϕ_x can also be calculated to the second order:

$$\begin{aligned} R^2 &= -\frac{d^2}{2\mu}(\epsilon a_4)^2 + d\epsilon a_4\cos\Omega x + \frac{d(\epsilon a_4)^2}{12\Omega^2}\left(\frac{c}{a}+\frac{e}{b}\right)\cos 2\Omega x + e \qquad (119)\\ \phi_x &= \frac{\epsilon a_4}{\mu\Omega(1+\alpha^2)}\left[e\sin\Omega x - \frac{\epsilon a_4}{24\Omega^2}\left(6d\Omega^2+\frac{7e^2}{a\Omega^2}+\frac{7ce}{a}\right)\sin 2\Omega x\right] \end{aligned}$$

So clearly R and ϕ_x are independent of λ. Similarly, the different signs of a_4 will give the same solution up to a half-period translation. This solution is the one observed in the numerics when passing the Eckhaus instability for underlying wavevector $q=0$. Linear stability analysis reveals [171] that the $q=0$ state, the most stable state under the long wavelength perturbations, becomes unstable when the size of the system is such that the smallest possible nonzero wavenumber k satisfies

$$k^2 < -\frac{2\mu(1+\alpha\beta)}{1+\alpha^2} \equiv \kappa^2\,.$$

It is easy to see that $\kappa^2 = \omega_1^2$ up to order (ρ^4).

For our parameter choices $\mu = 1, \alpha = 1.5, \beta = -1.2$, the bifurcation size of the system is $L_0 = \frac{2\pi}{\kappa} = 8.95492$. In the following, we will first prove the stability of our solutions near the bifurcation point. Then we will compare them with the stable solutions observed in numerics.

4.5.2.1 Stability analysis

Assume that $A = R\exp(i\phi)$ where $R, \phi \in \mathbb{R}$ is an exact solution of (70). The perturbed solution is assumed to be $\bar{A} = (R + r)\exp i(\phi + \theta)$, where $r, \theta \in \mathbb{R}$ is the perturbation on the amplitude and phase, separately. Substitute it into (70), keeping only the linear terms in r and θ. We have

$$\begin{aligned} r_t &= (\mu - \phi_x^2 - \alpha\phi_{xx} - 3R^2)r + r_{xx} - 2\alpha\phi_x r_x \\ &\quad -(2R\phi_x + 2\alpha R_x)\theta_x - \alpha R\theta_{xx} \qquad (120) \\ R\theta_t &= (\omega - \alpha\phi_x^2 + \phi_{xx} - 3\beta R^2)r + \alpha r_{xx} + 2\phi_x r_x \\ &\quad +(2R_x - 2\alpha R\phi_x)\theta_x + R\theta_{xx}\,, \qquad (121) \end{aligned}$$

where in (121) we have used $\phi_t = -\omega$. To study the stability of the starting solution A, we treat these equations as an eigenvalue problem for a two-component vector, *i.e.*, we let $r_t = \sigma r$, $\theta_t = \sigma\theta$ and investigate the spectra σ of the linear operator resulting from (120) and (121) in the C^1 continuous periodic function space. As the CGLe has global phase invariance, the eigenvalue equations always have solution $(r, \theta) = (0, \theta_0)$ with eigenvalue $\sigma = 0$. At the same time, spatial translational invariance implies that another eigenmode has $\sigma = 0$. As a result, saying that the solution is stable means that it is stable up to a phase and a spatial translation, and that all other eigenmodes have eigenvalues with negative real parts.

Invoking the expression for R, ϕ_x to the second order of ϵ, the coefficients of various terms of r, θ and their derivatives in (120) and (121) become explicit functions of x. The resulting linear operator on (r, θ) has even parity due to the symmetry of our solution, and we can consider the even and odd modes of r, θ separately. If we set $\epsilon = 0$, i.e., the starting state A is a plane wave state, then $\cos(n\Omega x)$ and $\sin(n\Omega x)$ are the eigenfunctions of the unperturbed linear operator. They give the stability spectrum of the plane waves. Now, let us move a little (to the order of ϵ) beyond the bifurcation point. The eigenfunctions are still $\cos(n\Omega x)$ and $\sin(n\Omega x)$ up to ϵ corrections. For example, if the even solutions are considered first, we assume that to the first order the eigenfunctions are (the time dependence for r, θ has been suppressed):

$$\begin{aligned} r &= m_1\cos(n\Omega x) + \epsilon(m_0\cos((n-1)\Omega x) + m_2\cos((n+1)\Omega x)) \qquad (122) \\ \theta &= n_1\cos(n\Omega x) + \epsilon(n_0\cos((n-1)\Omega x)) + n_2\cos((n+1)\Omega x))\,, \qquad (123) \end{aligned}$$

where n is a non-negative integer. Note that we do not include the terms such as $\epsilon^2\cos((n \pm 2)\Omega x)$ in the above expressions because they induce corrections of order ϵ^3 or higher in the eigenvalues. Now if we substitute (122) and (123) into the eigenvalue equations and identify the coefficients of $\cos(n\Omega x), \cos((n-1)\Omega x)$ and $\cos((n+1)\Omega x)$, a set of six homogeneous

linear equations for $m_0, m_1, m_2, n_0, n_1, n_2$ can be derived. The determinant of the coefficient matrix will give an eigenvalue equation for σ. The resulting expression is too complicated to merit being displayed here.

Before bifurcation, the HOS is stable. The first instability occurs for $n = 1$ mode, one eigenvalue of which is very close to 0 near the bifurcation point, being negative before and positive after. Meanwhile, for $n > 1$ modes, the corresponding eigenvalues have negative real parts bounded away from zero. As the bifurcating solution emerges continuously from the HOS, near the bifurcation point ($\epsilon \ll 1$) the perturbed linear operator has all the eigenvalues with negative real parts away from 0 for $n > 1$ and one eigenvalue close to 0 for $n = 1$. So, we only need to check the stability of our solutions for $n = 1$.

For convenience, we can fix parameters α and β to any values allowed by (97) and perform the above stability analysis of the solution.

The numerical values we used are $\mu = 1.0, \alpha = 1.5, \beta = -1.2, a_4 = 1$. The eigenvalue equation is then

$$\begin{aligned} 7.9860\epsilon^2\sigma + (56.423 - 63.394\epsilon^2)\sigma^2 + (82.564 - 75.135\epsilon^2)\sigma^3 \\ +(45.022 - 28.859\epsilon^2)\sigma^4 + (10.923 - 4.3059\epsilon^2)\sigma^5 \\ +(1.0 - 0.18864\epsilon^2)\sigma^6 \quad = \quad 0\,. \end{aligned}$$

$\sigma = 0$ corresponds to the neutral mode associated with the global phase invariance. All others solutions have negative real parts. The $\sigma_- = -0.14154\epsilon^2$ solution is the interesting one. If we use the same parameter values to calculate the stability of the HOS, the eigenvalue equation for $n = 1$ is

$$\epsilon^2(-0.21122 - 0.26402\sigma) + 2.98462\sigma + \sigma^2 = 0\,.$$

To the second order in ϵ, we have $\sigma = -2.98462 - 0.19325\epsilon^2$ or $\sigma_+ = 0.07077\epsilon^2$. The later positive eigenvalue indicates that the plane wave solution is not stable. We note that $2\sigma_+ = -\sigma_-$ to order ϵ^2 which indicates a supercritical pitchfork bifurcation. We have proved that this equality holds exactly at the bifurcation point for any values of α and β, and this justifies the above numerical checks. Under perturbation the HOS will evolve to the modulated amplitude solution given above. When the instability is saturated, the corresponding eigenvalue for the MAW is negative. If we change the sign of a_4 or use the other value of λ, the eigenvalue does not change, as expected.

If we alternatively consider the odd-parity function space $\{\sin(n\Omega x)\}_{n\in\mathbb{N}}$, we obtain the following eigenvalue equation:

$$\begin{aligned} (28.2115 - 33.6568\epsilon^2)\sigma + (27.1763 - 21.2703\epsilon^2)\sigma^2 + (8.92308 - \\ 4.04125\epsilon^2)\sigma^3 + (1 - 0.19287\epsilon^2)\sigma^4 = 0\,. \end{aligned}$$

This equation is quartic because for $n = 1$ only two modes $\sin\Omega x$ and $\sin 2\Omega x$ are used. Now $\sigma = 0$ corresponds to the neutral mode associated with the spatial translation of the CGLe. Other eigenvalues of the equation have negative real parts bounded away from 0.

To summarize, our solution is stable in the whole phase space of the CGLe, up to a phase and a spatial translation.

In ref [135], B. Janiaud *et al.* have investigated the stability of traveling waves near the Eckhaus instability in Benjamin-Feir stable regime. They derived a necessary condition for the bifurcation to be supercritical and located the corresponding regions as two strips in the α, β parameter space. We have studied the stationary MAWs in the Benjamin-Feir unstable regime and found that the bifurcation from the HOS to MAWs is always supercritical, even when parameter values lay outside of the region given in ref [135].

In ref [190], application of the perturbation method to the zeroth order (ϵ^0) equation gave nonzero eigenvalue $\lambda_0 = 2/\beta$. This can not be correct since the zeroth order equation just gives the stability of the unstable HOS. Furthermore, in the Galerkin projection calculation in [190], somewhat surprisingly the $N = 1$ truncation was found to give a better result than the $N = 2$ truncation. In our case, if we used only the first order expressions for R, ϕ_x in (120) and (121), we could not get the correct eigenvalues even near the bifurcation point, and thus are absolutely forbidden to extend the result to the next bifurcation.

4.5.2.2 Comparaison with numerical integration of the CGLe

In our numerical simulations we employed a pseudo-spectral method to evolve equation (70) using 128 modes. For system size $L < L_0$, we always recover the HOS ($q = 0$). For L slightly larger than L_0, however, the solution relaxes to the modulated amplitude solution (119) for any smooth initial condition we have tried. Figure 11 compares the stable steady solutions obtained by the two methods.

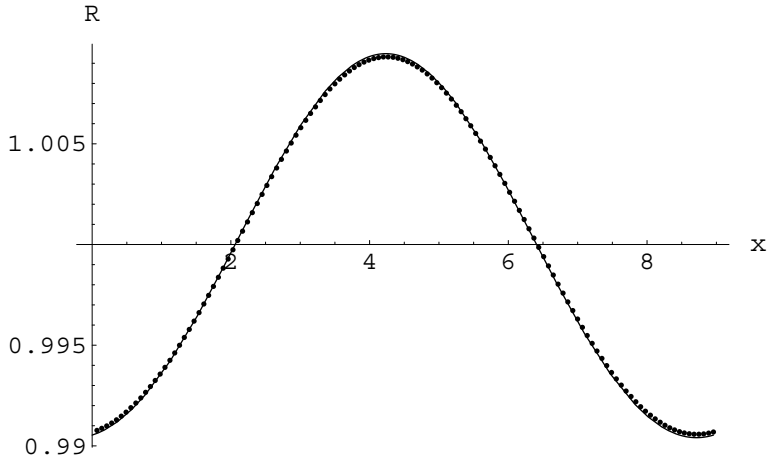

Figure 11: Spatial profiles of the amplitude R for $\mu = 1, \alpha = 1.5, \beta = -1.2, L = 8.958$ from numerical simulation (dots) and the approximate solution (119) (solid line). The agreement is good, with the discrepancy mainly due to the long relaxation time close to the bifurcation point.

4.6 Summary

After reviewing the basic properties of the 1-d CGle, we reformulated the equation for its stationary solutions as a fourth-order ODE for a variable P that can be interpreted as the

modulation of the amplitude squared of a plane wave solution. This reformulation enabled us to prove the existence of stationary MAW solutions in the two limit cases corresponding to the bifurcation of the trivial solution $A = 0$ (case I), and to the bifurcation of the plane wave solution of zero wavenumber (case II).

We proved the stability of MAW solutions for the full CGLe in a finite box with periodic boundary conditions in case II near the onset of plane wave instability. We tested our analytical results by comparison of numerical integrations of the full CGLe with our approximate analytical solutions.The MAWs continue to exist when the size L is increased. In case I, unstable periodic hole solutions were shown to exist. This could not be inferred from any phase equation: around the defect point $A = 0$, the amplitude behaves non-analytically, namely piecewise affinely, and the phase is not defined.

The analysis of MAWs bifurcating from a plane wave with wavenumber $0 < q < 1$ should be similar to the study of case II. It would be interesting to study the higher order instabilities of MAWs when the system size is increased beyond the region in which our analysis takes place. It has been observed that stationary symmetrical MAWs bifurcate into uniformly-propagating asymmetrical ones via a drift-pitchfork bifurcation. This happens when L is increased as a consequence of the growth of the amplitude of the modulation, and the increase of the spectral richness of the MAW solution. Moreover, MAWs are expected to be the building blocks of phase turbulence, and the analytical analysis of their global stability may lead to a characterization of the suspected transition between phase and defect chaos in the CGLe [**?**, **?**].

CHAPTER V

$1-D$ KURAMOTO-SIVASHINSKY EQUATION AND ITS STEADY SOLUTIONS

The $1-d$ Kuramoto-Sivashinsky equation (KSe) is one of the simplest nonlinear PDEs that exhibit spatiotemporal chaos. As we will show, its asymptotic dynamics is equivalent to a finite set of ODEs, even in the chaotic regime. The study also helps us understand the phase dynamics of the CGLe discussed in chapter 4. In this chapter we discuss basic properties and the steady solutions of the KS equation. After deriving the KSe as a phase description of the CGLe in sect. 5.1, we present some of its properties under the periodic boundary condition in sect. 5.2. In sect. 5.3, we concentrate on the steady solutions of the KSe. In addition to reviewing others' work, we numerically determined the steady solutions most relevant to the phase space dynamics. They will be used in the calculation of periodic orbits in the next chapter.

5.1 Derivation

The KS equation is a generic equation that describes the evolution of the phase of coupled oscillating systems near the onset of spatial instability. Here we take the CGLe (70) as an example and derive the KSe near the onset of first spatial instability. Consider perturbations on the homogeneous oscillating state, *i.e.*, let $A(x,t)$ take the form

$$A(x,t) = (1+\rho(x,t))e^{i(-\beta t+\phi(x,t))}\,. \tag{124}$$

Substituting (124) into the CGLe (with $\mu = 1$), we get the exact evolution equation for $\rho(x,t)$ and $\phi(x,t)$,

$$\rho_t = -2\rho - 3\rho^2 - \rho^3 + \rho_x - \alpha(1+\rho)\phi_{xx} - 2\alpha\rho_x\phi_x - (1+\rho)(\phi_x)^2\,, \tag{125}$$

$$\begin{aligned}(1+\rho)\phi_t &= -2\beta\rho - 3\beta\rho^2 - \beta\rho^3 + \alpha\rho_{xx} + (1+\rho)\phi_{xx} \\ &\quad +2\rho_x\phi_x - \alpha(1+\rho)(\phi_x)^2\,.\end{aligned} \tag{126}$$

For small perturbations, we only need to retain linear terms in (125), (126), and thus are able to use the Fourier modes to study the stability. Let

$$\begin{aligned}\rho(x,t) &= \rho_0 e^{i(\omega t-kx)} \\ \phi(x,t) &= \phi_0 e^{i(\omega t-kx)}\,,\end{aligned}$$

and by substituting them into the linear equations for ρ and ϕ, we get the relation

$$\begin{aligned}(i\omega + 2 + k^2)\rho_0 - \alpha k^2\phi_0 &= 0 \\ (2\beta + \alpha k^2)\rho_0 + (i\omega + k^2)\phi_0 &= 0\,,\end{aligned} \tag{127}$$

which implies

$$i\omega = -(1+k^2) \pm \sqrt{1-2\alpha\beta k^2 - \alpha^2 k^4}\,.$$

One solution always has negative real part which is stable and the other solution may change the sign of the real part under system parameter changes. The latter one induces spatial instability and its dispersion relation for small k becomes

$$i\omega = -(1+\alpha\beta)k^2 - \frac{1}{2}\alpha^2(1+\beta^2)k^4 + O(k^6)\,, \tag{128}$$

which implies that the long wavelength modes become unstable first and evolve very slowly (at a time scale $1/t \sim (1+\alpha\beta)k^2$). To the lowest order, the phase thus satisfies a diffusion equation

$$\partial_t \phi = \nu \nabla^2 \phi\,, \tag{129}$$

with $D = 1+\alpha\beta$. If $D > 0$ (the so-called Benjamin-Feir-Newell criterion), the phase will tend to be spatially uniform and the asymptotic state is the homogeneously oscillating state. If $D < 0$, (129) leads to unphysical blow-ups so higher order and nonlinear terms should be included to saturate the instability. Comparing the relative size of each term in (125) and (126) at the onset of instability, we find that in (125), -2ρ on the right hand side implies a fast decay of ρ and thus ρ is small and slaved to the gradient of ϕ. From (127), we see that

$$\frac{\rho_0}{\phi_0} \approx \frac{|\alpha|}{2}k^2\,, \tag{130}$$

which shows $\rho_0 \to 0$ as $k \to 0$, as argued above. In view of (130) and (128), near the onset of spatial instability, the scalings are like

$$x \sim \epsilon\,,\ t \sim \epsilon^2\,,\ \phi \sim 1\,,\ \rho \sim \epsilon^2\,.$$

Inserting into (127) and equating the terms of order ϵ^2, we get

$$\begin{aligned} 0 &= -2\rho - \alpha\phi_{xx} - (\phi_x)^2 \\ \phi_t &= -2\beta\rho + \phi_{xx} - \alpha(\phi_x)^2\,, \end{aligned}$$

or

$$\phi_t = D\phi_{xx} + \lambda(\phi_x)^2\,, \tag{131}$$

where $\lambda = \beta - \alpha$. Crossing the BFN instability, (131) becomes unstable and we have to retain higher order terms to stabilize it. The simplest choice is to include the fourth order term in (128) and we find that

$$\phi_t = D\phi_{xx} + \lambda(\phi_x)^2 - \mu\phi_{xxxx}\,, \tag{132}$$

where $\mu = \frac{1}{2}\beta^2(1+\alpha^2)$. To be consistent with the scaling relation, the fourth and the second order terms must have comparable size, which means $D \sim k^2$ and thus implies that (132) holds near the onset of instability and in the limit of large system size. In practice, (132) and its variants hold under less restrictive conditions and are able to describe the time evolution of a spatially extended system in quite large parameter range. In the following we are interested in the case where $D < 0$.

5.2 Basic Properties

The KS equation was initially derived as a phase equation by Kuramoto and Tsuzuki for a system of reaction-diffusion equations [153]. Sivashinsky derived it independently in the context of small perturbations of unstable flame fronts [228]. The equation also describes falling films on an inclined surface [229, 17], interfacial instability between two concurrent viscous fluids [127] and unstable drift waves in plasmas [38, 207]. By rescaling t, x and u in (132), we obtain

$$u_t = (u^2)_x - u_{xx} - \nu u_{xxxx}\,, \tag{133}$$

where ν is a viscosity-like parameter which controls the rate of dissipation in the system. The first term on the right of (133) is the nonlinear convection term which induces interaction between different Fourier modes. In average, it transfers energy from the low wavenumber modes to higher ones. The second term is an anti-diffusion term which pumps energy to the system and makes it unstable. The last term dissipates energy and stabilizes the system.

5.2.1 Symmetry and Fourier modes

Eq (133) is space and time translationally invariant. It also preserves antisymmetric solutions, *i.e.*, if $u(x,0) = -u(-x,0)$, then $u(x,t) = -u(-x,t)$ for any $t > 0$. It is Galilean invariant, *i.e.*, if $u(x,t)$ is a solution, then $c + u(x + 2ct, t)$ with c an arbitrary constant, is also a solution.

We will study (133) in a periodic interval of size L. L will be used as the control parameter with ν fixed. In the literature the renormalized length $\tilde{L} = \frac{L}{2\pi\sqrt{\nu}}$ is also used as the bifurcation parameter. In view of the periodic boundary condition $u(x,t) = u(x+L,t)$, we expand $u(x,t)$ in Fourier modes,

$$u(x,t) = \sum_k a_k(t) e^{ikqx}\,, \tag{134}$$

where $a_k \in \mathbb{C}$ and $q = 2\pi/L$ is the basic wavenumber. The reality of u implies that $a_k^* = a_{-k}$. Eq (133) then takes the form

$$\dot{a_k} = [(kq)^2 - \nu(kq)^4]a_k + ikq \sum_{m=-\infty}^{\infty} a_{k-m}a_m\,, \tag{135}$$

where $\dot{a_k}$ denotes the time derivative of a_k. Note that $\dot{a_0} = 0$, so a_0 is a conserved quantity. By Galilean invariance, we may set $a_0 = 0$ without loss of generality.

From (135), we see that the origin $u(x,t) \equiv 0$ has Fourier modes as the stability eigenvector and at most a finite of them are unstable. See in figure 12 how the linear eigenvalue depends on the wavenumber. Considering that this dependence is an even function of the wavenumber, we only show the positive part. It is easy to see that when $|kq| \in (0, 1/\sqrt{\nu})$, the corresponding Fourier modes are unstable. The most unstable modes has $|kq| = 1/\sqrt{2\nu}$ and defines the scale of basic building blocks of the spatiotemporal dynamics of the KSe in large system size limit as shown later. In a periodic box, as the set of wavenumbers is discrete, finite gaps exist between different eigenvalues and the gap increases quickly with the increase of wavenumbers. Based on this special spectral structure, various properties of the KSe are derived [245].

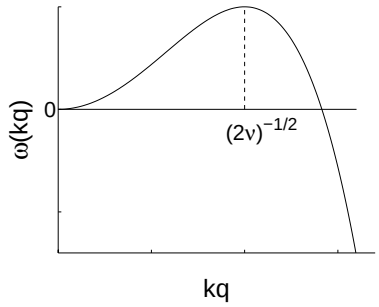

Figure 12: The stability eigenvalue of $u(x,t) \equiv 0$ versus the wavenumber kq.

5.2.2 Origin is the global attractor for small L

For L small enough, as shown above, all the Fourier modes become linearly stable so the origin is a local attractor. In fact, for $L < 2\pi\sqrt{\nu}$, we show that $u(x,t) = 0$ is also a global attractor. We denote the integral of a function A over $[0, L]$ by $\langle A \rangle$, *i.e.*,

$$\langle A \rangle = \int_0^L A(x,t)\, dx\,.$$

Multiplying both sides of (133) by $u(x,t)$ and then integrate, we have

$$\frac{1}{2}\langle u^2 \rangle_t = \frac{2}{3}\langle (u^3)_x \rangle - \langle u u_{xx} \rangle - \nu \langle u u_{xxxx} \rangle = \langle u_x^2 \rangle - \nu \langle u_{xx}^2 \rangle\,, \tag{136}$$

since $\langle (u^3)_x \rangle = 0$ due to the periodic boundary condition. For the same reason the partially integrated parts equal to zero. $\langle u \rangle_t$ means taking derivative with respect to time. Substitute (134) into the right hand side of (136), we get

$$\frac{1}{2}\langle u^2 \rangle_t = \sum_{k=-\infty}^{\infty} |a_k|^2 (kq)^2 (1 - \nu (kq)^2)\,. \tag{137}$$

It is easy to see that when $L < 2\pi\sqrt{\nu}$, each term on the right hand side of (137) is less than or equal to 0. So in this case, we conclude that

$$\langle u^2 \rangle_t \leq 0$$

$' ='$ holds only for $u \equiv 0$. When $u \not\equiv 0$, $\langle u^2 \rangle_t < 0$, so $\langle u^2 \rangle$ keeps decreasing, the solution to (133) approaching $u(x,t) = 0$. So we have proved that the origin is a global attractor when $L < 2\pi\sqrt{\nu}$.

5.2.3 Inertial manifold

When L is large (or infinite), near the laminar solution $u(x,t) = 0$, a band of Fourier modes with wave numbers $|kq| < 1/\sqrt{\nu}$ are unstable with the observed patterns dominated by the most unstable mode, with $|kq| = 1/\sqrt{2\nu}$. Away from $u = 0$, the instability of these lower modes is balanced by the collective action of all the modes through the nonlinear

convection term $(u^2)_x$, not like in the CGLe case where the stability is saturated by the nonlinear "diagonal terms" of the form $a_n \Sigma_k a_k^* a_k$ [40].

It has been shown that the solution $u(x,t)$ is analytic in x at any time $t > 0$ if $u(x,0)$ is analytic, and thus the amplitudes of the high k modes decay at least exponentially [39]. In fact, an absorbing ball $\mathscr{B}$ exists such that all trajectories will be contained in it after a finite time interval depending on the initial conditions. The ω-limit set of $\mathscr{B}$ is thus the global attractor in the infinite-dimensional phase space of the KSe. The strong damping of the higher modes exerted by the super-viscosity term u_{xxxx} produces a finite-dimensional invariant manifold Σ which is compact and attracting. With these properties, it has been named *inertial manifold* [85, 86, 245]. All solutions converge exponentially to Σ and therefore Σ contains the global attractor. Σ acts like a global center manifold and a finite number of Fourier modes are enough to pin it down. The rest higher modes are contained in the geometrical constraints that define Σ [192]. Various numerical procedures have been proposed to approximate inertial manifolds [84].

Though the fractal dimension of the global attractor and the inertial manifold can be rigorously estimated $d(X) \leq 1 + \text{const}\, \nu^{9/40} \tilde{L}^{3/2}$ (see ref. [132] and references therein), it is generally believed that in an extended system the fractal dimension grows linearly with the system size [214, 239, 74]. In practice, people tend to use much fewer modes to do the simulation than given by the above estimate. When restricted to the inertial manifold, the flow of the KSe is equivalent to that of a finite set of ODEs. In this sense, the KSe is accessible by the "low-dimensional" dynamical system analysis. In practice, we get the set of ODEs that define the dynamics on the inertial manifold by substitute the approximate constraint equations into the equations of motion of lower Fourier modes [246].

5.3 Steady solutions of the KSe

Though the KS equation is a nonlinear PDE and exhibits spatiotemporally chaotic behavior when the system size is big enough, it shows characteristics of low-dimensional dynamics, which is analytically justified by the study of inertial manifolds. From the trivial state $u \equiv 0$ towards the onset of the chaotic behavior, the system experiences a series of bifurcations in which steady solutions play an important role and set up the scale of the building blocks of spatiotemporal chaos. In certain parameter range, the steady solutions are directly related to the observed dynamics. For example, the n-cell state [91] is stable at discrete windows for arbitrary large system size. Another example is the localized near-solitory waves observed in experiments and numerical simulation [33]. These highly-separated waves are not stable and their evolution is governed by the weak interaction originating from the exponential tails of their profiles.

Equilibria are the simplest invariant sets in the phase space, their distribution and the connections between them form the coarsest geometrical frame for organizing phase space orbits [103]. The steady solutions of the KSe satisfies

$$(u^2)_x - u_{xx} - \nu u_{xxxx} = 0\,.$$

We can integrate once to get

$$u^2 - u_x - \nu u_{xxx} = c\,, \tag{138}$$

where c is an integration constant. Its value determines the property of solutions of (138). In the following calculation, without loss of generality we may set $\nu = 1$.

Written in the form of a $3-d$ dynamical system, (138) becomes

$$\begin{aligned} u_x &= y \\ y_x &= w \\ w_x &= u^2 - y - c\,. \end{aligned} \tag{139}$$

It is clear that the flow defined by (139) is volume preserving. Notice that the system has the time reversal symmetry,

$$x \to -x, \quad u \to -u, \quad y \to y, \quad w \to -w\,.$$

From (139), we see that

$$(u+w)_x = u^2 - c\,.$$

Therefore, if $c < 0$, $u+w$ increases without bounded with $x \to \infty$. Every solution escapes to infinity and (139) has no bounded solutions. If $c = 0$, the origin $(0,0,0)$ is the only bounded solution. Other solutions go to infinity when $x \to \infty$ and/or $x \to -\infty$. If $c > 0$, interesting dynamics may happen and depending on the value of c, the set of bounded solutions can be extremely complicated. In the following, we only discuss this case. Again, the dynamics of (139) is organized at the coarsest level by its own equilibria and possible connections between them.

When $c > 0$, system (139) has two stationary points $c_+ = (\sqrt{c}, 0, 0)$ and $c_- = (-\sqrt{c}, 0, 0)$. Linearizing the flow around c_+, we obtain the stability eigenvalues $2\lambda_1\,, -\lambda_1 \pm i\lambda_2$ with

$$\lambda_1 = \frac{1}{\sqrt{3}} \sinh\phi,\ \ \lambda_2 = \cosh\phi\,,$$

where $\sinh 3\phi = 3\sqrt{3c}$. So, c_+ has a $1-d$ unstable manifold and a $2-d$ stable manifold along which solutions spiral in. Because of the time reversal symmetry, c_- has similar manifolds with reversed stability properties. The escaping orbits still dominate and it can be shown that the escaping orbits take up a large subset in the phase space [23]. This creates great trouble for numerical calculation as most of the orbit will escape even near a compact invariant set. Bisection technique is used by the early authors [128] and evolves into straddle-saddle scheme later on [195, 185]. All these methods involve the time and effort consuming evolving-refining procedures. To efficiently locate important compact solutions, the variational technique developed in [156] shows its strength as we will show later.

5.3.1 Heteroclinic and homoclinic Connections

It is well known that equation (138) has an exact heteroclinic solution

$$u = a_1 \tanh(kx) + a_2 \tanh^3(kx)\,, \tag{140}$$

for the specific value $c = -\frac{30k^2}{19}(304k^4 - 40k^2 + 1)$ where

$$a_1 = 60k^3 - \frac{30k}{19}\,,\ a_2 = -60k^3\,,\ k^2 = \frac{11}{76} \text{ or } k^2 = -\frac{1}{76}\,.$$

When $k^2 = -1/76$, the hyperbolic tangent becomes ordinary tangent and there are poles on the real axis. Near the singulariy, u goes like like

$$u(x) \approx \frac{-60}{(x - x_0)^3}\,,\ x \to x_0\,.$$

All the blow-up solutions possess singularities of the same type [23]. In general, the existence and structure of connections depend on parameter c in a very complicated way.

According to the stability analysis of the stationary points of (139), naive counting scheme [259] tells that: there are structurally stable spiraling heteroclinic connections between c_+ and c_- for any $c > 0$. Connections may exist connecting the $1-d$ and the $2-d$ manifolds for discrete values of c. Due to time reversal symmetry, the two $1-d$ manifolds are sometimes able to connect to each other to form asymptotically monotonic connection. The exact solution (140) is an example.

When c is large, system behavior is quite simple. Let's do the following rescaling of coordinates

$$u \to \sqrt{c}u\,,\ x \to \frac{x}{c^{1/6}}\,.$$

(138) then becomes

$$u^2 - c^{-1/3}u - u_{xxx} = 1\,.$$

In the limit $c \to \infty$, we get

$$u_{xxx} = u^2 - 1\,.$$

McCord studied this system and proved that the antisymmetric heteroclinic orbit connecting the two equiliria is the only bounded nonconstant solution [172]. For c large enough, Michelson argued that the heteroclinic orbit remains the unique bounded curve [174]. This orbit has been numerically observed down to $c = 0.07$ [128] and can be found in normal form analysis for $c \ll 1$ [32].

When c decreases from large values, new connections with more zeroes are born through saddle-node bifurcations. They all lie on the 2-d manifolds of $c_\pm$ and so possess structural stablility. There exists a lower bound $c_{max} \approx 1.1252$ such that these orbits limit to an odd periodic orbit by having infinitely many zeroes at $c = c_{max}$. When $c < c_{max}$, the set of connections has intricate geometrical structure. Lau [159] has studied the formation and bifurcation of the intersectons of 2-d manifolds of $c_\pm$ and found that they form a cocoon-like tangle in the phase space. He named the whole process the "cocoon" bifurcation.

In [128], if a heteroclinic orbit involves spiraling, it is called an oscillatory shock, otherwise, a regular shock. Homoclinic connections are called solitory waves. More specificly, in the far field, the oscillatory shock behaves like

$$u \to \pm\sqrt{c} + b_\pm e^{\mp\lambda_1 x}\cos(\lambda_2 x + \phi_\pm)\,,\ x \to \pm\infty\,, \tag{141}$$

the regular shock behaves like

$$u \to \mp\sqrt{c} + a_{\pm} e^{\mp 2\lambda_1 x}\,,\ x \to \pm\infty\,, \tag{142}$$

and the solitary wave near c_+ behaves like

$$\begin{aligned} u &\to \sqrt{c} + a e^{2\lambda_1 x}\,, \qquad x \to -\infty \\ u &\to \sqrt{c} + b e^{-\lambda_1 x}\cos(\lambda_2 x + \phi)\,, \qquad x \to +\infty\,, \end{aligned} \tag{143}$$

where $a, a_{\pm}, b, b_{\pm}$ are arbitrary constants and $\phi, \phi_{\pm}$ are adjustable parameters to match asymptotics when $x \to \pm\infty$. The three categories are investigated numerically at different c values in [128] and families of solutions are found. These connecting orbits can be classified according to their topology relative to the two equilibria [143].

The asymptotic approach can sometimes be rather tricky. For example, when $c \to 0^+$, although an asymptotic expansion appears to establish the existence of regular shocks, there are actually none. Only the "asymptotics beyond all orders" reveals the truth [105]. Yang carried out the asymptotic analysis further on the existence and properties of the connections [275]. He showed that in the weak-shock limit, *i.e.*, $0 < c \ll 1$, the oscillatory shocks can only be antisymmetric, otherwise oscillatory and monotonic waves of exponentially small but growing amplitude will be excited. He also showed that under certain conditions, the solitary wave forms when the stable and unstable manifold of an equilibrium connects.

Numerically, the asymptotic solutions are taken as the initial condition and shooting scheme is invoked to determine the connections. The integration constant c and the azimuthal angle ϕ can be used as variable matching parameters. There are two ways of shooting. The first is to shoot from one point and check whether it reaches the other point; the other is to shoot from both points and match them at some intermediate point. I prefer the second method as matching away from the equilibria is easier and more accurate.

5.3.2 Periodic Solutions of the steady equation

Having in mind above discussion about the intricate set of connections, we expect that the set of periodic solutions could be extremely complicated. Yet a bifurcation analysis in Fourier space simplifies the classification a lot if we are only concerned with the periodic solutions [103]. For a fixed system size L, the periodic solutions satisfy the equation

$$[(kq)^2 - (kq)^4]a_k + ikq \sum_{m=-\infty}^{\infty} a_{k-m} a_m = 0\,. \tag{144}$$

We have proved in sect. 5.2.2 that when the system size is smaller than 2π, the laminar state $u \equiv 0$ is the global attractor. So there is no nontrivial periodic solution with period smaller than 2π. Next we check the linear stability of the laminar state. When the nonlinear term $(u^2)_x$ is removed in (133), the remaining linear equation has Fourier modes as eigenvectors with eigenvalues

$$\omega_k = (kq)^2 - (kq)^4\,.$$

If we take the system size L as the bifurcation parameter, every time L crosses $2n\pi\,, n \in \mathbb{N}$, there is a pitchfork bifurcation where n-cell states are generated. They form an invariant circle due to the translational invariance of (133). In the antisymmetric space, they corresponds to two points, being half-period translates of each other, and of the form

$$u(x,t) = -2\sum_k b_{kn}\sin(knx)\,,$$

where $b_{kn} \in \mathbb{R}$. By rescaling u, x and ν, the n-cell states transform to each other.

The bifurcation of the n-cell states is well described in [103]. The stability matrices associated with these states decompose into non-interacting blocks due to the symmetries present. Each block corresponds to a subharmonic perturbation and contains two separate subsectors corresponding to cosine and sine components in the tangent space. At each bifurcation, two anti-symmetric solutions (being translates of each other) are generated with additional asymmetric solutions. For small long-wavelength perturbations, the anti-symmetric solution can be viewed as a modulated n-cell state.

With the increase of L these steady periodic solutions may bifurcate into more complicated ones. For any fixed period L, however, the number of steady periodic solutions are finite up to spatial translation. This fact can be explained as follows. The existence of the inertial manifold [245] bounds the size of all Fourier components and the stationary points should live on the compact inertial manifold. This manifold and the dynamics on it can be described by smooth functions of a finite number of Fourier modes. On a finite-dimensional compact manifold, a smooth function can only have a finite number of zeros. So, the steady states, as the zeros of the smooth velocity field on the inertial manifold, are finitely many.

When L is small, the number of steady solutions are small and their energy concentrates on the low wavenumber end of the Fourier spectrum. These solutions may be obtained by solving the truncated version of (144). When L increases, the number of steady solutions increases exponentially. Like the laminar solution, a steady solution bifurcates every time when L expands a certain amount close to some average value. In the limit of infinite system size $L \to \infty$, there are infinitely many steady solutions. To understand the structure of these solutions, we have to study the phase space of the $3-d$ dynamical system (139).

The mass generation of periodic orbits are closely related to the connecting orbits in the phase space. Kent and Elgin conjectured that all the bounded orbits originate from the unique heteroclinic orbits at $c \gg 1$ through a series of bifurcations [143]. The existence of the periodic and connecting orbits may be rigorously established by computer-assisted topological arguments [251]. At the qualitative level, the existence of the complicated set of periodic orbits is deducible from the Shil'nikov construction of horseshoes for homoclinic orbits or heteroclinic cycles [106]. There are infinitely many horseshoes associated with this construction and each horseshoe will generate infinitely many periodic orbits. So, the orbit structure of the phase space becomes extemely complicated when this construction is possible. But there is no problem for the periodic orbit theory as periods of these orbits increase very fast and the required low-period orbits can be found numerically without much difficulty.

5.3.3 Phase space structure at small c

In the limit $c \to 0^+$, perturbation technique can be employed to analyze properties of (139). For simplicity, let $c = \epsilon^2$, $\epsilon > 0$. Make a change of variables

$$(u, y, w) \to \epsilon(u, y, w) .$$

(139) becomes

$$\begin{aligned} u_x &= y \\ y_x &= w \\ w_x &= -y + \epsilon(u^2 - 1) . \end{aligned} \tag{145}$$

To the zeroth order, (145) is linear, the general solutions is

$$\begin{aligned} u &= \tilde{y}\sin(x) - \tilde{w}\cos(x) + \tilde{u} \\ y &= \tilde{y}\cos(x) + \tilde{w}\sin(x) \\ w &= -\tilde{y}\sin(x) + \tilde{w}\cos(x) , \end{aligned} \tag{146}$$

where $\tilde{u}, \tilde{y}, \tilde{w}$ are constants and will be used as dependent variables in the perturbation analysis. Substitute (146) into (145), and we get equations for $\tilde{u}, \tilde{y}, \tilde{w}$,

$$\begin{aligned} \tilde{u}_x &= \epsilon(u^2 - 1) \\ \tilde{y}_x &= -\epsilon\sin(x)(u^2 - 1) \\ \tilde{w}_x &= \epsilon\cos(x)(u^2 - 1) \end{aligned} \tag{147}$$

Multi-scale averaging method may be used to analyze (147). For example, do the following change of variables,

$$\tilde{y} = \bar{y} + \epsilon y_1(\bar{u}, \bar{y}, \bar{w}, x) + \epsilon^2 y_2(\bar{u}, \bar{y}, \bar{w}, x) + \cdots ,$$

with similar expressions applied to the other two variables, $\tilde{u}$ and $\tilde{w}$. To the third order of ϵ, we get (for notation simplicity we replace $\bar{u}, \bar{y}, \bar{w}$ by u, y, w)

$$\begin{aligned} u_x &= \epsilon[\frac{1}{2}(y^2 + w^2) + u^2 - 1] + \epsilon^3[4u^4 + \frac{7}{4}(y^2 + w^2) - \frac{271}{288}(y^2 + w^2)^2 \\ &\quad + \frac{1}{8}u^2(-32 + 9(y^2 + w^2))] \\ y_x &= -\epsilon uy + \frac{\epsilon^2}{24}(36u^2 w - w^3 - wy^2) + \frac{\epsilon^3}{36}[153u^3 y - 9uy - 41uy(y^2 + w^2)] \\ w_x &= -\epsilon uw - \frac{\epsilon^2}{24}(36u^2 y - y^3 - yw^2) + \frac{\epsilon^3}{36}[153u^3 w - 9uw - 41uw(y^2 + w^2)] . \end{aligned}$$

Let $\rho = y^2 + w^2$, we get a 2-d dynamical system

$$\begin{aligned} u_x &= \epsilon(\frac{1}{2}\rho + u^2 - 1) + \epsilon^3(4u^4 + \frac{7}{4}\rho - \frac{271}{288}\rho^2 + \frac{1}{8}u^2(-32 + 9\rho)) \\ \rho_x &= \epsilon 2u\rho + \frac{\epsilon^3}{18}(153u^3\rho - 9u\rho - 41u\rho^2) . \end{aligned} \tag{148}$$

This is a 2-d autonomous system with $(x-)$time reversal symmetry, *i.e.*, the system is

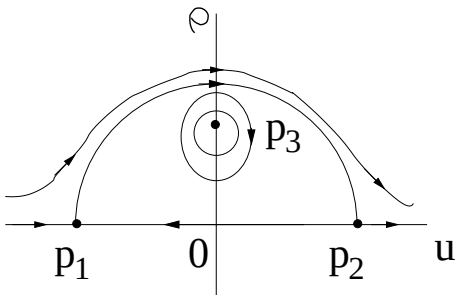

Figure 13: Phase diagram of (148) to the lowest order.

invariant under

$$u \to -u\,, \rho \to \rho\,, x \to -x\,.$$

H.-T. Chang obtained a similar expression to the lowest order of ϵ using the normal form analysis [32]. To $O(\epsilon^2)$, the phase diagram of system (148) is shown in figure 13. There are three stationary points $p_1\,, p_2\,, p_3$ where p_1 and p_2 correspond to the two stationary points of (139) and p_3 to the odd periodic orbit generated when c crosses zero. As shown in [139], this orbit always exists for small $c > 0$ and has the form

$$u = -\sqrt{2}\epsilon \sin(\Omega x) + \frac{\epsilon^2}{3}\sin(2\Omega x) + \cdots\,,$$

where $\Omega = 1 - \epsilon^2/6 + \cdots$. The existence of this orbit and the structurally stable heteroclinic connection implies an extremely complicated phase space structure as consequence of the Conley index theory [42] and Shil'nikov construction [106]. In figure 13, we have two heteroclinic connections between p_1 and p_2. The one on the $\rho = 0$ axis corresponds to the regular shock mentioned before and the other one to a 2-d connection manifold of (139). Between these connections, the area is filled with periodic orbits, corresponding to invariant tori of (139), whose periods increase indefinitely upon approaching the connections.

The dynamics described above is not structurally stable. It depicts, however, a qualitative picture valid to all orders of ϵ, which seems to say that through change of coordinates, the system (139) becomes an integrable system. This *cannot* be correct as complicated dynamical behavior is observed in (139) even for small values of c. The contradiction is due to the nonconvergence of the series of coordinate changes

$$\tilde{y} \to \bar{y} + \epsilon y_1 + \epsilon^2 y_2 + \cdots\,.$$

For this reason, many features of the dynamics observed in figure 13 are not present in (139). For example, there are no continuous families of invariant tori or 2-d heteroclinic connection, and the connection on $\rho = 0$ does not exist for small $c > 0$, as noted above. In fact the separation of the $1-d$ manifolds can be estimated using the analysis beyond all orders [105]. Similar situations are frequently encountered in Hamiltonian mechanics [125, 150]. On the other hand, many features of (148) are kept in (139). For example, some of the invariant tori would survive the higher order perturbations [186] and one structurally stable heteroclinic connection persists as a remnant of the $2-d$ connection manifold. During the process, infinitely many periodic orbits will be generated.

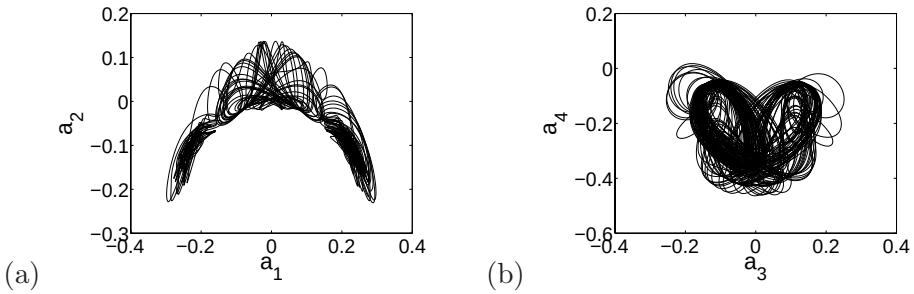

Figure 14: (a) a_1, a_2 projection of a typical phase orbit of (135); (b) a_3, a_4 projection of the same orbit; $L = 38.5\,, \nu = 1\,,$ 16 Fourier modes truncation.

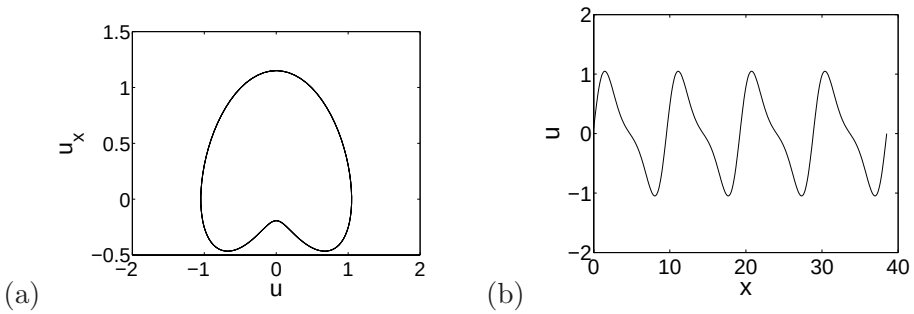

Figure 15: The first antisymmetric steady solutions of (135),$L = 38.5\,, \nu = 1\,.$ (a) u, u_x projection in the 3-d phase space of (139); (b) The profile of the same orbit on the interval $[0, L]$;

5.3.4 Variational approach

Because we take the periodic boundary conditions $u(x,t) = u(x+L,t)$, it is of great interest to find dynamically important steady solutions with a given spatial period L. (144) may be directly solved for the steady solution. But as we remarked previously, the number of solutions increases rapidly with L, if L is not too small, there are quite many low-period orbits and we have to classify them according to their importance as we believe that only a few of them are closely related to the asymptotic dynamics of (133). Empirically, we know that an equilibrium is important if a typical phase orbit passes its neighborhood frequently. On a plane, through observation of the phase orbit we may quickly identify those important equilibria. In high dimensional space, even if the steady solutions are found, it is not straightforward to determine which ones are important.

Figure 14 shows a typical phase orbit of the KSe in the antisymmetric solution space with periodic boundary conditions. It consists of three parts, the parts on sides communicating with the part in the middle. We pick up any point on the typical orbit. It corresponds to a antisymmetric loop in the phase space $\mathcal{M}$ of (139) and so can be used to initialize the search for a periodic orbit in $\mathcal{M}$. Using the technique developed in [156], we found several dozen periodic orbits of (139) for $L = 38.5\,, \nu = 1$. Not all of them are antisymmetric and some of them may not even be important. So we re-initialize the search by taking the average of an orbit segment with the hope that the typical phase orbit will pass through the neighborhood of important steady solutions often. In this way, the number of relevant steady solutions is greatly reduced. There are around 10 solutions with 4 of them antisymmetric. We display them in figure 15, figure 16, figure 17, and figure 18.

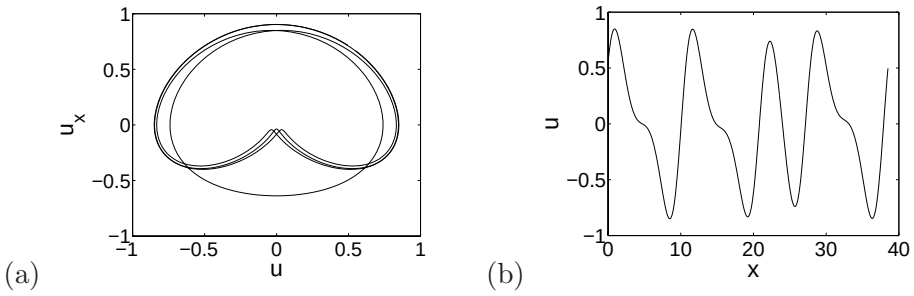

Figure 16: The second antisymmetric steady solutions of (135),$L = 38.5\,, \nu = 1\,.$ (a) u, u_x projection in the 3-d phase space of (139); (b) The profile of the same orbit on the interval $[0, L]$;

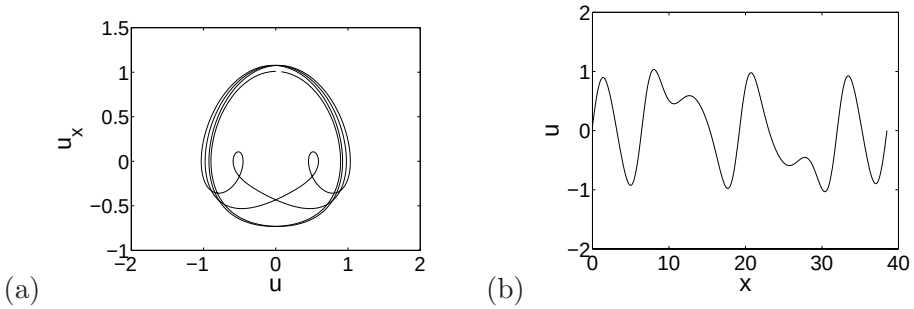

Figure 17: The third antisymmetric steady solution of (135),$L = 38.5\,, \nu = 1\,.$ (a) u, u_x projection in the 3-d phase space of (139); (b) The profile of the same orbit on the interval $[0, L]$;

The steady solutions in figure 15 and figure 16 live in the middle part while the ones in figure 17 and figure 18 live on its sides. Close inspection reveals that they have different topology relative to the equilibria on the u, u_x projection plane of $\mathcal{M}$. In figure 15 and figure 16, the orbits circles circle the two stationary points as a whole and u has 4 peaks on $[0, L]$. In figure 17 and figure 18, the orbits sometimes circle only one of the equilibria and u has 6 peaks. Now, we may conclude that there is a qualitative difference between the middle part and the side parts in figure 14. A typical orbit has 4 peaks in the middle part and 6 peaks in the side parts. The communication between the middle and side parts indicates transitions between these two states.

5.3.5 Other bounded solutions

Besides stationary points, heteroclinic connections and periodic orbits, there are other more complicated invariant sets like invariant tori and chaotic trajectories. Interestingly, almost all these solutions exhibit the characteristic cellular structure - the average distances between maxima or minima approximately equal a constant value close to $2\sqrt{2}\pi$, the wavelength of the most unstable mode.

The periodic orbits can be either elliptic or hyperbolic. When they are elliptic, the Poincaré map associated with the periodic orbit is measure preserving and Moser's twist mapping theorem implies that, the flow defined by (139) possesses an infinite set of invariant tori surrounding the periodic orbit [174]. When a periodic orbit is hyperbolic, there exists

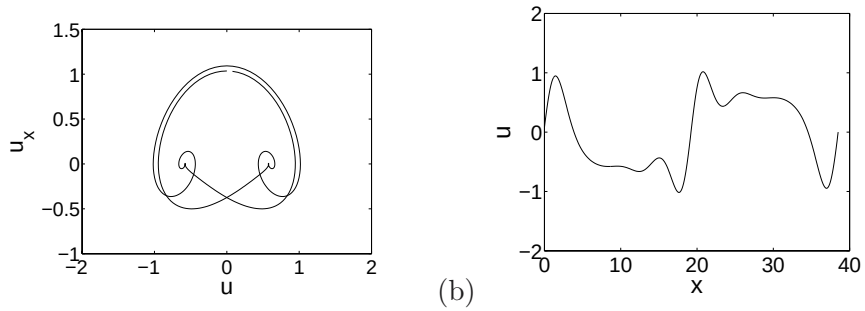

Figure 18: The fourth antisymmetric steady solutions of (135),$L = 38.5\,, \nu = 1\,.$ (a) u, u_x projection in the 3-d phase space of (139); (b) The profile of the same orbit on the interval $[0, L]$;

Cantor-type set of chaotic solutions which weave between periodic ones. This can be double-checked by constructing horseshoes from the connections.

5.4 Summary

In this chapter, we derived the KSe as a phase equation from the CGLe. Eq (133) is a general phase equation in a space-time translationally invariant system when the system crosses the long wavelength instability [152]. We discussed its basic property, in particular, its inertial manifold. We also give a rather detailed account of its steady solutions. It turns out that even the structure of steady solutions are rather complex. Lots of efforts have been made to illucidate the spatial behavior of these solutions.

Steady solutions are important because they set up the coarsest frame for the typical phase space motion. According to their distribution and property, the phase space is divided into qualitatively different parts. Each part has its own dynamics and there are orbits commuting between different parts. In the next chapter, we will investigate all these dynamics in detail and build a much more clear picture of the SIS.

CHAPTER VI

SPATIOTEMPORAL DYNAMICS OF THE 1-D KURAMOTO-SIVASHINSKY EQUATION

6.0.1 Bifurcation sequence

One fundamental problem in the dynamical systems approach to turbulence is that [47]: are transitions to chaos true routes to turbulence? This is not obvious since usual dynamical systems have only a few degrees of freedom with no spatial features, while systems described by a PDE have infinitely many degrees of freedom with possibly intricate spatial structures. The KSe provides the simplest example of a nonlinear PDE that exhibits extremely rich dynamical behavior [133] and that can be tackled within the framework of dynamical system theory.

For small system size L, the dynamics and bifurcation sequence are thoroughly investigated both numerically and analytically [132, 144, 6, 124]. When $L < 2\pi\sqrt{\nu}$, the origin is the global attractor, with no interesting spatial structure. With L passing $2\pi\sqrt{\nu}$, a supercritical bifurcation generates a stationary attractor with one spatial hump . Due to the spatial translation invariance of the KSe, there exists a continous family of such solutions with different phases. The next bifurcation produces stable travelling wave attractor. The consecutive one stabilize the heteroclinic cycles where solutions "burst" intermittently: they stay quite long as a quasi-steady wave and then switch rapidly to a translated quasi-steady state and continue to repeat this process indefinitely. A new bifurcation follows with heteroclinic cycles replaced by stationary two-hump stable equilibria. (Later on stable equilibria with n humps are observed with energy concentrating on the nth Fourier modes. A class of such steady attractive solutions are analyzed by Frisch *et. al* [91] and called cellular solution as they exhibit the so-called viscoelastic behavior under long-wave perturbations.) The next two bifurcations again give travelling waves and heteroclinic cycles, one after another. Then, chaos mounts on the stage with the two-cellular and three-cellular states competing with each other. Armbruster *et. al* showed that four complex modes are enough to produce all the basic features of the system for a considerably large range of system sizes [6]. But for the full spatiotemporal chaos, we need more modes.

6.0.2 Spatiotemporal chaos and recurrence patterns

J. Hyman and B. Nicolaenko [133] went on to explore dynamics on larger intervals and found that regular and chaotic regions appear alternatively. Intermittency and metastable states are observed for various parameter ranges. For the system size sufficiently large, strange equilibria appear which contain broad spectra of Fourier modes. These equilibrium points bring spatial complexity to the solution and are believed to play an important role in the formation of eventual large-scale spatiotemporal chaos. These points correspond to

periodic solutions on the chaotic sets of the ODE for steady solutions of the KSe and were identified by Michelson [175].

Locally coherent structures are frequently observed even in the fully spatiotemporal chaotic regime. The aforementioned cellular structures are the most commonly encountered ones. They are a well-defined entity, moving only slightly chaoticly, interacting weakly with each other except at some discrete space-time points where they are annihilated or created, leaving almost constant local cell densities. We can take a portion of the profile of $u(x,t)$ and after small modification of the boundary parts extend it periodically to the whole real axis to get a new profile. For a considerable amount of time, the evolution of these two profiles agrees fairly well, especially in the central part [58, 124]. These observations show that the full chaotic system consists of almost constant number of spatially localized cells or subsystems. They look rather similar and have few internal degrees of freedom which are controllable. They communicate with each other weakly and mainly through their boundaries.

From a dynamical system point of view, the coherent structures with short periods live and are stable in some invariant subspaces of the full phase space. In the spatiotermporal chaos regime, the modes in the orthogonal (infinite-dimensinal) space provide perturbations which drag solutions out of those subspaces and make them chaotic. If the resulted solutions are still close to the subspaces, they will bear many structural resemblance to the originally stable patterns with chaoticity caused by the weak interaction between them. The whole pattern forms out of instabilities of different levels and the chaotic dynamics just exhibits their competition and mutual saturation. In the periodic orbit theory, the most important recurrent patterns are captured by the shortest UPOs, which encode the coarsest structure of the attractor in the phase space and contain the most unstable directions in their unstable manifolds. Longer cycles resolve more detailed structures and thus more subtle instabilities. This direction was first pursued by Christiansen *et. al* [36]. Using Newton-Raphson method, they located several hundred UPOs in the anti-symmetric space of the KSe with periodic boudary condition at the onset of spatiotemporal chaos, and accordingly established symbolic dynamics. Thus the structure of the strange attractor was clearly displayed and the physical averages are computable via trace formula.

6.1 Proposed study

We will now extend this exploration to the full solution space of the KSe with possibly more complex attracting sets. We will study the spatiotemporal chaotic dynamics from two aspects: locally and globally. The global investigation includes finding UPOs, establishing symbolic dynamics, constructing intrinsic coordinate on the SIS and identifying the most important instabilities. The local study will construct a class of models based on the cellular structures of the KSe and the concept of inertial manifold. Roughly, the strong correlations in short distances will be built into the equation while the long distance correlations will be modeled by the interaction between cells. Next, the geometrical constraints that depict the inertial manifold will be used to refine our models.

6.1.1 Periodic orbit investigations

In our preliminary investigations, we encountered the difficulty of detecting UPOs in a high-dimensional system with chaotic dynamics. Motivated by this challenge, we developed a new variational method for finding UPOs in general flows (see chapter 3). If some coarse picture of the dynamics is available, we may put into the phase space a rough guess in form of a loop represented by a set of points, and our variational method will drive it toward a real periodic orbit. So far, the method appears to be stable and efficient for handling spatiotemporally chaotic dynamics. It has been applied to the KSe with periodic boundary condition in the search of antisymmetric cycles at $\nu = 0.01500$, and we have succeeded in finding some of the shortest orbits [156].

I propose to carry out all the detailed steps to analyze the structure of the SIS and the spatiotemporal dynamics on them in the medium turbulent regime [133].

6.1.1.1 Qualitative dynamics and Fourier modes

It is always wise to develop a qualitative picture of the system dynamics before attempting an indepth investigation. Bifurcation sequences studied by Nikolaenko *et al* indicates that complex chaotic behavior sets in at $\nu = 0.01580$, and that it persists for small ν [133]. Our preliminary results show that as ν decreased, more and more stationary solutions appear, and that the chaotic attractor grows bigger and more complicated. 2-tori are generated through Hopf bifurcation of periodic orbits but higher-dimensional tori seem unlikely to occur, which is consistent with the claim made by Ruelle and Takens [216]. The local unstable manifolds of shortest periodic orbits found so far never achieve a dimension higher than two. This seems to contradict with the linear growth of the fractal dimension of the SIS with the system sizes [243]. We will investigate this apparent contradiction in detail. On the other hand, among the over 100 equilibria which we found in the phase space, only the least unstable ones seem to be relevant to the chaotic dynamics. There might exist UPOs with many unstable directions [278], but they do not participate in the asymptotic dynamics. We will check this out.

How many Fourier modes we should keep is a serious problem. The optimal choice is using the least number of them to capture the interesting dynamics to the precision we want. For numerical computation, this is actually all we can do, since what we observe on the computer is always some coarsed version of the true dynamics. From a mathematical point of view, we often have relatively small number of active modes, and the rest are either slaved to the active ones or can be viewed as small perturbations. The structural stability of short UPOs will guarantee the faithfulness of our numerical calculation. The coarsening procedure will be checked and the qualitative features of the dynamics will be defined in terms of properties of UPOs.

6.1.1.2 Periodic orbits and symbolic dynamics

After we have gained confidence in our accuracy in Gälekin truncations, and developed a qualitative picture of the high-dimensional flow, we shall apply our variational method. The

the shortest cycles we shall initialize the search with the qualitative knowledge we have, or start the evolution from UPOs found at bigger ν's.

After we have some UPOs, we may calculate the eigenvalues and the expanding eigenvector of the Jacobian. One or more Poincaré section can be chosen such that it intersects the UPOs transversely. Mark the UPOs as well as the unstable directions on the Poincaré section and try to visualize the image of the SIS. With more UPOs, the image would become more clear. Curvilinear coordinates are then established along unstable manifolds of periodic points on the Poincaré section. After very coarse maps are established on these coordinates, we may construct the symbolic dynamics and then use it to guess the location of other UPOs [36]. More UPOs that are found can in turn be used to get more accurate symbolic dynamics. I plan to procceed in this iterative way, finding more and more UPOs, down to the machine precision. One important observation is that the line approximation to the SIS is valid as long as the SIS is quasi-one dimensional. More general, we may need topological methods [181] to establish the symbolic dynamics as discussed above in Chapter 3.

6.1.1.3 Phase space structure and dynamical averages

Though symbolic dynamics usually give good enough description of the phase dynamics on the SIS, we would like to obtain more information about the generating mechanism, the organization, the possible changes of the SIS. It is then very helpful to know other invariant objects in the phase space. Stationary points are the simplest among them. Each one of them is an isolated island around which the flow is near linear and characterized by the center point. They communicate with each other or with other invariant set along stable and unstable manifolds. So the stationary points impose the roughest organization of the phase space dynamics. It is good to know around which stationary point a UPO or one portion of a UPO circulates.

Our strategy to determine the correspondence between the UPOs and stationary points will be to implement numerically the homotopy evolution driven by our variational method. We have now two phase spaces: the full phase space $\mathscr{M}_1$ that has Fourier components as its axis and the four-dimensional phase space $\mathscr{M}_2$ of the ODEs that describe the steady solutions for the KSe. Stationary points in $\mathscr{M}_1$ correspond to periodic orbits in $\mathscr{M}_2$. Pick any point on a UPO in $\mathscr{M}_1$. It represents a periodic spatial profile (note the periodic boundary condition) on the interval $[0, L]$ and can be represented by a loop in $\mathscr{M}_2$. We evolve this loop toward a periodic orbit in $\mathscr{M}_2$ by our variational method. The corresponding equilibrium in $\mathscr{M}_1$ is the center for the original UPO segment. In this way, we can locate in $\mathscr{M}_1$ those equilibria which are the important in organizing the dynamics.

After a substantial set of UPOs has been found, we may use trace formula to calculate the dynamical averages like correlation functions, average energy, Lyapunov exponents, fractal dimensions of the SIS. If the symbolic representation is obtained, the topological entropy or K-entropy can also be estimated. Through the study of the organization of the UPOs by the stationary points, typical as well as the special dynamical behavior will be checked and explained. On the other hand, we may transform the dynamics back onto the real axis and study various transport properties.

6.1.2 Local model investigation

Another part of the plan will be an attempt to describe the dynamics from a local interaction perspective. As mention in sect. 6.0.2, in the spatiotemporal chaotic regime of the KSe, a large number of well-defined local cellular states interacting with each other provides a quite suggestive picture of the structure of dynamics over large spatial intervals. This point of view suggests that we may partition the large interval into smaller ones and study more controllable dynamics on each subinterval. The dynamics on the full interval is restored by introducing interactions between the small systems on the subintervals. Two problems naturally arise: how to partition the interval and how to introduce the interactions.

There are two requirements for the partition. First, the subinterval should be big enough to accomodate the local coherent structure with fairly well-defined local dynamics. Second, the subinterval should be small enough such that the dynamics inside it is simple enough to be in our control. The interaction should be local and capture the dynamics predicted by the original PDE. For a comparison of the dynamics on the full interval with that on the subinterval, it is good if the interaction only distorts weakly the equations of motion on the subinterval. The following can be done on the KSe:

- The subinterval can be conveniently chosen to contain some integer number of cellular structures. The local interaction is introduced by combining the equations of motion of neighboring cells. How many cells chosen in a subinterval and how to combine these and derive the approximate equations is an open problem, essential to implementing this approach.
- After the partition and interaction are chosen, we obtain a new dynamical system with a greatly reduced dimension compared to the Gälerkin truncation of the original PDE. This model is supposed to reproduce its dynamics qualitatively; we have to check and validate this claim. Second, we may compare the dynamics on one cell with interaction to that without so as to determine the effects of the interaction to the cell dynamics and thus how well the cellular structure constitute the spatiotemporal chaos.
- If we succeed in the above two steps, we may vary the size of the interval and check two things. First, for some intermediate intervals, the competition between the dominant modes and the impact of this competition to the global dynamics will be investigated by the cell dynamics. Typical periodic orbits will be found to interprete this competition. Second, we may check dynamics on large intervals. The physical averages based on the cell dynamics will be calculated and compared to the values given in [133].

6.1.3 Averaged patterns

For turbulence in an infinite domain, any long-time average is uniform in space. In experiments, the boundary of the container breaks this, for example, the wall area is different from the central area. The boundaris impose geometrical constraints and the long-time average of appropriate physical quantities can have nontrivial spatial structure. This kind of

boundary effects were observed both in experiments and in numerical calculations [278, 79]. As short periodic orbits dominate the dynamics, we hope to interpret this phenomenon from structures of the UPOs as well as from the interaction between the cell and the boundary. As the short orbits are robust under small parameter variations, it is convenient for us to trace the change of the stucture when the boundary conditions varies. From the point of view of local models, as the boundary effects to cells is quite simple, the nature of the averaged structure will be quite clear.

CHAPTER VII

SUMMARY

Dynamical systems and turbulence have been a focus of research for centuries. Various approaches: numerical, analytical, algebraic, geometrical, statistical, topological, scaling, field theoretic, *etc.*, have been developed, and the advantagous stategy should combine all these methods. In a sense, periodic orbit theory is a strong candidate. It has been applied to many low-dimensional chaotic systems with a remarkable success. We are committed to generalizing this theory to study of spatiotemporal chaos (turbulence) in spatially extended systems. As a modest first step, here we have studied two $1-d$ PDEs on a compact domain with the periodic condition: the CGLe and the KSe.

The CGLe differs from the KSe in that it describes two interacting scalar fields while the KSe only depicts one. In the chaotic regime of the CGLe, topological defects appear and vanish at discrete space-time points, but the field in the KSe is always smooth. As the KSe can be derived as a phase equation from the CGLe [22], we may check the relationship of their dynamics and get a better understanding of both.

In the CGLe, we have investigated the onset of spatiotemporal chaos from a bifurcation point of view. Near the bifurcation point, the dynamics is regular or weakly chaotic, so analytical treatment is possible. We have also checked the role played by the invariant structures and tried to find their dynamical explanations. This system is an illumination of the idea that finitely many recurrent patterns may make up the key building blocks of the spatiotemporal chaos.

In the KSe, the structure of the SIS and the chaotic dynamics on it are explored using the periodic orbit approach. After checking the qualitative aspects of the dynamics, a complete set of UPOs up to some length is found and approximate symbolic dynamics established at the same time. Here, a variational method devised for high-dimensional unstable flows is applied for finding UPOs. Stationary points are found and their relation to the set of UPOs is studied, from which the qualitative structure of the phase space is dicussed. Finally, dynamical averages are calculated and typical patterns are picked up, which may be compared with the experimental or numerical observations.

The validity and applicability of the periodic orbit theory presupposes that the system is hyperbolic, so our calculatons depend much on the hyperbolicity assumption. Most systems in the interesting parameter regimes are not hyperbolic, and frequently intermittency plays an essential role. In some systems, the SIS and intermittency coexist. How to treat all these different cases and how to weigh different invariant sets in one dynamical system are open problems, important, and demanding real effort. The periodic orbit theory is making progress in this direction on 'simple' systems.

In long run, the hope is that we can apply the periodic orbit theory to real-world problems, such as the Navier-Stokes equation under given boundary conditions, and use calculated results to match or predict experimental data, or to check and modify the assumptions underlying specific turbulence models. More analytical tools for analyzing the invariant set and UPOs and more powerful numerical methods for detecting UPOs are waiting to be created, a task requiring a collaborative effort between people from many disciplines.

APPENDIX A

REMARKS ON THE JACOBIANS FOR THE GENERAL FLOW

Let's consider a general autonomous flow defined by the equation

$$\frac{d}{dt}x(t) = f(x(t)) \tag{149}$$

where $x \in \mathbb{R}^n$ and $f(.)$ is a smooth vector function. This flow will give an orbit $\phi(t, x)$ to each point x in the phase space,

$$\phi : \mathbb{R} \times \mathbb{R}^n \mapsto \mathbb{R}^n$$

which satisfies $\phi(0, x) = x$. For the invertible flow, $\phi(t, x)$ also satifies the full group property,

$$\phi(t2, \phi(t1, x)) = \phi(t2 + t1, x)$$

Actually, in this case, $\phi(t, x)$ forms a one-parameter family of transformations. The Jacobian associated with an orbit is defined as

$$J^t(x) = \frac{\partial}{\partial x}\phi(t, x)$$

which describes the relative movement of the neighbouring points around the given orbit. Following the group property of $\phi(t, x)$, if $\phi(t_1, \tilde{x}) = x$, then by chain rule,

$$J^{t_1+t}(\tilde{x}) = J^t(x)J^{t_1}(\tilde{x}) \tag{150}$$

It is not hard to check that the Jacobian J^t satisfies the following equation,

$$\frac{d}{dx}J^t(x) = AJ^t$$

where $A(x) = \frac{\partial}{\partial x}f(x)$ is the gradient of the velocity field. If we have a periodic orbit of period T, then J^T is called monodromy matrix whose eigenvalues are independent of the starting point. Of course, the eigenvectors will be different for different starting points. However, they could be related by the natural evolution along the flow. Suppose that along the periodic orbit, there are two points $\tilde{x}, x$ with $\phi(t_1, \tilde{x}) = x$. If $\vec{\Lambda}$ is an eigenvector of $J^T(\tilde{x})$, i.e. $J^T(\tilde{x})\vec{\Lambda} = \lambda\vec{\Lambda}$, then $J^{t_1}(\tilde{x})\vec{\Lambda}$ is an eigenvector of $J^T(x)$ of the same eigenvalue as shown below by repeated use of (150),

$$J^T(x)(J^{t_1}(\tilde{x})\vec{\Lambda}) = J^{t_1}(\tilde{x})J^{T-t1}(x)J^{t_1}(\tilde{x})\vec{\Lambda} = J^{t_1}(\tilde{x})(J^T(\tilde{x})\vec{\Lambda}) = \lambda(J^{t_1}(\tilde{x})\vec{\Lambda})$$

In practical calculations, Poincare sections are frequently utilized and the flow itself is treated as a map on the Poincare section. Periodic orbits then become finite point sets and the corresponding Jacobians depend not only on the position but also the orientation of the Poincare section. The questions arise that whether the eigenvalues of the Jacobians are invariant and how they are related to those of the flow. We will see in the following

that the $n-1$ eigenvalues of the map are the same as the corresponding ones of the flow, independent of the choice of the Poincare section.

For simplicity, let's assume that the Poincare section is defined by $x_1 = 0$ and we have found a periodic orbit with the starting point on the Poincare section. The Jacobian in the full phase space is denoted by $J = (J_{.1}, \cdots, J_{.n})$, where $J_{.k}$ is the kth column of the Jacobian matrix. We denote it this way because it is the resulting point having evolved for one period of the neighbouring point in the kth direction around the periodic point on the Poincare section. Generally, $J_{1k} \neq 0$, which means that the final point is not on the Poincare section. If we bring it back along the flow to the Poincare section, then the corresponding Jacobian of the Poincare map will be constructed for the periodic orbit. The back-flying time t_k should satisfy $t_k v_1 = J_{1k}$ where v_1 is the first component of the velocity at the periodic point. Then $t_k = J_{1k}/v_1$ and $\tilde{J}_{.k} = J_{.k} - t_k \vec{v}$ would be the corresponding vector on the Poincare section. The Jacobian of the map could be written as

$$\tilde{J} = (\tilde{J}_{.1}, \cdots, \tilde{J}_{.n}) = J - \vec{v}\vec{t} \tag{151}$$

where $\vec{t} = col(t_1, \cdots, t_n)$ and $col(.)$ denotes the column vector. Now suppose that we have an eigenvector $\vec{\Lambda}$ of J, i.e. $J\vec{\Lambda} = \lambda\vec{\Lambda}$. We claim that $\tilde{\Lambda} = \vec{\Lambda} - t_\lambda \vec{v}$ is an eigenvector of $\tilde{J}$ of the same eigenvalue λ, where $t_\lambda = \frac{\Lambda_1}{v_1}$. In fact,

$$\begin{aligned} \tilde{J}\tilde{\Lambda} &= (J - \vec{v}\vec{t})(\vec{\Lambda} - t_\lambda \vec{v}) \\ &= \lambda\vec{\Lambda} - t_\lambda \vec{v} - \vec{v}(\vec{t}\cdot\vec{\Lambda}) + t_\lambda \vec{v}(\vec{t}\cdot\vec{v}) \\ &= \lambda\vec{\Lambda} - \lambda t_\lambda \vec{v} = \lambda\tilde{\Lambda} \end{aligned}$$

During the above calculation, we have used

$$\begin{aligned} \vec{t}\cdot\vec{\Lambda} &= \sum_i t_i\Lambda_i = \sum_i \frac{J_{1i}}{v_1}\Lambda_i = \lambda\frac{\Lambda_1}{v_1} = \lambda t_\lambda \\ \vec{t}\cdot\vec{v} &= \frac{v_1}{v_1} = 1 \end{aligned}$$

since $J\vec{\Lambda} = \lambda\vec{\Lambda},\ J\vec{v} = \vec{v}$. Note that $\tilde{v} = \vec{v} - \vec{v} = 0$, which will give the zero eigenvalue of $\tilde{J}$. In the full space, $\tilde{J}$ is still an $n \times n$ matrix with the first row filled with zeros. The reduced $(n-1)\times(n-1)$ matrix which is a restraint of $\tilde{J}$ on the Poincare section is given just by deleting the first row and column of $\tilde{J}$.
For the whole discussion above to be valid, $v_1 \neq 0$ should always hold, i.e. the flow should be transversal to the Poincare section. The reduced Jacobian is therefore the Jacobian in the transversal direction, the invariance of whose eigenvalues justifies the use of the notation J^T in Chapter 7.

APPENDIX B

COMPARISON OF NEWTON DESCENT WITH VARIATIONAL PRINCIPLE IN HAMILTONIAN SYSTEM

Variational principle in Lagrangian mechanics is explained. Its usage in calculating periodic orbits is discussed and compared with the Newton descent method in ref. [156].

B.1 Variational principle in Hamiltonian systems

Variational principle is a powerful tool in theoretical physics. In Hamiltonian mechanics, it plays such a central role that much of the recent development of the subject is based on it, analytically or numerically. The variational formulation of mechanics is also a convenient bridge between classical mechanics and other branches of physics like statistical physics, quantum physics.

Although the following formulation is valid for the most general case, for brevity, we just consider a particle with unit mass ($m = 1$) moving in the 3-d space under the influence of the external potential $V(q,t)$. Newton's second law tells us that the acceleration $a(t) = \frac{d^2q}{dt^2}$ is proportional to the external force $f = -\frac{\partial V}{\partial q}$, that is

$$a(t) = -\frac{\partial V}{\partial q}\,. \tag{152}$$

Eq.(152) describes the motion locally while variational principle gives a global view of particle orbits. We can describe the dynamics in either the configuration (Lagrangian formulation) or the phase space (Hamiltonian formulation). In configuration space, the important physical quantity is the Lagrangian

$$L(q,\dot{q},t) = \dot{q}^2/2 - V(q,t)\,. \tag{153}$$

The equation of motion is determined by requiring the variation of the action integral

$$S = \int_{t_1}^{t_2} dt\, L(q,\dot{q},t) \tag{154}$$

to be dependent only on the surface terms [64].

In the most general case, the path varies in the configuration space with

$$q(t) \to q'(t') = q(t) + \delta q(t)\,, \quad t \to t'(t) = t + \delta t(t)\,. \tag{155}$$

These equations define the variation δq and δt in terms of the original variables: q and t. The time change induces a change in the integration measure in (154) by

$$\delta(dt) = d(t+\delta t) - dt = dt\frac{d}{dt}\delta t(t)\,.$$

In many applications, the time is not varied and we use δ_0 instead of δ to indicate this variation, *i.e.* $\delta_0 t = 0$. The variation of $q(t)$ is then to the highest order given by

$$\delta q(t) = q'(t+\delta t) - q(t) = q'(t) - q(t) + \delta t\frac{dq'(t)}{dt} := \delta_0 q(t) + \delta t\frac{dq(t)}{dt}\,.$$

Similarly,

$$\delta\dot{q}(t) = \delta_0\dot{q}(t) + \delta t\frac{d}{dt}\dot{q} = \frac{d}{dt}(\delta q) - \dot{q}\frac{d}{dt}\delta t\,.$$

So, the variation of the action S is

$$\begin{aligned}
\delta S &= \int_{t_1}^{t_2} L\,\delta(dt) + \delta L\,dt \\
&= \int_{t_1}^{t_2} dt\,L\frac{d}{dt}\delta t + \left(\frac{\partial L}{\partial q}\delta q + \frac{\partial L}{\partial\dot{q}}\delta\dot{q} + \frac{\partial L}{\partial t}\delta t\right) \\
&= \int_{t_1}^{t_2} dt\,\frac{d}{dt}(L\delta t + \frac{\partial L}{\partial\dot{q}}\delta q - \dot{q}\frac{\partial L}{\partial\dot{q}}\delta t) + \\
&\quad \int_{t_1}^{t_2} dt\,\left[\frac{\partial L}{\partial q} - \frac{d}{dt}(\frac{\partial L}{\partial\dot{q}})\right]\delta q + \left[\frac{\partial L}{\partial t} + \frac{d}{dt}(\dot{q}\frac{\partial L}{\partial\dot{q}} - L)\right]\delta t\,. \qquad (156)
\end{aligned}$$

As usual, we may define the conjugate momentum $p := \frac{\partial L}{\partial\dot{q}}$; and the Hamiltonian $H = \dot{q}\frac{\partial L}{\partial\dot{q}} - L$. According to our variational principle, the variation of the action with respect to a classical orbit only comes from the surface term,

$$\delta S = (p\,\delta q - H\,\delta t)|_{t_1}^{t_2}\,,$$

so the rest term in (156) should be identically zero. The variations δq give the equation

$$\frac{\partial L}{\partial q} - \frac{d}{dt}\left(\frac{\partial L}{\partial\dot{q}}\right) = 0\,. \qquad (157)$$

This is the famous Euler-Lagrangian equation and is able to produce the equation of motion in terms of the generalized coordinates. It is easy to see that if q is a cyclic coordinate (absent from L), the conjugate momentum p is a conserved quantity. The variations δt give the equation

$$\frac{dH}{dt} = -\frac{\partial L}{\partial t}\,. \qquad (158)$$

If the potential V is independent of time, then $\frac{dH}{dt} = 0$, *i.e.*, $H = E$ is a constant. In other words, if time t is treated as a coordinate and is cyclic, Hamiltonian H would be the corresponding conjugate momentum and is conserved. In fact, (158) can be directly derived from (157) since we have the identity

$$\frac{\partial L}{\partial t} + \frac{d}{dt}\left(\dot{q}\frac{\partial L}{\partial\dot{q}} - L\right) = -\left[\frac{\partial L}{\partial q} - \frac{d}{dt}(\frac{\partial L}{\partial\dot{q}})\right]\dot{q}\,.$$

With this observation, up to the surface term, δS depends only on $\delta_0 q$. The variation δt in time can well be contained in the position variation δq, which leaves some arbitrariness in the time parametrization of the loop as long as numerical calculation is concerned. For the same reson, the only equation that the particle trajectory has to satisfy is (157), the right hand side of which is the gradient of S with respect to δq (or $\delta_0 q$).

B.2 Newton descent and variational principle

If we are seeking a periodic orbit of known period T, we may set $\delta t = 0$, and the variational principle in this case reads

$$\delta S = \int_{t_1}^{t_2} dt \left[\frac{\partial L}{\partial q} - \frac{d}{dt}\left(\frac{\partial L}{\partial \dot{q}}\right)\right] \delta_0 q = 0\,. \tag{159}$$

So, the periodic orbit is a critical point (minimum, maximum or saddle) of the action functional. If the periodic orbit is an extremum (minimum or maximum), gradient-descent method [205, 50, 80] could be used. The more general way is to solve directly the zero gradient condition (157). Go back to the simple case and assume that v does not contain time explicitly, *i.e.*, $L(q,\dot{q}) = \frac{1}{2}\dot{q}^2 - v(q)$. The q gradient of S is then

$$g(q) := f(q) - \ddot{q} = a - \tilde{a}\,, \tag{160}$$

where $a := f(q)$ and $\tilde{a} := \ddot{q}$ make the notations consistent with those in [156]. We would like to find zeros of (160) in the loop space $\{q(t) : q(t) = q(t+T), t \in [0,T]\}$. Different approaches can be applied at this point. In view of the periodic boundary condition, Helleman and Bountis [119] derived the gradient $g(\hat{q})$ in Fourier space and use Newton's method to locate its zeros.

In the more complicated case, Newton descent is a efficient method for finding zeros of $g(q)$. Let's review the Newton descent method in the Hamiltonian case. Our starting equation is

$$\frac{\partial}{\partial \tau}(\tilde{a} - \lambda^2 a) = -(\tilde{a} - \lambda^2 a)\,. \tag{161}$$

As the period T is known by assumption it is convenient to set $\lambda = 1$. Then (161) is equivalent to

$$\frac{\partial}{\partial \tau}\, g(q) = -g(q)\,, \tag{162}$$

or more explicitly,

$$\frac{\delta g(q)}{\delta q} \cdot \frac{\partial q}{\partial \tau} = -g(q)\,. \tag{163}$$

This is just the infinitesimal version of Newton's method. As we make the loop deformation continuous, we call it *Newton descent*. Therefore basically, Newton descent is a variant of Newton's method for locating zeros of the stationary variation condition $g(q) = 0$. In practice, we can choose to work in the configuration q-space or in the Fourier $\hat{q}$-space. In q-space numerical calculation, the large matrix derived from the left hand side of (163) is sparse, which is easier for inversion, especially in high-dimensional space. When we work in $\hat{q}$-space, much fewer modes are sufficient to capture the essential shape of the periodic orbit if it is 'simple' (high frequency components are highly supressed).

Solve (163) for $\delta_0 q$ and the corresponding variation in S is given by

$$\delta S = -\int_{t_1}^{t_2} dt\, g(q) \left(\frac{\delta g}{\delta q}\right)^{-1} (q) g(q)\, \delta\tau\,. \tag{164}$$

If the loop $q(t)$ is close to a periodic orbit, we can check where δS heads. Near a minimum (maximum), all the eigenvalues of $\frac{\delta g}{\delta q}$ being positive (negative), δS is therefore decreasing (increasing) to make S approach its minimum (maximum) value. Near a saddle, situation becomes more complicated: δS could be positive or negative. But (162) ensures that $g(q)$ always approaches zero and thus $q(t)$ evolves toward a periodic orbit.

In chapter 3, we introduced the following cost functional

$$F^2[\tilde{x}] = \frac{1}{2\pi} \oint_{L(\tau)} ds\ (\tilde{v}(\tilde{x}) - \lambda v(\tilde{x}))^2\ . \tag{165}$$

The Newton descent flow always decreases F^2 and every solution of (157) minimizes F^2. However, F^2 is not equivalent to the action integral S in the Lagrangian mechanics, because there may be local minima (maxima, saddle) of (165) that are not solutions to (157). So, stationary variation condition $\delta F^2 = 0$ may not yield solutions that are physical while $\delta S = 0$ always does. At a critical point S assumes any value while F^2 can only take value 0 in order to identify a true solution of the original equation. The Newton descent (162) directly searches zeros of $g(q)$, which is better than ordinary minimization of F^2 (see chapter 9 of [205]).

B.3 Conclusion

From the above comparison, we see that the basic equation of Lagrangian mechanics can be derived from the variational principle. The principle is also applicable analytically or numerically to determining periodic orbits, when the desired orbit is an extremum of the action integral. If the periodic orbit appears as a saddle which is the case in many instances, we cannot apply the principle directly. In practice, various versions of Newton's method are used to locate zeros of the gradient of the action. The Newton descent is one variant of Newton's method among others.

APPENDIX C

THEOREMS USED IN THE PROOFS

We use successive approximation method to prove the existence of modulated amplitude waves. Below are listed several theorems from the theory of nonlinear oscillations taken from Hale's monograph [112].

Consider the system of equations

$$\dot{z} = Az + \epsilon Z(\tau, z, \epsilon) \tag{166}$$

where A is a constant matrix, $\epsilon, \tau \in \mathbb{R}$, and $z, Z \in \mathbb{R}^n$. Z is a continuous function of τ, z, ϵ, periodic in τ of period T. In the following, we only consider the case that Z is a smooth function. Without loss of generality, A can always be assumed to have the standard form

$$A = \text{diag}(0_p, B),$$

Where 0_p is a $p \times p$ zero matrix and B is a constant matrix with the property that the equation $\dot{y} = By$ has no nontrivial periodic solution of period T. Under these settings, if the successive approximation is applied to (166), we have

Theorem C.0.1 *Given $d > b > 0$, there is an $\epsilon_1 > 0$ such that for any given constant p vector $a, \|a\| < b$ and real $\epsilon, |\epsilon| < \epsilon_1$, there is a unique function*

$$z^*(\tau) = z(\tau, a, \epsilon), \text{ with } \sup_{\tau} \|z^*(\tau)\| < d$$

which has continuous first derivative with respect to τ and satisfies

$$\dot{z^*} = Az^* + \epsilon Z(\tau, z^*, \epsilon) - \epsilon P_0 Z(\tau, z^*, \epsilon).$$

Furthermore, $z(\tau, a, 0) = a^*$, $a^* = \text{col}(a, 0)$, $P_0(z^*) = a^*$, and $z(\tau, a, \epsilon)$ has continuous first derivatives with respect to a, ϵ.

P_0 is defined as a projection operator on the Banach space S of continuous periodic functions of period T. If $f \in S$, write $f = \text{col}(g, h)$ where g is a p vector and h is a $n - p$ vector, then

$$P_0(f) = \text{col}\left(T^{-1} \int_0^T g(t)\, dt, 0\right)$$

So, P_0 brings an element f in S to a constant vector which has the average values of g over one period as the first p components and zeros as the rest components. The equation satisfied by z^* is different from (166) by a constant vector. By a proper choice of the starting vector a, we may make this constant vector zero to obtain a solution for the system (166). The mathematical statement is give by the following theorem.

Theorem C.0.2 *Let $z(\tau, a, \epsilon)$ be the function given by the Theorem C.0.1 for all $\|a\| \leq b < d, |\epsilon| \leq \epsilon_1$. If there exist an $\epsilon_2 \leq \epsilon_1$ and a continuous function $a(\epsilon)$ such that*

$$P_0 Z(\tau, z(\tau, a(\epsilon), \epsilon), \epsilon) = 0, \text{ with } \|a(\epsilon)\| \leq b \text{ for } |\epsilon| \leq \epsilon_2 \tag{167}$$

then $z(\tau, a(\epsilon), \epsilon)$ is a periodic solution of system (166) for $\|\epsilon\| \leq \epsilon_2$. Conversely, if system (166) has a periodic solution $\bar{z}(\tau, \epsilon)$, of period T, $\|\bar{z}(\tau, \epsilon)\| \leq d, |\epsilon| \leq \epsilon_2$, then $\bar{z}(\tau, \epsilon) = z(\tau, a(\epsilon), \epsilon)$.

Therefore, the existence of a continuous function $a(\epsilon)$ satisfying (167) is a necessary and sufficient condition for the existence of a periodic solution of system (166) of period T. As we do not know the exact functional form of the periodic solution, the condition (167) could not be solved explicitly. But by using implicit function theorem, we can show that the substitution into (167) of a proper approximate function of $z(\tau, a, \epsilon)$ leads to the existence condition for periodic solutions.

Theorem C.0.3 *In the system (166), let*

$$Z = \text{col}(X, Y), \quad z = \text{col}(x, y)$$

where X, x are p vectors and define

$$X_0(x, y, \epsilon) = \frac{1}{T} \int_0^T X(\tau, x, y, \epsilon) d\tau.$$

If there is a p vector $a_0, \|a_0\| < d$, such that

$$X_0(a_0, 0, 0) = 0, \quad \det \left[\frac{\partial X_0(a_0, 0, 0)}{\partial x} \right] \neq 0 \tag{168}$$

then there exists an $\epsilon_1 > 0$ and a periodic function $z(\tau, \epsilon), |\epsilon| \leq \epsilon_1$, of system (166) of period T with $z(\tau, 0) = \text{col}(a_0, 0)$.

If we need to determine other parameters as a function of ϵ in practical applications, similar theorems could be derived. Specifically, in the main text we consider the period T as a function of ϵ. It is clear that theorem C.0.3 applies if we suppose $T(\epsilon)$ is continuous in ϵ and bounded for $|\epsilon| \leq \epsilon_1$. Furthermore, despite the use of the zeroth approximation in the above theorem, the nth approximation could be used instead. If *simple* (non-vanishing determinant) solutions to the determining equations can be found for ϵ in the neighborhood of 0 then system (166) has a periodic solution.

If the system which we are studying possesses certain symmetries, we can prove the existence of particular symmetric solutions by a simplified version of determining equations. Let us define the symmetry first.

Definition C.0.1 *Let $\dot{z} = f(\tau, z)$, where $z, f \in \mathbb{R}^n$, be a system of differential equations. It is said to have the property E with respect to Q if there exists a nonsingular matrix Q such that*

$$Q^2 = I \quad Qf(-\tau, Qz) = -f(\tau, z) \quad QP_0 = P_0 Q$$

where P_0 is the projection operator defined before.

Under this symmetry assumption the following theorems apply:

Theorem C.0.4 *Suppose* $Q = \mathrm{diag}(Q_1, Q_2)$ *where* Q_1 *is a* $p \times p$ *matrix. If system (166) has property E with respect to this* Q *for all* ϵ*. If* $a, \|a\| \leq b$*, is a* p *vector and* $a^* = \mathrm{col}(a, 0)$ *is a* n *vector, chosen in such a way that* $Qa^* = a^*$*, then the solution* $z(\tau, a, \epsilon)$ *satisfies the relation*

$$Qz(-\tau, a, \epsilon) = z(\tau, a, \epsilon)$$

and consequently,

$$Z(-\tau, z(-\tau, a, \epsilon), \epsilon) = -Qz(\tau, z(\tau, a, \epsilon), \epsilon)$$

Theorem C.0.5 *If the* j*-th element of the diagonal of the matrix* Q_1 *in Theorem C.0.4 is* $+1$*, then the* j*-th equation in the determining equations is equal to zero for every vector* a^* *in Theorem C.0.4.*

The system (94) derived here from the 1-D CGLe has this symmetry, so the number of determining equations can be reduced using these two theorems.

REFERENCES

[1] Ablowitz, M. J. and Clarkson, P. A., *Solitions, Nonlinear Evolution Equations and Inverse Scattering*. Cambridge: Cambridge University Press, 1992.

[2] Angenent, S. B., "The periodic orbits of an area preserving twist-map," *Commun. Math. Phys.*, vol. 115, pp. 353–374, 1988.

[3] Aranson, I. S. and Kramer, L., "The world of complex Ginzburg-Landau equation," *Rev. Mod. Phys.*, vol. 74, pp. 99–143, 2002.

[4] Aranson, I. S. and Kramer, L., "The world of the complex Ginzburg-Landau equation," *Rev. Mod. Phys.*, vol. 74, pp. 99–143, 2002.

[5] Armbruster, D., Guckenheimer, J., and Holmes, P., "Heteroclinic cycles and modulated travelling waves in systems with o(2) symmetry," *Physica D*, vol. 29, pp. 257–282, 1988.

[6] Armbuster, D., Guckenheimer, J., and Holmes, P., "Kuramoto-Sivashinsky dynamics on the center-unstable manifold," *SIAM J. Appl. Math.*, vol. 49, no. 3, pp. 676–691, 1989.

[7] Arnold, V. I., "Kolmogorov's hydrodynamic attractors," *Proc. R. Soc. Lond. A*, vol. 434, no. 1890, pp. 19–22, 1991.

[8] Arnol'd, V. I., *Ordinary Differential Equations*. New York: Springer, 1992.

[9] Artuso, R., Aurell, E., and Cvitanović, P., "Recycling of strange sets: I. cycle expansions," *Nonlinearity*, vol. 3, p. 325, 1990.

[10] Artuso, R., Cvitanović, P., and Tanner, G., "Cycle expansions for intermittent maps," *Proc. Theo. Phys. Supp.*, vol. 150, pp. 1–21, 2003.

[11] Aubry, S., "Anti-integrability in dynamical and variational problems," *Physica D*, vol. 86, pp. 284–296, 1995.

[12] Auerbach, D., Cvitanović, P., Eckmann, J.-P., Gunaratne, G., and Procaccia, I., "Exploring chaotic motion through periodic orbits," *Phys. Rev. Lett.*, vol. 58, p. 23, 1987.

[13] Baker, N. H., Moore, D. W., and Spiegel, E. A., "Aperiodic behavior of a non-linear oscillator," *Quatr. J. Mech. and Appl. Math.*, vol. 24, p. 391, 1971.

[14] Bazhenov, M., Bohr, T., Gorshkov, K., and Rabinovich, M., "The diversity of steady state solutions of the complex Ginzburg-Landau equation," *Phys. Lett. A*, vol. 217, p. 104, 1996.

[15] Bekki, N. and Nozaki, K., "Formations of spatial patterns and holes in the generalized Ginzburg-Landau equation," *Phys. Lett.*, vol. 110A, pp. 133–135, 1985.

[16] Ben-Naim, E. and Krapivsky, P. L., "Growth and structure of stochastic sequences," *J. Phys. A: Math. Gen.*, vol. 35, pp. L557–L563, 2002.

[17] Benney, D. J., "Long waves in liquid films," *J. Math. Phys*, vol. 45, pp. 150–155, 1966.

[18] Biham, O. and Wenzel, W., "Characterization of unstable periodic orbits in chaotic attractors and repellers," *Phys. Rev. Lett.*, vol. 63, p. 819, 1989.

[19] Biham, O. and Wenzel, W., "Unstable periodic orbits and the symbolic dynamics of the complex hénon map," *Phys. Rev. E*, vol. 42, no. 8, p. 4639, 1990.

[20] Biham, O., Chandre, C., and Cvitanović, P. sect. *"Cyclists relaxation method"*, in ref. [50].

[21] Biró, T. S., Matinyan, S. G., and Müller, B., *Chaos and Gauge Field Theory.* Singapore: World Scientific, 1994.

[22] Bohr, T., Jensen, M. H., Paladin, G., and Vulpiani, A., *Dynamical Systems Approach to Turbulence.* No. 7 in Cambridge Nonlinear Science Series, Cambridge: Cambridge University Press, 1998.

[23] Bouquet, S., "Hamiltonian structure and integrability of the stationary Kuramoto-Sivashinsky equation," *J. Math. Phys.*, vol. 36, no. 3, p. 1242, 1995.

[24] Brandenburg, A., "Computational aspects of astrophysical MHD and turbulence," in *Advances in Nonlinear Dynamos* (Ferriz-Mas, A. and Núñez, M., eds.), pp. 269–344, London: Taylor & Francis, 2003. `astro-ph/0109497`.

[25] Brodin, G. and Lundberg, J., "Nonlinear surface waves in a plasma with a diffuse boundary," *Phys. Plasmas*, vol. 1, p. 96, 1994.

[26] Broer, H. W., Osinga, H. M., and Vegter, G., "Algorithms for computing Normally Hyperbolic Invariant Manifolds," *Z. Angew. Math. Phys.*, vol. 48, p. 480, 1997.

[27] Brusch, L., Torcini, A., and Bär, M., "Nonlinear analysis of the Eckhaus instability: modulated amplitude waves and phase chaos with nonzero average phase gradient," *Physica D*, vol. 174, no. 1-4, pp. 152–167, 2003.

[28] Brusch, L., Torcini, A., van Hecke, M., Zimmermann, M. G., and Bär, M., "Modulated amplitude waves and defect formation in the one-dimensional complex Ginzburg-Landau equation," *hysica D*, vol. 160, pp. 127–148, 2001.

[29] Brusch, L., Torcini, A., van Hecke, M., Zimmermann, M. G., and Bär, M., "Modulated amplitude waves and defect formation in the one-dimensional complex Ginzburg-Landau equation," *Physica D*, vol. 160, pp. 127–148, 2001.

[30] Brusch, L., Zimmermann, M. G., van Hecke, M., Bär, M., and Torcini, A., "Modulated amplitude waves and the transition from phase to defect chaos," *Phys. Rev. Lett.*, vol. 85, no. 1, p. 86, 2000.

[31] Cariello, F. and Tabor, M., "Painlevé expansions for nonintegrable evolution equations," *Physica D*, vol. 39, p. 77, 1989.

[32] Chang, H.-C., "Travelling waves on fluid interfaces: Normal form analysis of the Kuramoto-Sivashisky equation," *Phys. Fluids*, vol. 29, no. 10, p. 3142, 1986.

[33] Chang, H. C., "Wave evolution on a falling film," *Ann. Rev. Fluid Mech.*, vol. 26, pp. 103–136, 1994.

[34] Chaté, H., "Spatiotemporal intermittency regimes of the one-dimensional complex Ginzburg-Landau equation," *Nonlinearity*, vol. 7, pp. 185–204, 1994.

[35] Chaté, H. and Manneville, P., "Transition to turbulence via spatiotemporal intermittency," *Phys. Rev. Lett.*, vol. 58, no. 2, p. 112, 1987.

[36] Christiansen, F., Cvitanović, P., and Putkaradze, V., "Spatiotemporal chaos in terms of unstable recurrent patterns," *Nonlinearity*, vol. 10, p. 55, 1997.

[37] Christiansen, F. chapter *"Fixed points, and how to get them"*, in ref. [50].

[38] Cohen, B. I., Krommes, J. A., Tang, W. M., and Rosenbluth, M. N., "Nonlinear saturation of the dissipative trapped-ion mode by mode coupling," *Nucl. Fusion*, vol. 16, pp. 971–991, 1972.

[39] Collet, P., Eckmann, J. P., Epstein, H., and Stubbe, J., "Analyticity for the Kuramoto-Sivashinsky equation," *Physica D*, vol. 67, pp. 321–326, 1993.

[40] Collet, P., Eckmann, J. P., Epstein, H., and Stubbe, J., "A global attracting set for the Kuramoto-Sivashinsky equation," *Commun. Math. Phys.*, vol. 152, pp. 203–214, 1993.

[41] Collet, P., Eckmann, J.-P., and Lanford, O. E., "Universal properties of maps on an interval," *Commun. Math. Phys.*, vol. 76, p. 211, 1980.

[42] Conley, C., *Isolated Invariant Sets and the Morse Index*. Providence, RI: AMS, 1978.

[43] Conte, R., *The Painlevé property: one century later*. New York: Springer, 1999.

[44] Creutz, M., *Quantum Fields on the Computer*. Singapore: World Scientific, 1992.

[45] Cross, M. C. and Hohenberg, P. C., "Pattern formation outside of equilibrium," *Rev. Mod. Phys*, vol. 65, no. 3, p. 851, 1993.

[46] Cross, M. C. and Hohenberg, P. C., "Pattern formation outside of equilibrium," *Rev. Mod. Phys.*, vol. 65, no. 3, 1993.

[47] Cross, M. C. and Hohenberg, P. C., "Spatiotemporal chaos," *Science*, vol. 263, no. 5153, pp. 1569–1570, 1994.

[48] Cvitanović, P., *Universality in Chaos*. Bristol: Adam Hilger, 1989. Second Edition.

[49] Cvitanović, P., "Periodic orbits as the skeleton of classical and quantum chaos," *Physica D*, vol. 51, p. 138, 1991.

[50] Cvitanović, P., Artuso, R., Mainieri, R., Tanner, G., and Vattay, G., *Chaos: Classical and Quantum*. Copenhagen: Niels Bohr Institute, 2003. ChaosBook.org.

[51] Cvitanović, P., Dettmann, C. P., Mainieri, R., and Vattay, G., "Trace formulas for stochastic evolution operators: Weak noise perturbation theory," *J. Stat. Phys.*, vol. 93, p. 981, 1998.

[52] Cvitanović, P. and Eckhardt, B., "Periodic orbit expansions for classical smooth flows," *J. Phys. A*, vol. 24, p. L237, 1991.

[53] Cvitanović, P. and Eckhardt, B., "Symmetry decomposition of chaotic dynamics," *Nonlinearity*, vol. 6, p. 277, 1993. `chao-dyn/9303016`.

[54] Cvitanović, P. and Hansen, K. T., "Bifurcation structures in maps of hnon type," *Nonlinearity*, vol. 11, p. 1233, 1998.

[55] Cvitanović, P. and Lan, Y., "Turbulent fields and their recurrences," in *Proceedings of 10th International Workshop on Multiparticle Production: Correlations and Fluctuations in QCD* (Antoniou, N., ed.), (Singapore), World Scientific, 2003. `nlin.CD/0308006`.

[56] Cvitanović, P., "Invariant measurement of strange sets in terms of cycles," *Phys. Rev. Lett.*, vol. 61, p. 2729, 1988.

[57] Cvitanović, P., "Chaotic field theory: a sketch," *Physica A*, vol. 288, p. 61, 2000. `nlin.CD/0001034`.

[58] Dankowicz, H., Holmes, P., Berkooz, G., and Elezgaray, J., "Local models of spatio-temporally complex fields," *Physica D*, vol. 90, pp. 387–407, 1996.

[59] Daviaud, F., Lega, J., Bergé, P., Coullet, P., and Dubois, M., "Spatio-temporal intermittency in a 1d convective pattern: theoretical model and experiments," *Physica D*, vol. 55, pp. 287–308, 1992.

[60] Davidchack, R. L. and Lai, Y.-C., "Efficient algorithm for detecting unstable periodic orbits in chaotic systems," *Phys. Rev. E*, vol. 60, p. 6172, 1999.

[61] Dettmann, C. P. and Cvitanović, P., "Cycle expansions for intermittent diffusion," *Phys. Rev. E*, vol. 56, p. 6687, 1997.

[62] Devaney, R. L., *An Introduction to Chaotic Dynamical systems*. Red-wood City: Addison-Wesley, 1989.

[63] Diakonos, F. K., Schmelcher, P., and Biham, O., "Systematic computation of the least unstable periodic orbits in chaotic attractors," *Phys. Rev. Lett.*, vol. 81, p. 4349, 1998. `chao-dyn/9810022`.

[64] Dittrich, W. and Reuter, M., *Classical and Quantum Dynamics:From Classical Paths to Path Integrals*. New York: Springer, 2001.

[65] Doebner, H. D. and Goldin, G. A., "Properties of nonlinear schrödinger equations associated with diffeomorphism group representations," *J. Phys. A*, vol. 27, pp. 1771–1780, 1994.

[66] Doelman, A., "Finite-dimensional models of the Ginzburg-Landau equation," *Nonlinearity*, vol. 4, pp. 231–250, 1991.

[67] Doelman, A., "Breaking the hidden symmetry in the Ginzburg-Landau equation," *Physica D*, vol. 97, pp. 398–428, 1996.

[68] Doering, C. R., Gibbon, J. D., Holm, D. D., and Nikolaenko, B., "Exact Lyapunov dimension of the universal attractor for the complex Ginzburg-Landau equation," *Phys. Rev. Lett.*, vol. 59, no. 26, pp. 2911–2914, 1987.

[69] Doering, C. R., Gibbon, J. D., Holm, D. D., and Nikolaenko, B., "Low-dimensional behaviour in the complex Ginzburg-Landau equation," *Nonlinearity*, vol. 1, pp. 279–309, 1988.

[70] Du, M. L. and Delos, J. B., "Effect of closed classical orbits on quantum spectr: Ionization of atoms in a magnetic field," *Phys. Rev. Lett.*, vol. 58, no. 17, p. 1731, 1987.

[71] Eckman, J.-P. and Collet, P., *Iterated Maps on the Interval as Dynamical Systems*. No. 1 in Progress in Physics, Boston: Birkhäuser, 1980.

[72] Eckmann, J.-P., "Roads to turbulence in dissipative dynamical systems," *Rev. Mod. Phys.*, vol. 53, p. 643, 1981.

[73] Eckmann, J.-P. and Ruelle, D., "Ergodic theory of chaos and strange attractors," *Rev. Mod. Phys.*, vol. 57, no. 3, p. 617, 1985.

[74] Eckmann, J. P. and Wayne, C. E., "Liapunov spectra for infinite chains of nonlinear oscillators," *J. Stat. Phys.*, vol. 50, pp. 853–878, 1988.

[75] Egolf, D. A. and Greenside, H. S., "Relation between fractal dimension and spatial correlation length for extensive chaos," *Nature*, vol. 369, p. 129, 1994.

[76] Egolf, D. A. and Greenside, H. S., "Characterization of the transition from defect to phase turbulence," *Phys. Rev. Lett.*, vol. 74, no. 10, p. 1751, 1995.

[77] Egolf, D. A., Melnikov, I. V., and Bodenschatz, E., "Importance of local pattern properties in spiral defect chaos," *Phys. Rev. Lett.*, vol. 80, p. 3228, 1998.

[78] Egolf, D. A., Melnikov, I. V., Pesch, W., and Ecke, R. E., "Mechanisms of extensive spatiotemporal chaos in Rayleigh-Bénard convection," *Nature*, vol. 404, p. 733, 2000.

[79] Eguíluz, V. M., Alstrøm, P., Hernández-García, E., and Piro, O., "Average patterns of spatiotemporal chaos: A boundary effect," *Phys. Rev. E*, vol. 59, no. 3, p. 2822, 1999.

[80] Falcolini, C. and de la Llave, R., "Numerical calculation of domains of analyticity for perturbation theories in the presence of small divisors," *J. Stat. Phys.*, vol. 67, pp. 645–666, 1992.

[81] Farmer, J. D. and Sidorowich, J. J., "Predicting chaotic time series," *Phys. Rev. Lett.*, vol. 59, no. 8, p. 845, 1987.

[82] Feigenbaum, M. J., "Quantitative universality for a class of nonlinear transformations," *J. Stat. Phys.*, vol. 19, p. 25, 1978.

[83] Foias, C. and Jolly, M. S., "On the numerical algebraic approximation of global attractors," *Nonlinearity*, vol. 8, pp. 295–319, 1995.

[84] Foias, C., Jolly, M. S., Kevrekidis, I. G., Sell, G. R., and Titi, E. S., "On the computation of inertial manifolds," *Phys. Lett. A*, vol. 131, p. 433, 1988.

[85] Foias, C., Nicolaenko, B., Sell, G. R., and Temam, R., "Inertial manifold for the Kuramoto-Sivashinsky equation," *C. R. Acad. Sci. I-Math*, vol. 301, no. 6, pp. 285–288, 1985.

[86] Foias, C., Nicolaenko, B., Sell, G. R., and Temam, R., "Inertial manifold for the Kuramoto-Sivashinsky equation and an estimate of their lowest dimension," *J. Math. Pure Appl.*, vol. 67, no. 3, pp. 197–226, 1988.

[87] Foias, C., Nicolaenko, B., Sell, G. R., and Témam, R., "Kuramoto-Sivashinsky equation," *J. Math. Pures et Appl.*, vol. 67, p. 197, 1988.

[88] Frisch, U., *Turbulence*. Cambridge, England: Cambridge University Press, 1996.

[89] Frisch, U., Hasslacher, B., and Pomeau, Y., "Lattice-gas automata for the navier-stokes equation," *Phys. Rev. Lett.*, vol. 56, pp. 1505–1508, 1986.

[90] Frisch, U., She, Z. S., and Sulem, P.-L., "Large-scale flow driven by the anisotropic kinetic alpha effect," *Physica D*, vol. 28, pp. 382–392, 1987.

[91] Frisch, U., She, Z. S., and Thual, O., "Viscoelastic behavior of cellular solutions to the Kuramoto-Sivashinsky model," *J. Fluid Mech.*, vol. 168, pp. 221–240, 1986.

[92] Gameiro, M., Kalies, W., and Mischailow, K., "Topological characterization of spatial-temporal chaos," *submitted*, vol. 1, no. 1, p. 1, 2003.

[93] García-Archilla, B., Novo, J., and Titi, E. S., "Postprocessing the Gälerkin method: a novel approach to approximate inertial manifolds," *SIAM J. Numer. Anal.*, vol. 35, no. 3, pp. 941–972, 1998.

[94] Garnier, N., Chiffaudel, A., Daviaud, F., and Prigent, A., "Nonlinear dynamics of waves and modulated waves in 1d thermocapillary flows," *Physica D*, vol. 174, no. 1-4, pp. 1–29, 2003.

[95] Ghidaglia, J. M. and Héron, B., "Dimension of the attractors associated to the Ginzburg-Landau partial differential equation," *Physica D*, vol. 28, pp. 282–304, 1987.

[96] Ghrist, R., den Berg, J. B. V., and Vandervost, R. C., *Morse theory on spaces of braids and Lagrangian dynamics*. ArXiv preprint. math.DS/0105082.

[97] Giona, M. and Adrover, A., "Nonumiform stationary measure of the invariant unstable foliation in hamiltonian and fluid mixing systems," *Phys. Rev. Lett.*, vol. 81, no. 18, p. 3864, 1998.

[98] Golé, C., "A new proof of the aubry-mather's theorem," *Math. Z.*, vol. 210, pp. 441–448, 1992.

[99] Gollub, J. P., "Order and disorder in fluid motion," *Proc. Natl. Acad. Sci. USA*, vol. 92, p. 6705, 1995.

[100] Golubitsky, M., Swift, J. W., and Knobloch, E., "Symmetries and pattern selection in Rayleigh-Bernard convection," *Physica D*, vol. 10, p. 249, 1984.

[101] Grassberger, P., Kantz, H., and Moenig, U., "On the symbolic dynamics of Hénon map," *J. Phys. A*, vol. 22, pp. 5217–5230, 1989.

[102] Grebogi, C., Hammel, S. M., Yorke, J. A., and Sauer, T., "Shadowing of physical trajectories in chaotic dynamics: Containment and refinement," *Phys. Rev. Lett.*, vol. 65, pp. 1527–1530, 1990.

[103] Greene, J. M. and Kim, J. S., "The steady states of the Kuramoto-Sivashinsky equation," *Physica D*, vol. 33, pp. 99–120, 1988.

[104] Griewank, A., "On automatic differentiation," in *Mathematical Programming: Recent Developments and Applications* (Iri, M. and Tanabe, K., eds.), pp. 83–108, Amsterdam: Kluwer Academic Publishers, 1989.

[105] Grimshaw, R. and Hooper, A. P., "The non-existence of a certain class of travelling wave solutions of the Kuramoto-Sivashinsky equation," *Physica D*, vol. 50, pp. 231–238, 1991.

[106] Guckenheimer, J. and Holmes, P., *Nonlinear Oscillations, Dynamical Systems, and Bifurcations of Vector Fields*. New York: Springer-Verlag, 1983.

[107] Guckenheimer, J. and Meloon, B., "Computing periodic orbits and their bifurcations with automatic differentiation," *SIAM J. Sci. Comp.*, vol. 22, no. 3, pp. 951 – 985, 2000.

[108] Gutzwiller, M. C., *Chaos in Classical and Quantum Mechanics*. New York: Springer, 1990.

[109] Gutzwiller, M., *Chaos in Classical and Quantum Mechanics*. New York: Springer-Verlag, 1990.

[110] Hale, J., *Ordinary Differential Equations*. New York: Wiley-Interscience, 1969.

[111] Hale, J. and Koçak, H., *Dynamics and Bifurcations*. New York: Springer-Verlag, 1991.

[112] Hale, J. K., *Oscillations in Nonlinear Systems*. New York: McGraw-Hill, 1963.

[113] Hale, J. K. and Magalhaes, L. T., *An Introduction to Infinite Dimensional Systems-Geometric Theory*. New York: Springer-Verlag, 1984.

[114] Hansen, K. T., "Remarks on the symbolic dynamics for the Hénon map," *Phys. Lett. A*, vol. 165, no. 2, pp. 100–104, 1992.

[115] Hansen, K. T., *Symbolic Dynamics in Chaotic systems*. PhD thesis, Uiversity of Oslo, Box 1048, Blindern, N-0316, Oslo, Norway, September 1993.

[116] Hao, B.-L., *Chao II*. Singapore: World Scientific, 1990.

[117] Hao, B.-L. and Zheng, W.-M., *Applied Symbolic Dynamics and Chaos*. Singapore: World Scientific, 1998.

[118] Hartman, P., *Ordinary Differential Equations*. New York: Wiley, 1964.

[119] Helleman, R. and Bountis, T., "Periodic solutions of arbitrary period, variational methods," *LNP*, vol. 93, p. 353, 1978.

[120] Hénon, M., *Generating Families in the Restricted Three-Body Problem II. Quantitative Study of Bifurcations*. New York: Springer, 2001.

[121] Hénon, M. and Heiles, C., "The applicability of the third integral of motion: Some numerical experiments," *Astron. J.*, vol. 69, p. 73, 1964.

[122] Henry, B. I., Watt, S. D., and Wearne, S. L., "A lattice refinement scheme for finding periodic orbits," *Anziam J.*, vol. 42E, pp. C735–C751, 2000.

[123] Hille, E., *Ordinary Differential Equations in the Complex Domain*. New York: Dover, 1997.

[124] Holmes, P., Lumley, J. L., and Berkooz, G., *Turbulence, Coherent Structures, Dynamical Systems and Symmetry*. Cambridge: Cambridge University Press, 1998.

[125] Holmes, P., Marsden, J., and Scheurle, J., "Exponentially small splittings of separatrices with applications to KAM theory and degenerate bifurcations," *Cont. Math., AMS*, vol. 81, pp. 213–244, 1988.

[126] Homburg, A. J., Osinga, H. M., and Vegter, G., "On the computation of invariant manifolds of fixed points," *Z. Angew. Math. Phys.*, vol. 46, p. 171, 1995.

[127] Hooper, A. P. and Grimshaw, R., "Nonlinear instability at the interface between two viscous fluids," *Phys. Fluids*, vol. 28, pp. 37–45, 1985.

[128] Hooper, A. P. and Grimshaw, R., "Travelling wave solutions of the Kuramoto-Sivashinsky equation," *Wave Motion*, vol. 10, pp. 405–420, 1988.

[129] Hopf, E., "A mathematical example displaying features of turbulence," *Comm. Appl. Math.*, vol. 1, pp. 303–322, 1948.

[130] Hopf, E., "The partial differential equation $u_t + uu_x = u_{xx}$," *Comm. Pure Appl. Math.*, vol. 3, pp. 201–230, 1950.

[131] Hunt, B. R. and Ott, E., "Optimal periodic orbits of chaotic systems," *Phys. Rev. Lett.*, vol. 76, p. 2254, 1996.

[132] Hyman, J. M. and Nicolaenko, B., "The Kuramoto-Sivashinsky equation: a bridge between pde's and dynamical systems," *Physica D*, vol. 18, pp. 113–126, 1986.

[133] Hyman, J. M., Nicolaenko, B., and Zaleski, S., "Order and complexity in the Kuramoto-Sivashinsky model of weakly turbulent interfaces," *Physica D*, vol. 23, pp. 265–292, 1986.

[134] Ince, E. L., *Ordinary Differential Equations*. New York: Dover, 1956.

[135] Janiaud, B., Pumir, A., Bensimon, D., Croquette, V., Richter, H., and Kramer, L., "The eckhaus instability for traveling waves," *Physica D*, vol. 55, p. 269, 1992.

[136] Janiaud, B., Pumir, A., Bensimon, D., Croquette, V., Richter, H., and Kramer, L., "The Eckhaus instability for travelling waves," *Physica D*, vol. 55, pp. 269–286, 1992.

[137] Jeffreys, H. and Jeffreys, B., *Methods of Mathematical Physics*. Cambridge: Cambridge University Press, 1999.

[138] Jensen, M. H., Bak, P., and Bohr, T., "Transition to chaos by interaction of resonances in dissipative systems," *Phys. Rev. A*, vol. 30, p. 1960, 1984.

[139] Jones, J., Troy, W. C., and MacGillivary, A. D., "Steady solutions of the Kuramoto-Sivashinsky equation for small wave speed," *J. Diff. Eqn.*, vol. 96, pp. 28–55, 1992.

[140] Kato, S. and Yamada, M., "Unstable periodic solutions embedded in a shell model turbulence," *Phys. Rev. E*, vol. 68, p. 025302, 2003.

[141] Kawahara, G. and Kida, S., "Periodic motion embedded in plane couette turbulence: regeneration cycle and burst," *J. Fluid Mech.*, vol. 449, pp. 291–300, 2001.

[142] Keller, H. B., *Numerical Methods for Two-Point Boundary-Value Problems*. New York: Dover, 1992.

[143] Kent, P. and Elgin, J., "Travelling-waves of the Kuramoto-Sivashinsky equation: period-multiplying bifurcations," *Nonlinearity*, vol. 5, pp. 899–919, 1992.

[144] Kevrekidis, I. G., Nicolaenko, B., and Scovel, J. C., "Back in the saddle again: a computer assisted study of the Kuramoto-Sivashinsky equation," *Siam J. Appl. Math.*, vol. 50, no. 3, pp. 760–790, 1990.

[145] Kevrekidis, I. G., Nicolaenko, B., and Scovel, J. C., "Back in the saddle again: a computer assisted study of the Kuramoto-Sivashinsky equation," *SIAM J. Applied Math.*, vol. 50, p. 760, 1990.

[146] Kolmogorov, A. N., "The local structure of turbulence in incompressible viscous fluid for very large reynolds numbers," *Proc. R. Soc. Lond. A*, vol. 434, no. 1890, pp. 9–13, 1991.

[147] Kook, H.-T. and Meiss, J. D., "Application of Newton's method to Lagrangian mappings," *Physica D*, vol. 36, pp. 317–326, 1989.

[148] Kook, H.-T. and Meiss, J. D., "Periodic orbits for reversible symplectic mappings," *Physica D*, vol. 35, pp. 65–86, 1989.

[149] Krasikov, I., Rodgers, G. J., and Tripp, C. E., "Growing random sequences," *J. Phys. A: Math. Gen.*, vol. 37, pp. 2365–2370, 2004.

[150] Kruskal, M., "Asymptotic theory of Hamiltonian and other systems with all solutons nearly periodic," *J. Math. Phys.*, vol. 3, no. 4, p. 806, 1962.

[151] Kuramoto, Y., "Diffusion-induced chaos in reaction systems," *Suppl. Progr. Theor. Phys.*, vol. 64, pp. 346–367, 1978.

[152] Kuramoto, Y., *Chemical Oscillations, Waves and Turbulence*. Berlin: Springer, 1984.

[153] Kuramoto, Y. and Tsuzuki, T., "Persistent propagation of concentration waves in dissipative media far from thermal equilibrium," *Progr. Theor. Phys.*, vol. 55, p. 365, 1976.

[154] Lamb, J. S. W. and Roberts, J. A. G., "Time reversal symmetry in dynamical systems: A survey," *Physica D*, vol. 112, p. 1, 1998.

[155] Lan, Y., *Dynamical systems approach to 1-d spatiotemporal chaos - A cyclist's view*. PhD thesis, School of Physics, Geogia Institute of Technology, Atlanta, Georgia, 2004. Not completed yet.

[156] Lan, Y. and Cvitanović, P., "Variational method for finding periodic orbits in a general flow," *Phys. Rev. E*, vol. 69, p. 016217, 2004.

[157] Lan, Y., Garnier, N., and Cvitanović, P., *Stationary modulated-amplitude waves in the 1D complex Ginzburg-Landau equation*. to appear in Phys. Rev. E.

[158] Landau, L. D., "On the problem of turbulence," *Akad. Nauk. Doklady*, vol. 44, p. 339, 1944.

[159] Lau, Y. T., "The "cocoon" bifurcations in three-dimensional systems with two fixed points," *Int. J. Bifur. Chaos*, vol. 2, pp. 543–558, 1992.

[160] Lawden, D. F., *Elliptic Functions and Applications*. New York: Springer-Verlag, 1989.

[161] Lega, J., "Traveling hole solutions of the complex ginzburg landau equation: a review," *Physica D*, vol. 269, pp. 152–153, 2001.

[162] Lorenz, E. N., "Deterministic nonperiodic flow," *J. Atmos. Sci.*, vol. 20, p. 130, 1963.

[163] Luce, B. P., "Homoclinic explosions in the complex Ginzburg-Landau equation," *Physica D*, vol. 84, pp. 553–581, 1995.

[164] Malomed, B. A. and Stenflo, L., "Modulational instabilities and soliton solutions of a generalized nonlinear schrödinger equation," *J. Phys. A*, vol. 24, pp. L1149–L1153, 1991.

[165] Mandelbrot, B. B., *The Fractal Geometry of Nature*. New York: WH Freeman Co., 1982.

[166] Manneville, P., *Dissipative structures and weak turbulence*. Boston: Academic Press, 1990.

[167] Manneville, P. and Chaté, H., "Phase turbulence in the two-dimensional complex Ginzburg-Landau equation," *Physica D*, vol. 96, pp. 30–46, 1996.

[168] Marsden, J. E. and McCracken, M., *The Hopf Bifurcation and its Applications*. Springer-Verlag, 1976.

[169] Martine, M. and Temam, R., "Nonlinear Gälerkin methods," *SIAM J. Numer. Anal.*, vol. 26, no. 5, pp. 1139–1157, 1989.

[170] Mather, J. N., "Variational construction of orbits of twist difeomorphisms," *J. Am. Math. Soc.*, vol. 4, pp. 207–263, 1991.

[171] Matkowsky, B. J. and Volpert, V., "Stability of plane wave solutions of complex Ginzburg-Landau equations," *Quart. Appl. Math.*, vol. LI, no. 2, pp. 265–281, 1993.

[172] McCord, C. K., "Uniqueness of connection orbits in the equation $y^{(3)} = y^2 - 1$," *J. Math. Anal. Appl.*, vol. 114, pp. 584–592, 1986.

[173] Melo, F., Umbanhowar, P., and Swinney, H. L., "Transition to parametric wave patterns in a vertically oscillated granular layer," *Phys. Rev. Lett.*, vol. 72, pp. 172–175, 1994.

[174] Michelson, D., "Steady solutions of the Kuramoto-Sivashinsky equation," *Physica 19D*, pp. 89–111, 1986.

[175] Michelson, D., "Steady solutions of the Kuramoto-Sivashinsky equation," *Physica D*, vol. 19, pp. 89–111, 1986.

[176] Michelson, D. M. and Sivashinsky, G. I., "Nonlinear analysis of hydrodynamic instability in laminar flames - ii. numerical experiments," *Acta Astr.*, vol. 4, pp. 1207–1221, 1977.

[177] Mischaikow, K., "Topological techniques for efficient rigorous computations in dynamics," *Acta Numerica*, p. 001, 2002.

[178] Mischaikow, K. and Mrozek, M., "Chaos in the Lorenz equations: a computer-assisted proof," *Bull. Amer. Math. Soc.(N.S.)*, vol. 32, p. 66, 1995.

[179] Mischaikow, K. and Mrozek, M., "Chaos in the Lorenz equations: A computer assisted proof part ii: Details," *Math. Comp.*, vol. 67, pp. 1023–1046, 1998.

[180] Mischaikow, K. and Mrozek, M., "The Conley index theory," in *Handbook of Dynamical Systems III: Towards Applications* (Fiedler, B., Iooss, G., and Kopell, N., eds.), Singapore: Elsevier Science B. V., 2003.

[181] Mischaikow, K., Mrozek, M., Reiss, J., and Szymczak, A., "Construction of symbolic dynamics from experimental time series," *Phys. Rev. Lett.*, vol. 82, no. 6, p. 1144, 1999.

[182] Montagne, R., Hernández-García, E., and Miguel, M. S., "Winding number instability in the phase-turbulence regime of the complex Ginzburg-Landau equation," *Phys. Rev. Lett.*, vol. 77, no. 2, p. 267, 1996.

[183] Moore, C., "Braids in classical gravity," *Phys. Rev. Lett.*, vol. 70, p. 3675, 1993.

[184] Moore, D. W. and Spiegel, E. A., "A thermally excited nonlinear oscillator," *Astrophys. J.*, vol. 143, p. 871, 1966.

[185] Moresco, P. and Dawson, S. P., "The PIM-simplex method: an extension of the PIM-triple method to saddles with an arbitrary number of expanding directions," *Physica*, vol. 126D, p. 38, 1999.

[186] Moser, J., *Stable and Random Motions in Dynamical Systems*. No. 77 in Ann. Math. Stud., Princeton: Princeton University Press, 1973.

[187] Newell, A. C., "Envelope equations," *Lect. Appl. Math.*, vol. 15, pp. 157–163, 1974.

[188] Newhouse, S. E., Ruelle, D., and Takens, F., "Occurrence of strange Axiom A attractors near quasi-periodic flows on $t^m (m = 3$ or more)," *Commun. Math. Phys.*, vol. 64, p. 35, 1978.

[189] Newton, P. K. and Sirovich, L., "Instabilities of Ginzburg-Landau equation: periodic solutions," *Quart. Appl. Math.*, vol. XLIV, no. 1, pp. 49–58, 1986.

[190] Newton, P. K. and Sirovich, L., "Instabilities of Ginzburg-Landau equation: secondary bifurcation," *Quart. Appl. Math.*, vol. XLIV, no. 2, pp. 367–374, 1986.

[191] Nicolaenko, B., Scheurer, B., and Temam, R., "Some global dynamical properties of the Kuramoto-Sivashinsky equations: nonlinear stability and attractors," *Physica D*, vol. 16, pp. 155–183, 1985.

[192] Nicolaenko, B., Scheurer, B., and Temam, R., "Some global dynamical properties of the Kuramoto-Sivashinsky equations:nonlinear stability and attractors," *Physica D*, vol. 16, pp. 155–183, 1985.

[193] Nozaki, K. and Bekki, N., "Pattern selection and spatiotemporal transition to chaos in the Ginzburg-Landau equation," *Phys. Rev. Lett.*, vol. 51, no. 24, p. 2171, 1983.

[194] Nozaki, K. and Bekki, N., "Exact solutions of the generalized Ginzburg-Landau equation," *J. Phys. Soc. Japan*, vol. 53, no. 5, pp. 1581–1582, 1984.

[195] Nusse, H. E. and York, J. A., "A procedure for finding numerical trajectories on chaotic saddles," *Physica*, vol. 36D, p. 137, 1989.

[196] Olver, P. J., *Applications of Lie Groups to Differential Equations*, vol. 107 of *GTM*. New York: Spring-Verlag, 1998.

[197] Oseledec, V. I., "A multiplicative ergodic theorem. liapunov characteristic numbers for dynamical systems," *Trans. Moscow Math. Soc.*, vol. 19, pp. 197–221, 1968.

[198] Pereira, N. R. and Stenflo, L., "Nonlinear schrödinger equation including growth and damping," *Phys. Fluid*, vol. 20, no. 10, pp. 1733–1734, 1977.

[199] Perko, L., *Differential Equations and Dynamical Systems*. New York: Springer-Verlag, 1991.

[200] Pingel, D., Schmelcher, P., and Diakonos, F. K., "Detecting unstable periodic orbits in chaotic continuous-time dynamical systems," *Phys. Rev. E*, vol. 64, no. 2, p. 026214, 2001.

[201] Pingel, D., Schmelcher, P., Diakonos, F., and Biham, O., "Theory and applications of the systematic detection of unstable periodic orbits in dynamical systems," *Phys. Rev. E*, vol. 62, p. 2119, 2000. `nlin.CD/0006011`.

[202] Poincaré, H., *New Methods in Celestial Mechanics*, vol. 13 of *History of Modern Physics and Astronomy*. New York: Springer-Verlag, 1992.

[203] Pomeau, Y. and Manneville, P., "Intermittent transition to turbulence in dissipative dynamical systems," *Commun. Math. Phys.*, vol. 74, p. 189, 1980.

[204] Porubov, A. V. and Velarde, M. G., "Exact periodic solutions of the complex Ginzburg-Landau equation," *J. Math. Phys.*, vol. 40, no. 2, p. 884, 1999.

[205] Press, W. H., Teukolsky, S. A., Vetterling, W. T., and Flannery, B. P., *Numerical Recipes in C*. Cambridge, England: Cambridge University Press, 1992.

[206] Pugh, C., "An improved closing lemma and a general density theorem," *Amer. J. Math.*, vol. 89, 1967.

[207] Quey, R. E. L., Mahajan, S. M., Rutherford, P. H., and Tang, W. M., "Nonlinear saturation of the trapped-ion mode," *Phys. Rev. Lett.*, vol. 34, pp. 391–394, 1974.

[208] Ramshankar, R. and Gollub, J. P., "Transport by capillary waves, part ii: Scalar dispersion and the structure of the concentration field," *Phys. Fluids A*, vol. 3, p. 1344, 1991.

[209] Rodriguez, J. D. and Sirovich, L., "Low-dimensional dynamics for the complex Ginzburg-Landau equation," *Physica D*, vol. 43, pp. 77–86, 1990.

[210] Rössler, O. E., "An equation for continuous chaos," *Phys. Lett. A*, vol. 57, p. 397, 1976.

[211] Rothstein, D., Henry, E., and Gollub, J. P., "Persistent patterns in transient chaotic fluid mixing," *Nature*, vol. 401, pp. 770–772, 1999.

[212] Rožděstvenskiĭ, B. and Janenko, N., *Systems of Quasilinear Equations and Their Applications to Gas Dynamics*. Providence, RI: AMS, 1983.

[213] Ruelle, D., *Statistical Mechanics, Thermodynamic Formalism*. Reading, MA: Addison-Wesley, 1978.

[214] Ruelle, D., "Large volume limit of the distribution of characteristic exponents in turbulence," *Commun. Math. Phys.*, vol. 87, pp. 287–302, 1982.

[215] Ruelle, D., "Conversations on nonequilibrium physics with an extraterrestrial," *Physics Today*, vol. 57, no. 5, pp. 48–53, 2004.

[216] Ruelle, D. and Takens, F., "On the nature of turbulence," *Commun. Math. Phys.*, vol. 20, p. 167, 1971.

[217] Rugh, H., "The correlation spectrum for hyperbolic analytic maps," *Nonlinearity*, vol. 5, p. 1237, 1992.

[218] Rybakowski, K. P., *The Homotopy Index and Partial Differential equations*. New York: Spring-Verlag, 1980.

[219] Sakaguchi, H., "Breakdown of the phase dynamics," *Prog. Ther. Phys.*, vol. 84, no. 5, pp. 792–800, 1990.

[220] Scheuer, J. and Malomed, B. A., "Stable and chaotic solutions of the complex Ginzburg-Landau equation with periodic boundary conditions," *Physica D*, vol. 161, pp. 102–115, 2002.

[221] Schmelcher, P. and Diakonos, F. K., "General appoach to the localization of unstable periodic orbits in chaotic dynamical systems," *Phys. Rev. E*, vol. 57, no. 3, p. 2739, 1998.

[222] Schöpf, W. and Kramer, L., "Small-amplitude periodic and chaotic solutions of the complex Ginzburg-Landau equation for a subcritical bifurcation," *Phys. Rev. Lett.*, vol. 66, no. 18, p. 2316, 1991.

[223] Schuster, H. G., *Deterministic Chaos: an introduction*. Weinheim: VCH Verlagsgesellschaft, 1995.

[224] Sepulchre, J.-A. and Mackay, R., "Localized oscillations in conservative or dissipative networks of weakly coupled autonomous oscillators," *Nonlinearity*, vol. 10, pp. 679–713, 1997.

[225] Shraiman, B. I., Pumir, A., van Saarloos, W., Hohenberg, P. C., Chaté, H., and Holen, M., "Spatiotemporal chaos in the one-dimensional complex Ginzburg-Landau equation," *Physica D*, vol. 57, pp. 241–248, 1992.

[226] Sidorov, N., Loginov, B., Sinitsyn, A., and Falaleev, M., *Lyapunov-Schmidt Methods in Nonlinear Analysis and Applications*, vol. 550 of *mathematics and its applications*. Dordrecht: Kluwer Academic Publishers, 2002.

[227] Sinai, Y. G., *Introduction to Ergodic Theory*. Princeton: Princeton University Press, 1976.

[228] Sivashinsky, G. I., "Nonlinear analysis of hydrodynamical instability in laminar flames - i. derivation of basic equations," *Acta Astr.*, vol. 4, p. 1177, 1977.

[229] Sivashinsky, G. I. and Michelson, D. M., "On irregular wavy flow of a liquid down a vertical plane," *Prog. Theor. Phys. Suppl.*, vol. 66, p. 2112, 1980.

[230] Smale, S., "Differentiable dynamical systems," *Bull. Amer. Math. Soc.*, vol. 73, pp. 747–817, 1967.

[231] Spalding, D. B., "Kolmogorov's two-equation model of turbulence," *Proc. R. Soc. Lond. A*, vol. 434, no. 1890, pp. 211–216, 1991.

[232] Sparrow, C., *The Lorenz Equations: Bifurcations, Chaos and Strange Attractors*. New York: Springer- Verlag, 1982.

[233] Spiegel, E. A., "Chaos: a mixed metaphor for turbulence," *Proc. Roy. Soc.*, vol. A413, p. 87, 1987.

[234] Stenflo, L. and Gradov, O. M., "Solitary surface-wave deformation of a plasma boundary," *Phys. Plasmas*, vol. 1, no. 8, p. 2804, 1994.

[235] Stenflo, L. and Yu, M. Y., "Plasma oscillons in spherically bounded magnetized plasmas," *Phys. Plasmas*, vol. 5, p. 3122, 1998.

[236] Stenflo, L. and Yu, M. Y., "Oscillons at a plasma surface," *Phys. Plasmas*, vol. 10, no. 3, pp. 912–913, 2003.

[237] Sterling, D. and Meiss, J. D., "Computing periodic orbits using the anti-integrable limit," *Phys. Lett. A*, vol. 241, pp. 46–52, 1998.

[238] Stoer, J. and Bulirsch, R., *Introduction to Numerical Analysis*. New York: Springer-Verlag, 1983.

[239] Strain, M. C. and Greenside, H. S., "Size-dependent transition to high-dimensional chaotic dynamics in a two-dimensional excitable media," *Phys. Rev. Lett.*, vol. 80, no. 11, pp. 2306–2309, 1998.

[240] Strogatz, S. H., *Nonlinear Dynamics and Chaos*. Studies in Nonlinearity, Cambridge Massachusetts: Perseus Publishing, 2000.

[241] Sweet, D., Nusse., H. E., and Yorke, J. A., "Stagger-and-step method: Detecting and computing chaotic saddles in higher dimensions," *Phys. Rev. Lett.*, vol. 86, no. 11, p. 2261, 2001.

[242] Szebehely, V., *Theory of Orbits*. New York: Academic Press, 1967.

[243] Tajima, S. and Greenside, H. S., "Microextensive chaos of a spatially extended system," *Phys. Rev. E*, vol. 66, p. 017205, 2002.

[244] Takáč, P., "Invariant 2-tori in the time-dependent Ginzburg-Landau equation," *Nonlinearity*, vol. 5, pp. 289–321, 1992.

[245] Temam, R., *Infinite-Dimensional Dynamical Systems in Mechanics and Physics*. No. 68 in Appl. Math. Sci., New York: Springer-Verlag, 1988.

[246] Temam, R., "Approximation of attractors, large eddy simulations and multiscale methods," *Proc. R. Soc. Lond. A*, vol. 434, no. 1890, pp. 23–39, 1991.

[247] Temme, N. M., *Special functions: an introduction to the classical functions of mathematical physics*. New York: Wiley-Interscience, 1996.

[248] Thomas, J. W., *Numerical Partial Differential Equations*. New York: Spring-Verlag, 1995.

[249] Tompaidis, S., "Numerical study of invariant sets of a quasi-periodic perturbation of a symplectic map," *Experimental Mathematics*, vol. 5, pp. 211–230, 1996.

[250] Torcini, A., "Order parameter for the transition from phase to amplitude turbulence," *Phys. Rev. Lett.*, vol. 77, no. 6, p. 1047, 1996.

[251] Troy, W. C., "The existence of steady solutions of the Kuramoto-Sivashinsky equation," *J. Diff. Eqn.*, vol. 82, pp. 269–313, 1989.

[252] und H. Frauenkron, A. T. and Grassberger, P., "Studies of phase turbulence in the one dimensional complex Ginzburg-Landau equation," *Phys. Rev. E*, vol. 55, p. 5073, 1997.

[253] van Hecke, M., "Building blocks of spatiotemporal intermittency," *Phys. Rev. Lett.*, vol. 80, p. 1896, 1998.

[254] van Hecke, M., "Building blocks of spatiotemporal intermittency," *Phys. Rev. Lett.*, vol. 80, no. 9, p. 1896, 1998.

[255] van Hecke, M., "Coherent and incoherent structures in systems described by the 1d CGLE: Experiments and identification," *Physica D*, vol. 174, p. 134, 2003.

[256] van Hecke, M., Hohenberg, P. C., and van Saarloos, W., "Amplitude equations for pattern forming systems," in *Fundamental Problems in Statistical Mechanics* (van Beijeren, H. and Ernst, M. H., eds.), vol. VIII, Amsterdam: North-Holland, 1994.

[257] van Hecke, M. and Howard, M., "Ordered and self-disordered dynamics of holes and defects in the one-dimensional complex Ginzburg-Landau equation," *Phys. Rev. Lett.*, vol. 86, no. 10, p. 2018, 2001.

[258] van Saarloos, W. and Hohenberg, P. C., "Pulses and fronts in the complex Ginzburg-Landau equation near a subcritical bifurcation," *Phys. Rev. Lett.*, vol. 64, no. 7, p. 749, 1990.

[259] van Saarloos, W. and Hohenberg, P. C., "Fronts, pulses, sources and sinks in generalized complex Ginzburg-Landau equations," *Physica D*, vol. 56, pp. 303–367, 1992.

[260] Varga, A. and Pieters, S., "Gradient-based approach to solve optimal periodic output feedback control problems," *Automatica*, vol. 34, no. 4, pp. 477–481, 1998.

[261] Viswanath, D., "The Lindstedt-Poincaré technique as an algorithm for finding periodic orbits," *SIAM Review*, vol. 43, pp. 478–496, 2002.

[262] Viswanath, D., "Symbolic dynamics and periodic orbits of the Lorenz attractor," *Nonlinearity*, vol. 16, pp. 1035–1056, 2003.

[263] Viswanath, D., "An extension of the Lindstedt-Poincaré algorithm for computing periodic orbits." unpublished.

[264] Vladimirov, S. V. and Yu, M. Y., "Boundary effects on the nonlinear interactions of surface waves," *Phys. Fluids B*, vol. 5, p. 2888, 1993.

[265] Vladimirov, S. V. and Yu, M. Y., "Coupled electron surface plasma wave solitons in slabs," *Phys. Lett. A*, vol. 184, p. 459, 1994.

[266] Voth, G. A., Haller, G., and Gollub, J. P., "Experimental measurements of streching fields in fluid mixing," *Phys. Rev. Lett.*, vol. 88, no. 25, p. 254501, 2002.

[267] Walters, P., *An introduction to ergodic theory.* New York: Speringer-Verlag, 1981.

[268] Weiss, J., "The Painlevé for partial differential equations.ii: Bäcklund transformation, lax pairs, and the schwarzian derivative," *J. Math. Phys.*, vol. 24, p. 1405, 1983.

[269] Weiss, J., "Bäcklund transformation and the Painlevé property," *J. Math. Phys.*, vol. 27, p. 1293, 1986.

[270] Weiss, J., Tabor, M., and Carnevale, G., "The Painlevé property for partial differential equations," *J. Math. Phys.*, vol. 24, p. 522, 1983.

[271] Wiggins, S., *Global Bifurcations and Chaos*. New York: Springer-Verlag, 1988.

[272] Wittenberg, R. W. and Holmes, P., "Scale and space localization in the Kuramoto-Sivashinsky equation," *Chaos*, vol. 9, no. 2, p. 452, 1999.

[273] Wolfram, S., *Cellular Automata and Complexity*. Red-wood City: Addison-Wesley, 1994.

[274] Yang, T.-H., Hunt, B. R., and Ott, E., "Optimal periodic orbits of continuous time chaotic systems," *Phys. Rev. E*, vol. 62, no. 2, p. 1950, 2000.

[275] Yang, T. S., "On travelling-wave solutions of the Kuramoto-Sivashinsky equation," *Physica D*, vol. 110, pp. 25–42, 1997.

[276] Yuan, G.-C., Yorke, J. A., Carroll, T. L., Ott, E., and Pecora, L. M., "Testing whether two chaotic one dimensional processes are dynamically identical," *Phys. Rev. Lett.*, vol. 85, no. 20, p. 4265, 2000.

[277] Zabusky, N. J. and Kruskal, M. D., "Interaction of "solitons" in a collisionless plasma and the recurrence of initial states," *Phys. Rev. Lett.*, vol. 15, p. 240, 1965.

[278] Zoldi, S. M. and Greenside, H. S., "Spatially localized unstable periodic orbits of a high-dimensional chaotic system," *Phys. Rev. E*, vol. 57, p. R2511, 1998.